UNCLASSIFIED

AD 270 928

Reproduced
by the

ARMED SERVICES TECHNICAL INFORMATION AGENCY
ARLINGTON HALL STATION
ARLINGTON 12, VIRGINIA

UNCLASSIFIED

WADC TECHNICAL REPORT 59-374

AIR FLOW CHARACTERISTICS OF PARACHUTE FABRICS
AT SIMULATED HIGH ALTITUDES

C. V. Seshadri
G. A. Brown
S. Backer
J. G. Krizik
D. M. Mellen

Massachusetts Institute of Technology

MARCH 1960

WRIGHT AIR DEVELOPMENT DIVISION

AIR FLOW CHARACTERISTICS OF PARACHUTE FABRICS AT SIMULATED HIGH ALTITUDES

C. V. Seshadri
G. A. Brown
S. Backer
J. G. Krizik
D. M. Mellen

Textile Division
Massachusetts Institute of Technology

MARCH 1960

WRIGHT AIR DEVELOPMENT DIVISION
AIR RESEARCH AND DEVELOPMENT COMMAND
UNITED STATES AIR FORCE
WRIGHT-PATTERSON AIR FORCE BASE, OHIO

FOREWORD

WADC TR 59-374

ABSTRACT

The air flow characteristics of parachute canopy cloth have been measured over an unusually wide range of test conditions. High altitude simulated tests (up to 150,000 feet) have shown the cloth to have markedly low flow rates, as may be predicted from a nozzle flow analogy. A method of predicting high altitude behavior has been proposed. Permeabilities of four cloths have been shown to be significantly dependent on their state of stress at the time of air flow measurement. The magnitude of this relationship is observed to be determined by the biaxial stress-strain behavior of each fabric. The air stream deflection tendency of thick canopy material has been verified and its cause investigated. The role of pore geometry in influencing cloth permeability has been explored.

PUBLICATION REVIEW

This report has been reviewed and is approved.

FOR THE COMMANDER:

C.A. WILLIS
Chief, Textile Branch
Non-Metallic Materials Division
Materials Laboratory

WADC TR 59-374

TABLE OF CONTENTS

WADC TR 59-374

LIST OF ILLUSTRATIONS

List of Illustrations (Cont'd)

List of Illustrations (Cont'd)

WADC TR 59-374

LIST OF TABLES

LIST OF SYMBOLS

a   Velocity of sound

α Filling deflection angle (see Fig. 25.2)

A   Flow area

A_a The apparent area through which the flow is directed

A_f The real area through which the flow is directed

β Warp deflection angle (see Fig. 25.2)

C   Effective porosity, see equation (3)

c_p Specific heat at constant pressure

$C_{w,f}$ Crimp in warp, filling

$d_{w,f}$ Yarn diameter, warp, filling

g_o Acceleration given to unit mass by unit force

G   Mass flow rate per unit area

G_s Mass flow rate through fabric with atmospheric conditions upstream of fabric, see equation (6)

H   Fabric thickness

J   Mechanical equivalent of heat

k   Ratio of specific heats

K_1, K_2 Constants in various equations

$L_{w,f}$ Length of warp, filling in unit cell

M   Mach number

p   pressure

p_2' Pressure downstream of fabric in mm Hg below atmospheric pressure

p_2'' Pressure downstream of fabric in cm Narcoil relative to McLeod gage pressure

$p_{w,f}$ Spacing between warp, filling yarns

Pressure at McLeod gage in mm Hg (Used as reference pressure for Narcoil manometer)

Q   Standard volume flow rate per unit area

Q'   Standard volume flow rate per unit area based on G_s

R   Gas constant

T   Absolute temperature

u   Average air velocity through fabric, based on apparent flow area and upstream density, see equation (4)

v   Air velocity

V   Velocity of free air stream, see equation (5)

$V_{r,1,2}$ Valve numbers (see Fig. 9)

w   Mass rate of flow

w_c Mass rate of flow through rotameter under arbitrary calibration conditions

w_r Mass rate of flow through rotameter under actual test conditions

Δp Pressure difference across fabric, $p_1 - p_2$

ρ Air density

ρ_s Air density at standard atmospheric conditions, 0.075 lbm/ft^3

ϕ Total deflection angle (see Fig. 25.2)

σ Stress in fabric lbs/in

Subscripts

c.   refers to conditions upstream of rotameter under arbitrary calibration conditions

e   refers to conditions at exit plane of nozzle

r   refers to conditions upstream of rotameter under actual test conditions

o   refers to atmospheric conditions

1   refers to conditions upstream of nozzle or fabric

2   refers to conditions downstream of nozzle or fabric

σ Stress in pounds per inch width

AIR FLOW CHARACTERISTICS OF PARACHUTE FABRICS AT SIMULATED HIGH ALTITUDES

INTRODUCTION

Satisfactory performance of cloth parachutes is dependent on parachute design, on fabrication efficiencies and on material properties. Strength and air permeability constitute the pertinent cloth properties which influence chute behavior. In particular, the permeability of chute materials has a strong effect on parachute opening reliability, on opening shock, on stability and on parachute drag.

The parachute designer has available numerous results of both model and full scale experiments in which cloth permeability is the controlled variable and parachute behavior characteristics are observed and recorded. Numerous emprical relationships have been recorded in this manner. A pertinent example is the dependence of the drag coefficient of a parachute on cloth permeability cited by Johns (1) and later by Hoerner (2).

Measurements of cloth air permeability are taken in the textile laboratory under rather arbitrary conditions of pressure differential, average air pressure, and sample size. The permeability units reported in the textile literature are volume flow per unit area per unit time for the given pressure differential. These data are often converted in the parachute literature to read in terms of effective porosity, a dimensionless number corresponding to the ratio of average air velocity through the parachute cloth to free stream velocity relative to the parachute. In laboratory calculations the effective porosity is taken as the ratio of the air permeability at a given pressure differential to that velocity of air whose dynamic pressure would equal the specified pressure differential. This definition becomes specific only when the air densities involved in the calculation of volume flow and velocities are specified, in other words, when it is stated explicitly that either upstream or downstream densities are used. It is important that the parachute designer recognize that different textile laboratories have used different conventions in reporting their data and frequently the specifics of the conventions are not sufficiently emphasized in summary and handbook presentations of the data.

Two variables of permeability testing which have not received sufficient attention to date are sample tensions and average air densities. Early work on air flow through textile structures has been restricted to the case of small pressure differentials above atmospheric pressure, hence, density variations during test and fabric stress build-up could be justifiably neglected. With the extension of parachute operations to excessively high speeds at high altitudes, cloth distortions and density changes must assume major roles in laboratory measurements of fabric flow behavior. The textile materials engineer must seek to control both of these parameters, as well as the parameter of pressure differential, for the parachute designer will now expect a more complete characterization of cloth behavior than that previously provided for low pressure differential atmospheric density applications.

This report presents the results of experiments and analyses conducted in the Textile Division, M.I.T., on the phenomena of air flow through parachute fabrics, with each of the three parameters controlled independently.

Part I deals with simulated high altitude flow and constitutes a study of density effects over a wide range of pressure differentials. Part II treats the stress buildup and accompanying fabric distortions as they influence air flow, independent of changes in pressure differential. This dual treatment provides the parachute designer with added dimensions of cloth characterization and, it is hoped will provide a worthwhile contribution to the field of retardation engineering.

This is not to imply that all parameters of cloth performance have now been adequately treated. As every rheologist knows, the mechanical behavior of synthetic organic fibers is dependent on such factors as rate of load, ambient temperature and humidity and previous mechanical history. These variables have been arbitrarily fixed in the experiments discussed in this report, as they have been in the majority of the airflow studies reported in the literature. Clearly, there is much more work to be done before a complete characterization can be provided for textile materials intended to be utilized in high speed parachutes and retardation devices.

WADC TR 59-374

2

I HIGH ALTITUDE FLOW

Introduction

The need for data on the permeability of parachute materials at high altitudes has become imperative in the context of present day defense requirements. Thus, with the increasing use of parachute-type devices to recover missile components and aid in the maneuverability of conventional aircraft, a knowledge of the performance of materials under actual conditions is necessary to enable the engineer to design efficient parachutes for use in every region of the Earth's atmosphere. This report presents data on conditions that obtain at sea-level, 50,000 feet, 100,000 feet and 150,000 feet. Experimental data on the effect of the temperature at these levels are not presented.

The materials include one experimental and three standard Air Force fabrics designated in the report as S3, S6, S8 and E10, respectively. These designations are a continuation of the system used in an earlier report (3) submitted by the Massachusetts Institute of Technology. Fabric specifications are listed in Appendix I. The data have been reported in the form of graphs of air-permeability expressed as cubic feet per minute per square feet versus differential pressure across the fabric in inches of water. A method of predicting the air permeability at altitudes higher than 150,000 feet as well as the relationships between the values at various altitudes is given. The effect of existing temperatures at higher altitudes will be two fold. 1) that due to the change in the density of the air and· 2) that due to the change in the viscoelastic properties of the material itself, an attempt has been made to predict the effect of temperature changes on the permeability of the materials as influenced by density only.

Description of the Atmosphere

The high altitude pressure simulation tests of this report were based on the definition of the standard atmosphere adopted by the National Advisory Committee for Aeronautics (4), (5). The values of pressure, temperature and density of the adopted standard are in fairly good agreement with average, annual values of these variables obtained at about latitude 40° in North America up to an altitude of about 20,000 metres (65,517 feet). Experimental values of atmospheric properties beyond this altitude have not yet been ratified and checked against the adopted standards.

WADC TR 59-374

The calculation procedures for the properties of the standard atmosphere have been described thoroughly elsewhere (4),(5),(6) and shall not be repeated here. The values of atmospheric pressure used in this report, at the altitudes of 50,000, 100,000 and 150,000 ft were 87.0, 8.04 and 1.08 mm of mercury, respectively; these are based on an arbitrary constant value of the gravitational acceleration. N.A.C.A. TN 1200 (5) also lists data that take into account the decrease in the acceleration of gravity with increasing altitude, and therefore are more precise. The difference in pressure is less than 1% at 50,000 but at 200,000 ft the pressure calculated by the latter procedure is about 7% higher than that calculated by the former.

Equipment

The high altitude permeometer was designed to supplement fixed compressor and steam-ejector facilities available in the laboratories of the contractor. These consisted of (a) high pressure compressor, pressure regulators, and air filters and (b) three stage steam-ejector and auxiliary instrumentation. The fixed facilities are described in Appendix II. In this section, only equipment constructed specially for the high altitude permeability tests is described.

The permeometer was designed to simulate only the pressure at the 50,000, 100,000 and 150,000 ft levels, but not the temperature. The tremendous range of temperatures encountered at these altitudes would have made the costs of temperature simulation prohibitive.

The permeometer is described with the aid of Figures 1, 2, 3, 4 and 5, the last two figures being photographs of the equipment and the steam-ejector respectively. The test chamber consisted of an 8" standard cast-iron cross, Figure 1. Two legs of the cross were used for lighting and viewing the sample during a test; the windows were cut out of 3/4" plexiglass sheets and were bolted to the cross by means of 8" pipe flanges. Thick, soft rubber gaskets were used between the flanges and the windows and the cross to ensure a good seal. The connection to the 6" tee of the ejector inlet was made through an 8" to 6" taper reducer and 6" ball valve. Since flanged joints were used on all the steel fittings in the equipment, special precautions were taken to seal the system, against leaks under the vacuum conditions encountered. Asbestos gaskets coated with Permatex No. 1* gasket compound were found to be effective for this purpose.

---

*Made by the Permatex Company, Huntington Station, Long Island, New York

The fourth leg of the cross was closed by means of a flange with an O-ring seal. Since the flange was removed frequently to change the sample, this method gave a more positive leakproof connection. The static pressure tap just ahead of the fabric specimen was also taken out through the flange.

Figure 2 shows the movable part of the permeometer, containing the sample clamping device, flow tube, control valves and the flow-meter. This unit was pushed back as a whole from the test chamber when a test specimen was changed in the jaws. The flange of Figure 1 was supported on a 3/4" plywood platform on wheels by means of rigidly mounted brackets welded to its sides. The jaw plate was attached to a short section of 2" pine which was threaded to the flange of Figure 1.

On the other side of the flange 2" streamline copper solder pipe and fittings were used. Figure 2 brings out one desired aim in the construction of the equipment, namely, a minimum of constrictions causing pressure losses.

Placing the valves after the flow meter instead of before, assured better flow control, though it produced more disturbance of the velocity profile just ahead of the fabric. However, since the flow took place only through a small area in the center of the fabric the approach profile should have been essentially flat.

A 2 inch gate valve was used for coarse control of the flow and a 3/4" needle valve, for fine control. Flow measurements were carried out with a Fischer & Porter Flowmeter and the pressures at the Flowmeter were read off from a calibrated compound test gage (30" Hg to 30 psig). A thermocouple well (not shown) and copper--constantan thermocouples were used to measure the temperature of the flowing air.

A solenoid valve actuated by a vacuum switch was used to shut off the air flowing through the fabric in case of failure. The relay in the vacuum switch was set at 4 mm mercury for the 150,000 foot tests and at 10 mm mercury for the 100,000 foot tests. The solenoid valve and a valve used in the calibration of the Flowmeter can be seen to the right of the Flowmeter in Figure 4.

Measuring instruments such as the pressure gage and the Flow-meter were calibrated; the former with the aid of a manometer and the latter using the laboratory's 250 cubic foot gasometer.
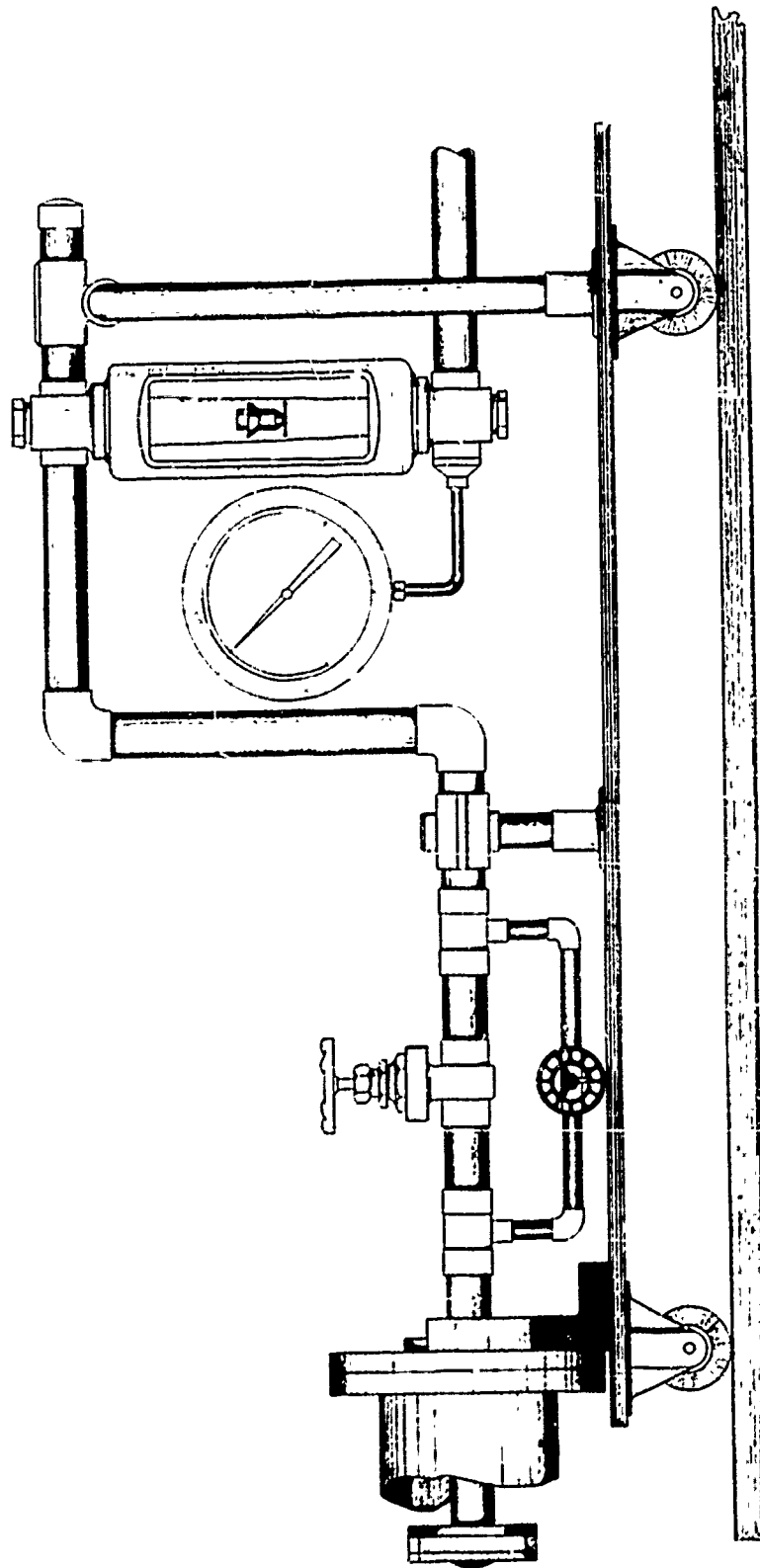
Figure 1.   LOW PRESSURE PERMEOMETER TEST SECTION
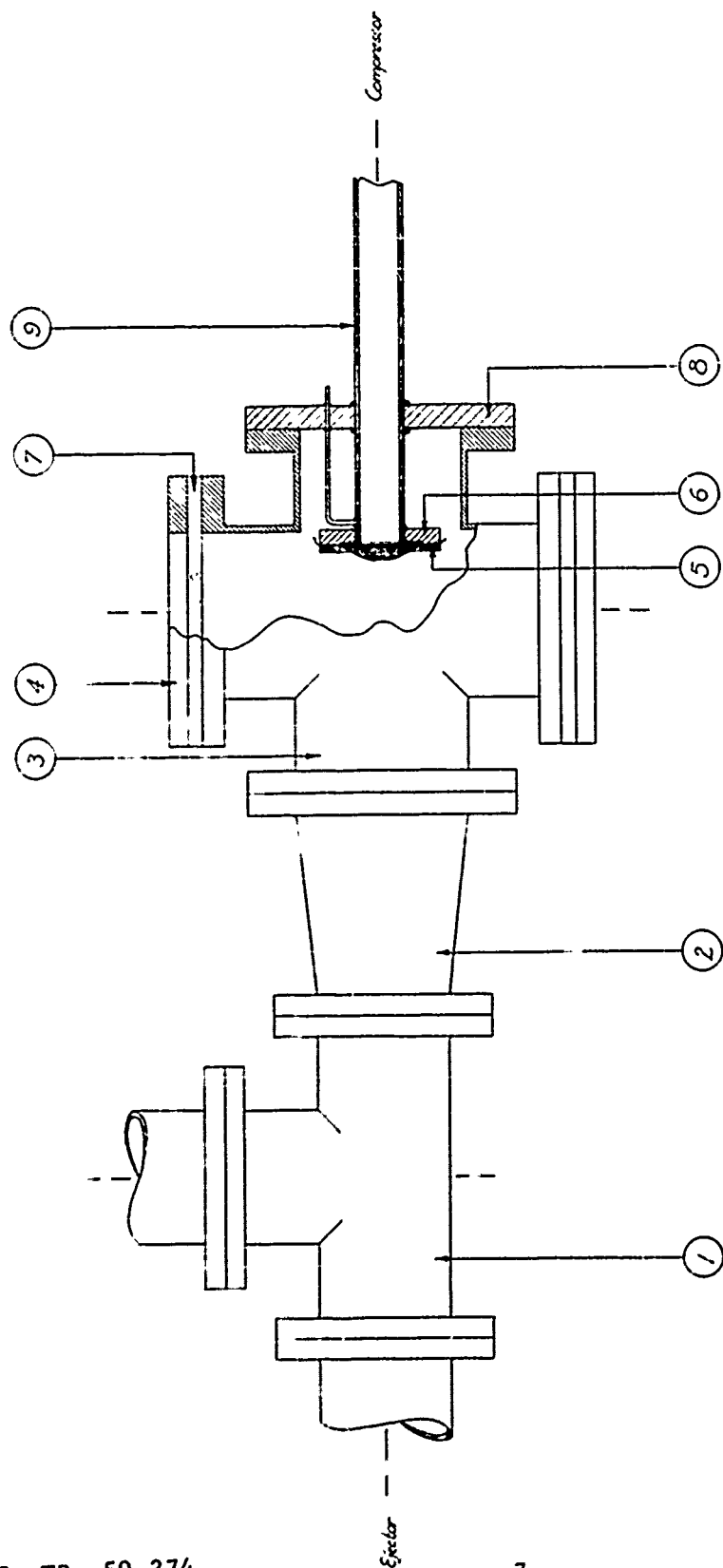
Figure 2.   LOW PRESSURE PERMEOMETER INLET SECTION

① 6" Tee
② 8" Taper Reducer
③ 8" Cross
④ 8" x 13¾" Flange
⑤ Jaw
⑥ Jaw Plate
⑦ Window
⑧ Jaw Flange
⑨ 2" Pipe

The fabric sample clamping device was similar to that used in a previous report (3) and was designed to test the permeability through a small area in the center under uniform biaxial stresses. Thus, the 4" square test specimen was backed up by a fortisan-rubber orifice diaphragm made in three sections. Two of these sections were cut out from a 0.010" rubber sheet in the form of 6" squares with holes along the sides corresponding to the bolt holes on the jaws. In the center, a 2" square was cut out to allow the orifice to be exposed to the airflow. Sandwiched in between was a 3" square orifice sheet of 3-ply rubber coated fortisan fabric with a 1 inch diameter circle cut out. This circle formed the only open area for air flow. In the case of the tests run at 150,000 feet altitude, the 1" orifice was replaced by a 3/4" orifice. Thus the fabric cum orifice diaphragm system comprised a flexible matrix of the test fabric, thin rubber diaphragm, orifice sheet, and thin rubber diaphragm. It has been shown (3) that such a system is satisfactory from the viewpoint of maintaining a constant exposed area and at the same time allowing the test fabric to bear all but a negligible amount of the flow derived loads.

The fabric specimen itself was prepared as follows: Nine inch squares were cut out from the yardage supplied by the Textile laboratories of W.A.D.C. at a sufficient distance from the edges to eliminate selvedge non-uniformity. These squares were then laid out on a pre-formed aluminum stencil which had holes along the sides corresponding to the threaded holes on the jaw-plate. The holes were marked on the fabric and then burned through with a soldering iron. Since these holes formed a 6" square, the extra 1.5" on each side of the square provided enough left over material for handling the test specimen in the clamp.

The pressure measuring system of the equipment presented a unique problem in that an 80-fold range of pressures was encountered i.e., 1 mm mercury at 150,000 feet to 87 mm mercury at 50,000 feet. Thus a combination of manometric devices was used since no one fluid could cover the whole range satisfactorily. Figure 3 shows all the manometers schematically. The manometer p_r was used to measure the pressure at the Flowmeter and the manometer p_1 to measure the static pressure just ahead of the fabric. Since the pressure at these points reached a maximum of 22 psig corresponding to a pressure drop of 1000 inches of water, the manometers were built in eight foot sections, and mercury was the measuring fluid. This may be seen from Figure 4. The valves V_r and V_1 were used to control the fluctuation of the column at the beginning of a run.

WADC TR 59-374

Figure 3. Pressure Measuring System
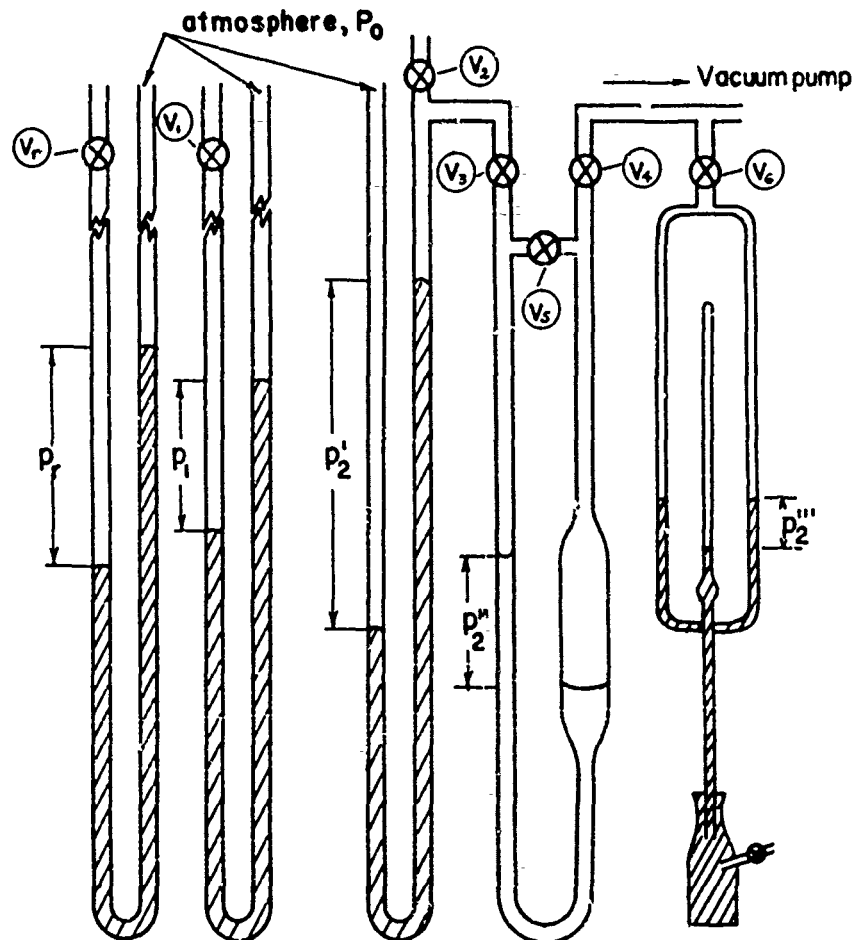
V_r From Flowmeter

V_1 From Fabric high pressure side

V_2 From Fabric low pressure side

V_3 V_4 V_5 Oil monometer controls

V_6 Mc Leod gage control

Note: Mercury barometer not shown

$$P_2 = P_0 - P_2' = P_2'' + P_2'''$$
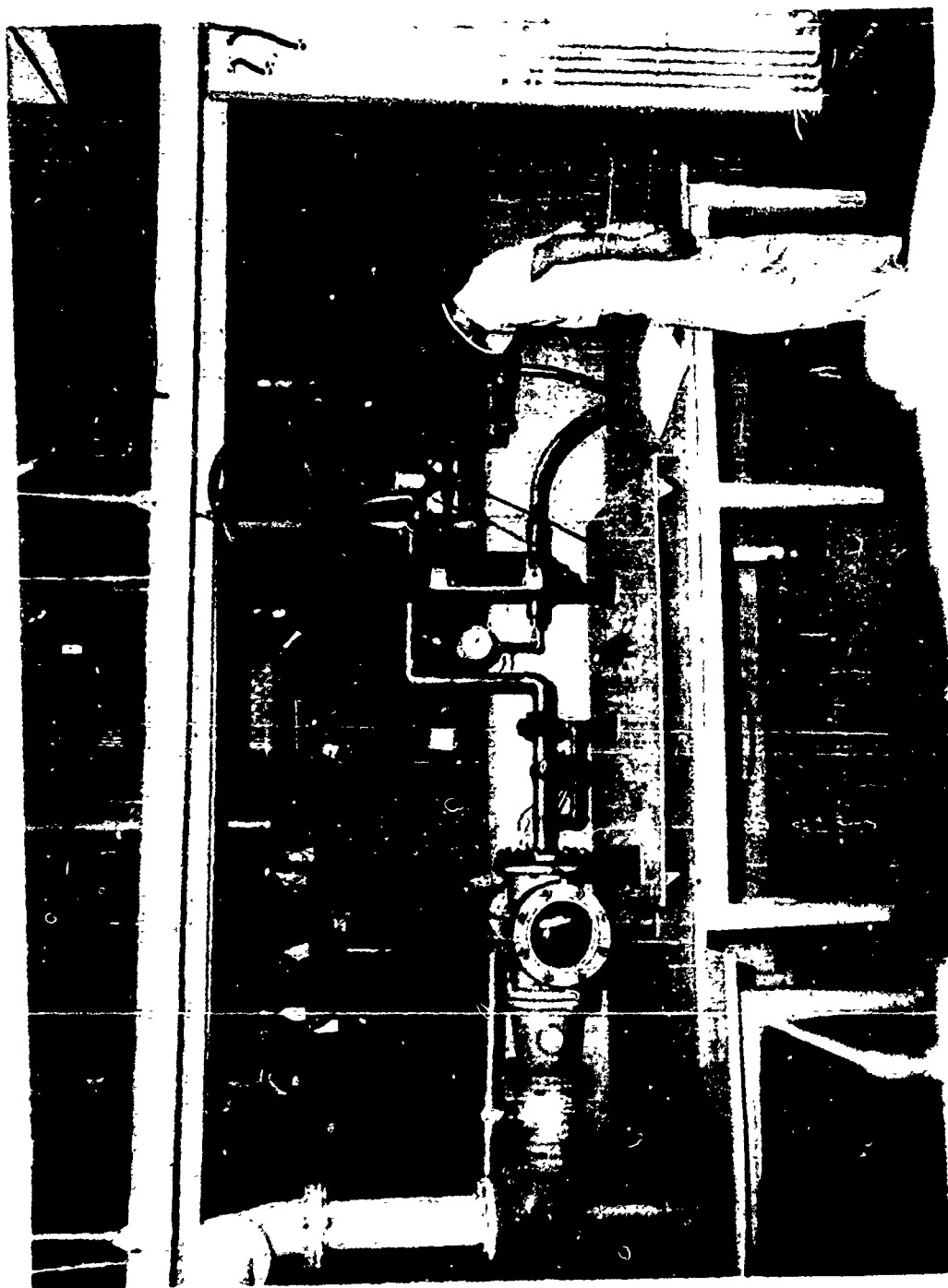
FIGURE 4.   LOW PRESSURE PERMEOMETER INSTALLATION

WADC   TR 59-374

10
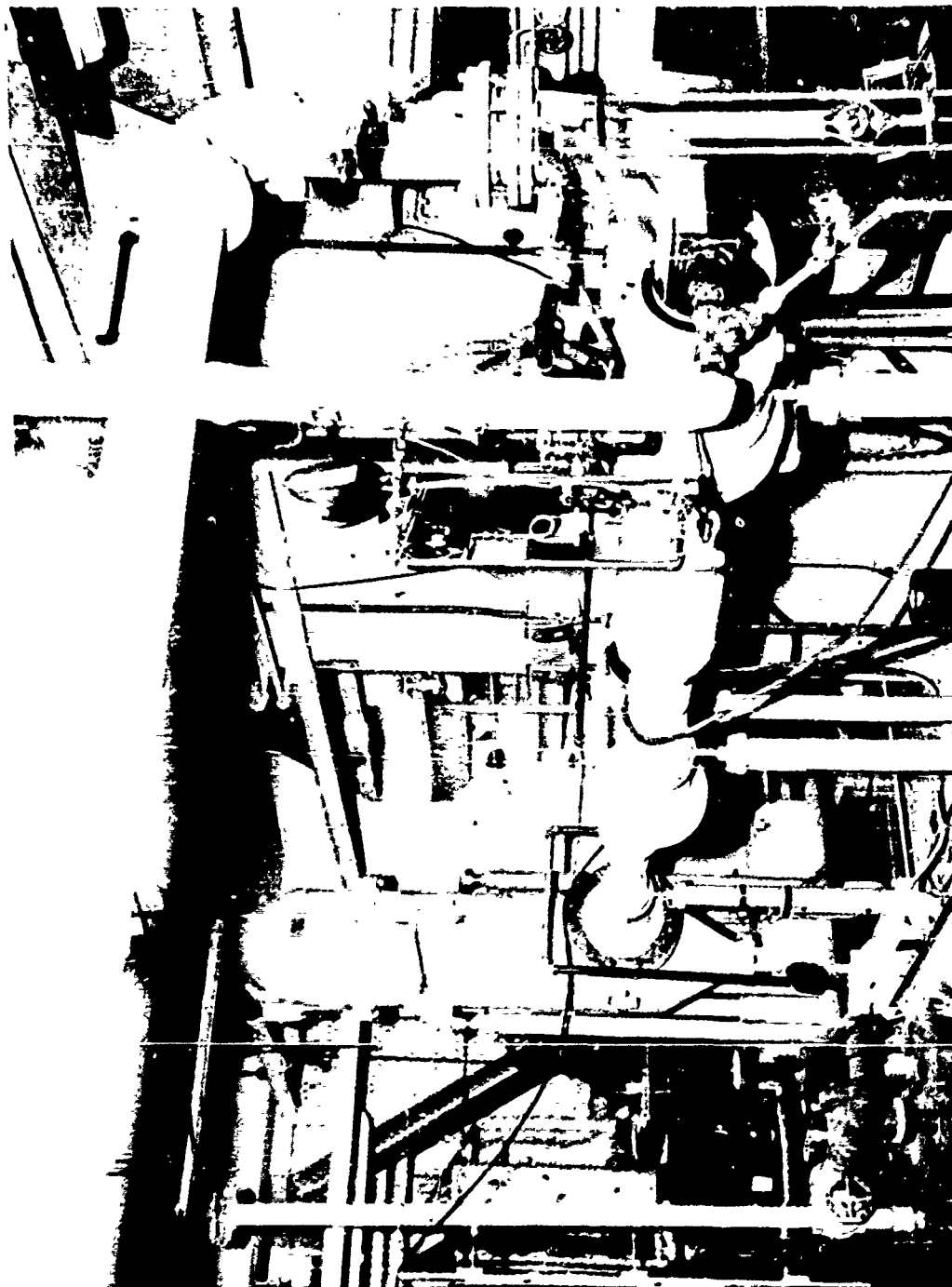
FIGURE 5. THREE STAGE STEAM EJECTOR

The system used to measure the low pressure on the high altitude side of the fabric was a composite of a mercury manometer, p_2', an oil manometer p_2'' and a McLeod Gage, p_2'''. The mercury manometer p_2' was only used at the 50,000 foot level; the oil manometer was used at the other altitudes. The oil used was a high molecular weight, low vapor pressure ester, Narcoil 40° and was selected to give greater accuracy when measuring low pressures. However, exposing one leg of the manometer to the atmosphere would have required a column more than 34 feet in length. Therefore, the oil manometer was used in conjunction with a vacuum pump, the pressure at the pump being measured by means of a calibrated McLeod gage.

The needle valve V_2 was used to control fluctuation and the high vacuum stopcocks V_3, V_4, V_5 and V_6 to regulate the initial lag in the columns and to de-gas the oil. A standard mercury barometer (not shown in Figure 3) was used to record atmospheric pressure at sea-level.

Procedure

The first step in the procedure was to mount the sample. The flange (Figure 1) was loosened and the carriage pushed back. The fabric and its backing was aligned in the jaw-plate and the jaws. were bolted tight over them. Care was taken to line up the warp and filling yarns with the sides of the jaws and keep as little slack as possible in the specimen. The test chamber was sealed up and the equipment was ready for use.

For the 50,000 foot runs, only the third stage of the ejector and the mercury manometer p_2' were used. For the other runs, all three stages of the ejector and the oil manometer system were used. The oil system merits special mention; otherwise, operation of the various stages of the ejector was the same.

The ejector was started up and allowed to come to equilibrium when dead-ended at its outlet to the permeometer. This usually took 10-15 minutes. Then the valve to the test chamber was opened very slowly, and atmospheric air was allowed to flow through the Flowmeter and the cloth. Coarse and fine control of the valves just ahead of the specimen allowed any setting of pressure drop to be maintained. At this stage valves V_r, V_1 and V_2, (Figure 3) were opened and measurements of of these three manometers, as well as the flow rate could be made. Once the pressure recording system was opened to the flow, control of these valves was no longer necessary.

---

*Narcoil 40 is highly refined di-Nonyl Phthalate supplied by the National Research Corporation, Newton Highlands, Massachusetts Density at 70° F = 0.968 gms/cc.

Before installation of the Narcoil 40 manometer in the system the oil was de-gassed for 2 weeks under a vacuum of 25 microns. The de-gassing consisted of closing stopcocks V_2 and V_3 and opening V_4, V_5 and V_6 to the vacuum pump (Figure 3). When no more bubbles came out of the oil, stop-cocks V_4 and V_5 were closed and this system was ready for use.

The 3 stages of the ejector were started up and allowed to come to equilibrium, dead-ended. The vacuum pump was started and allowed to come to equilibrium as shown on the McLeod gage. Then, valves V_3 and V_4 were opened slowly and simultaneously so that the oil columns balanced each other without being sucked out one way or the other. At this stage, the system was ready and permeability measurements could be made.

Except at the highest flow rates, it was necessary to bleed in at-mospheric air to the ejector through a needle valve at the first stage, in order to maintain a constant altitude. The setting of p_2' or p_2'' would depend on a) the barometer and b) the pressure drop across the fabric. Once the required pressure was calculated and marked off on the manometer board, fine control of the needle valve mentioned above was necessary to make up the quantity of air to fit the optimum mass flow vs. stage pres-sure relationship of the ejector. (See Appendix II) Thus at the high flow rates when the ejector could no longer 'pull' all the air being fed into it, the pressure and correspondingly the altitude would drop.

The compressor was not started until the pressure drop equalled the barometric leg. Thus both the pressure ahead and behind the fabric were sub-atmospheric up to a differential pressure of 406 in of water. At that stage the by-pass valves of the compressed air were opened until the com-pressor showed a steady output and then the air allowed to flow through the fabric.

Data and Data Processing

A run consisted of mounting the test sample, setting the "altitude" level of the test and measuring the permeability at differential pressure intervals up to 1000 in of water. In general, 3 runs were made at each altitude for the 4 fabrics S3, S6, S8 and E10. S6 and E10 being heavier fabrics, could be tested at 1000 in water pressure differential. S3 was found to break at the jaws if this differential exceeded 500 in water though it has been tested previously (7),(8) at the higher value.

The maximum "altitude" that could be reached by the equipment was 140,000 ft. However for reasons shown later the permeability was substan-tially the same as it would have been if the equipment had reached the 150,000 ft. level. The limits of "altitude" of the experiments were 49,500 $\pm$500 ft, 100,000 $\pm$1000 ft and 139,000 $\pm$ 1000 ft.

After calibration with the gasometer, the flowmeter was found to be accurate to $\pm$1%. The pressure gage at the flowmeter showed a negligible error over its whole range.

The data were calculated as shown on the sample calculation sheet, Table 1.

WADC TR 59-374

TABLE 1

SAMPLE CALCULATION SHEET

Fabric S6   Orifice Diameter 1"   Room Temperature 70°F.

Number	Item	Sample Data	Dimensions
1.	Barometric pressure, p_o	75.84	cm Hg
2.	McLeod gage, p_2'''	0.030	mm Hg
3.	Oil manometer, p_2''	11.10	cm oil
4.	Oil manometer (item 3 ÷ 1.405)	7.91	mm Hg
5.	Pressure behind fabric, p_2	7.94	mm Hg
6.	"Altitude" from graph	100,000	ft.
7.	Pressure ahead of fabric, p_1	49.04	cm Hg abs
8.	Differential pressure, $\triangle p$ (item 7 - item 5)	48.25	cm Hg
9.	Differential pressure, $\triangle p$ (item 8 x 5.34)	258	in H_2O
10.	Pressure ahead of Flowmeter P_r	29.33	in Hg abs
11.	Flow rate, w_c	17.99	lb/hr
12.	Correction factor ($\sqrt{\text{item } 10 \div 4.082'}$)	2.69	none
13.	Corrected flowrate, w_r (item 11 x item 12)	48.21	lb/hr
14.	Flow per unit area G (item 13 x 3.06)	147.5	lb/min ft^2
15.	Standard volumetric flow rate, Q (item 13 x 40.8; or item 14 ÷ 0.075)	1967	ft^3/min ft^2

Notes on Sample Calculation Sheets

The temperature of air was $70 \pm 3°$ F in all experiments because of the heat exchange system on the compressor line. Thus no temperature correction was necessary for the flow rate or for the manometric legs. The ratio of the density of mercury to that of Narcoil 40 is 14.05. Item 5 shows the calculation for the cases of the 100,000 ft and 150,000 ft runs. At the 50,000 ft level, the mercury manometer, p_2' was used. However, it was also used as a check at the former levels.

The flow rate, item 11, was calculated from the calibration curve of the Flowmeter (Appendix III). This rate, in lbs/hour of air had to be corrected to the test condition, since the Flowmeter was calibrated at pressures different from the test. This was done as follows: Let w_c, p_c, T_c be the mass flow rate, lb/hr, pressure ahead of Flowmeter and absolute temperature for the calibration conditions of the Flowmeter. Then at any other condition p_r and T_r the flow rate w_r (for the same float reading) is given by:

$$W_r = W_c \sqrt{\frac{p_r}{p_c}} \cdot \sqrt{\frac{T_c}{T_r}} \text{ lbs/hr} \tag{1}$$

The temperature ratio was equal to 1.0 in all the runs of this report. Items 14 and 15 represent the end results of the data processing. Special attention is drawn to them. Item 14 represents the mass flow rate per unit area of exposed fabric under the existing test conditions. Item 15 is the volume flow rate corresponding to item 14, assuming a standard air density of 0.075 lb/ft^3. This method of presenting the data differs from that of LaVier and Boteler (7), in that they present air permeability, - cubic feet of air per minute per square foot of fabric if the approach pressure is one atmosphere and the temperature 70°F. The reason for the change is explained in the section on Data Representation where previous work is evaluated.

For the present, it may be stated that the method used here is most convenient when dealing with compressible flow and makes no assumption as to the nature of the individual fabric pore, i.e., whether it is a nozzle or a sharp-edged orifice, etc. To convert the data of LaVier and Boteler (7) and others, a flow unit conversion coefficient for data taken at sea-level is enclosed in Part II. This conversion will only apply for 70°F air.

WADC TR 59-374

Data Representation

This section presents the experimental results of the simulated high altitude air flow studies in terms of standard volume flow rate per unit area, Q, and effective porosity, C, versus pressure drop across the fabric, $\triangle$p. As discussed previously the standard volume flow rate per unit area, Q, ft^3/min ft^2 is calculated from its definition.

$$Q = \frac{w/A}{\rho_s} \qquad (2)$$

where w, lb/min is the measured mass rate of flow through the fabric, A, ft^2, is the area of the fabric exposed to the air flow, and ρ_s is standard air density, 0.075 lb/ft^3. The effective porosity is calculated from its definition

$$C = \frac{u}{V} \qquad (3)$$

where

$$u = w/A \qquad (4)$$

and

$$V = \sqrt{\frac{2q_s \triangle p}{\rho_1}} \qquad (5)$$

Here u is assumed to represent an average air velocity through the fabric and is based on the measured mass flow rate, w, exposed fabric area, A and the actual air density ahead of the fabric, ρ_1 under test conditions. When atmospheric conditions prevail upstream of the fabric u and Q are the same. V is the velocity of an air stream of density ρ_1, which possesses a dynamic pressure equal to $\triangle$p.

La Vier and Boteler (7) (p. 13) have shown another method of calculating the data in their report. This method is based on an assumed behavior of the pores as being similar to an orifice in incompressible flow. Though not mentioned explicitly, La Vier's calculations (8) (page 19 item 28) are based on the same assumption. So are the three reports of the Fabric Research Laboratory (9) (10) (11) and a previous report of this laboratory (3). It is suggested here that this assumption is questionable. LaVier & Boteler start with the equation:

$$G = \sqrt{K \rho_1 \triangle p} \qquad (6)$$

where it is desired to express G the mass flow rate per unit area at test conditions in terms of a standard mass flow rate per area, G_s under the same conditions of pressure drop and with standard density, ρ_s ahead of the fabric A large amount of data is available (9) (10) (11) to show that the flow across a fabric is not necessarily proportional to the square root of the imposed pressure drop. Even if such a proportionality were true in incompressible flow, the use of equations (6) is unjustified when pressure drops of the order of 1500 in. of water are imposed across the fabric (8), with a downstream pressure equal to or less than atmospheric. Such conditions would lead to compressible flow within and downstream of the fabric. From equation (6) it follows that G_s can be written

$$G_s = G\sqrt{\rho_s / \rho_1} \tag{7}$$

or a standard volume flow rate per area, Q', can be defined from equation (7) as

$$Q' = G_s / \rho_s = G/\sqrt{\rho_1 \rho_s} \tag{8}$$

It is this quantity, Q', which has been reported in (7), (8), (9), (10) and (11) and not Q as defined by equation (2). It is obvious that Q and Q' are related by the simple equation

$$Q = Q'\sqrt{\rho_1 / \rho_s} \tag{9}$$

Table 2 summarizes the various forms of presenting data and factors for converting these forms to the effective porosity.

Figures 6-12 inclusive present the graphical relations between Q and Δp and c and Δp, respectively, for the test fabrics submitted by WADC.

TABLE 2

VARIOUS FORMS FOR PRESENTING AIR PERMEABILITY DATA FOR FABRICS

Reference	Method of Presenting Data	Conversion Factor To Effective Porosity, C
a. (3)(7)(8)(9)(10) (11)	Q'	Multiply by $0.00058/\sqrt{\Delta p}$
b. Present Research	Q	Multiply by $0.000159/\sqrt{\Delta p \rho_1}$
c. University of Minnesota (12)	C	--

WADC TR 59-374
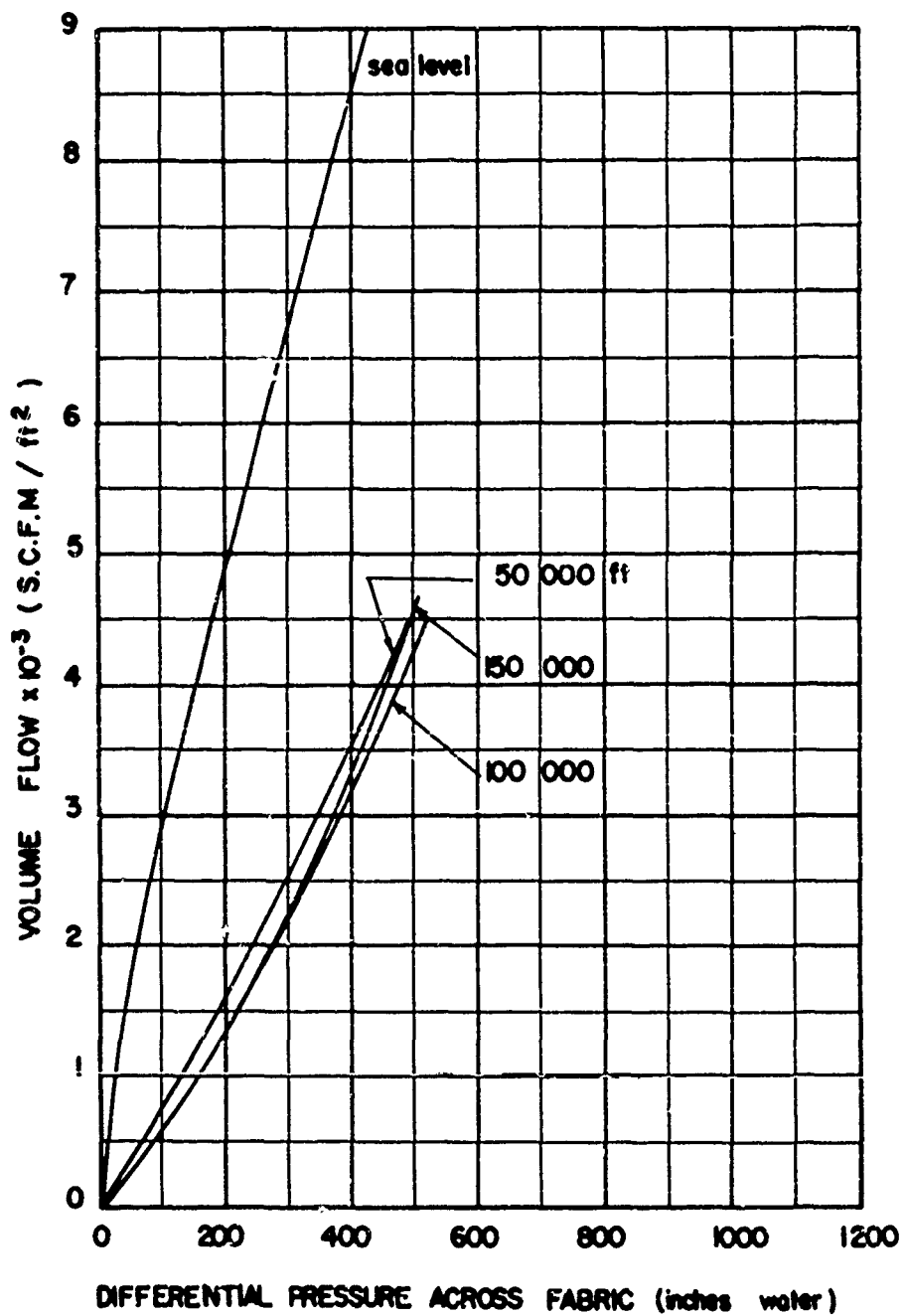
S-3 :   MIL- C - 7350 B   Type   I.

Figure 6.   Permeability of Fabric   S-3

S-6 : MIL-C - 8021 B Type II.
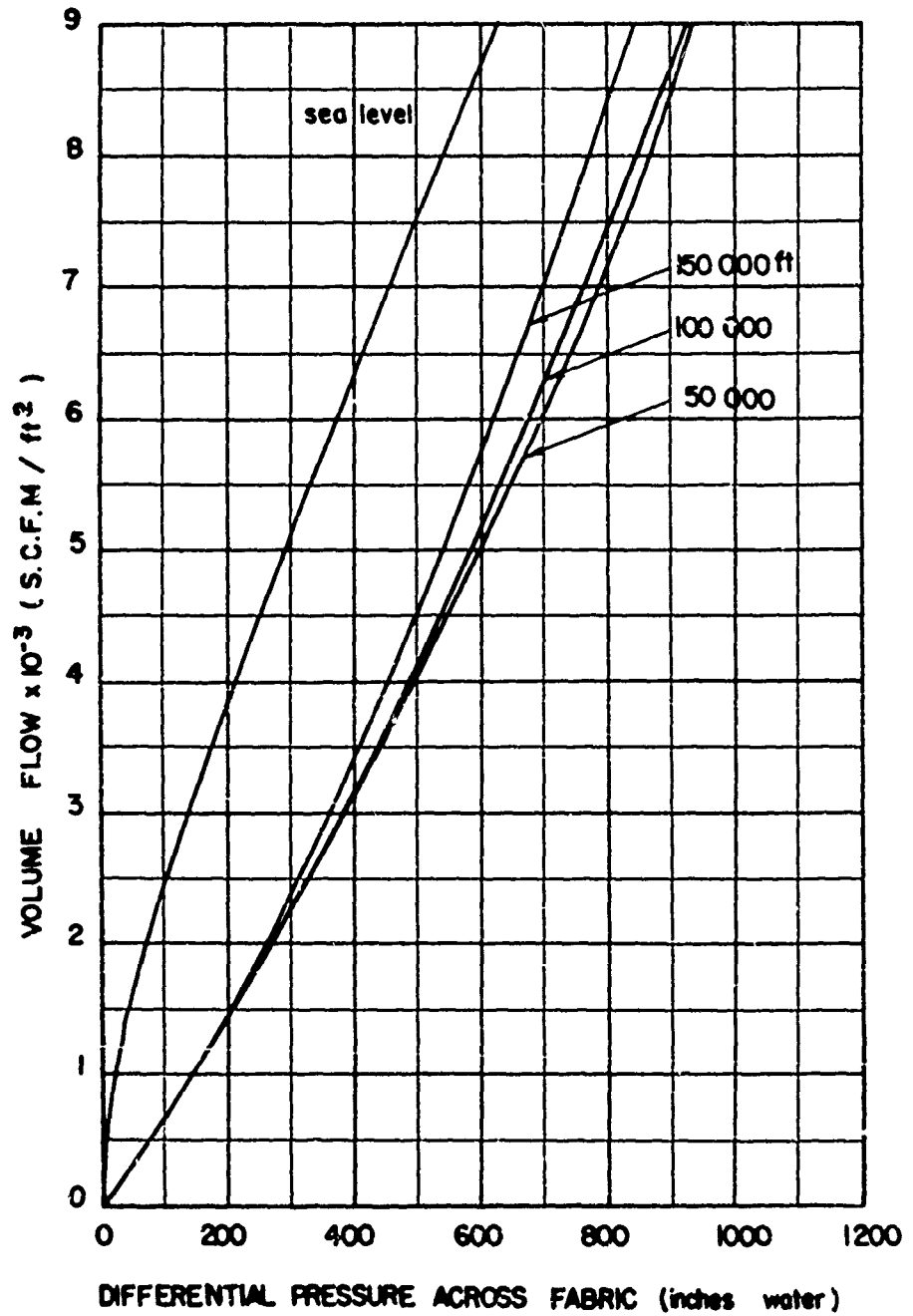
Figure 7. Permeability of Fabric S-6
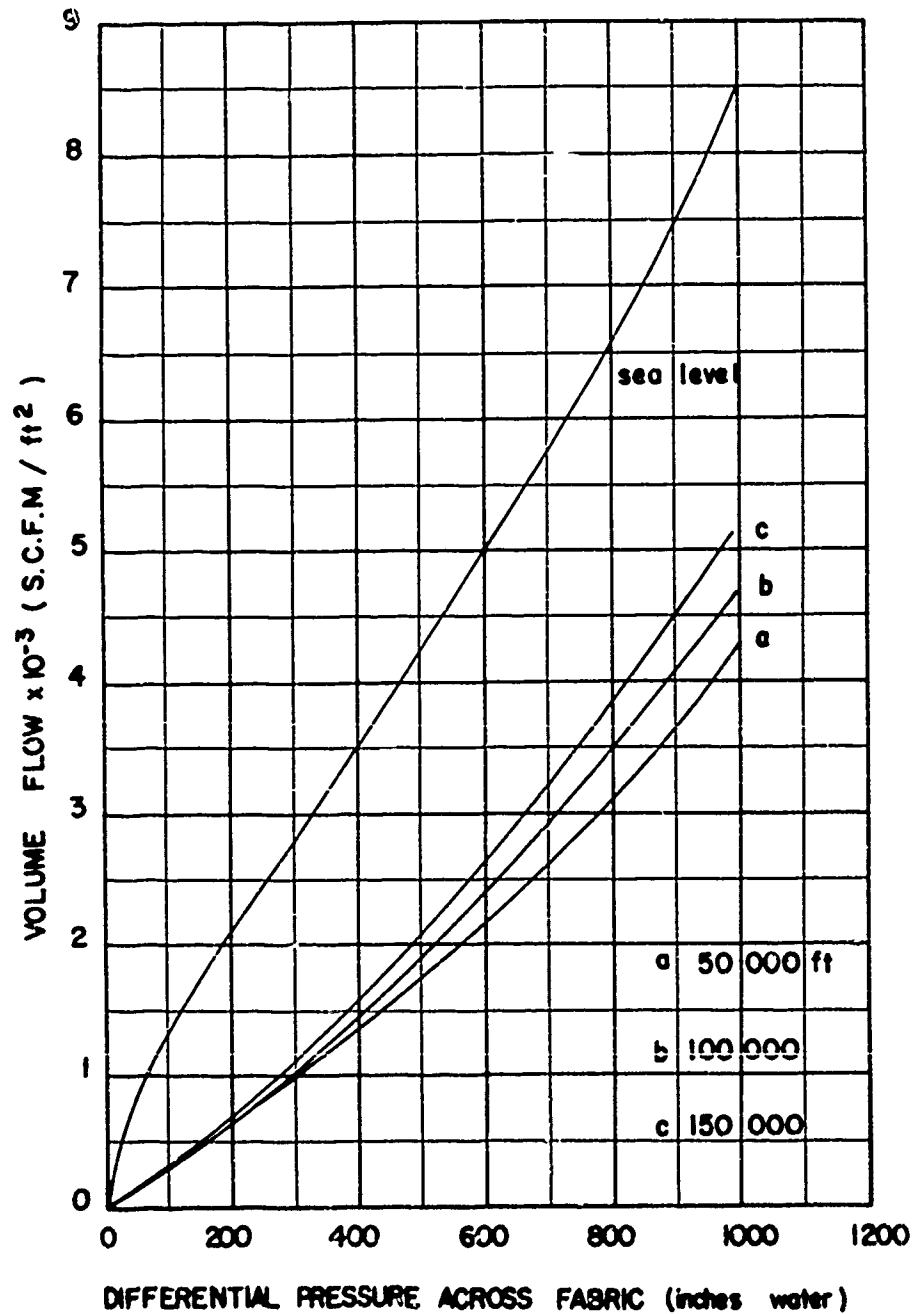
Figure 8.   Permeability of Fabric E-10
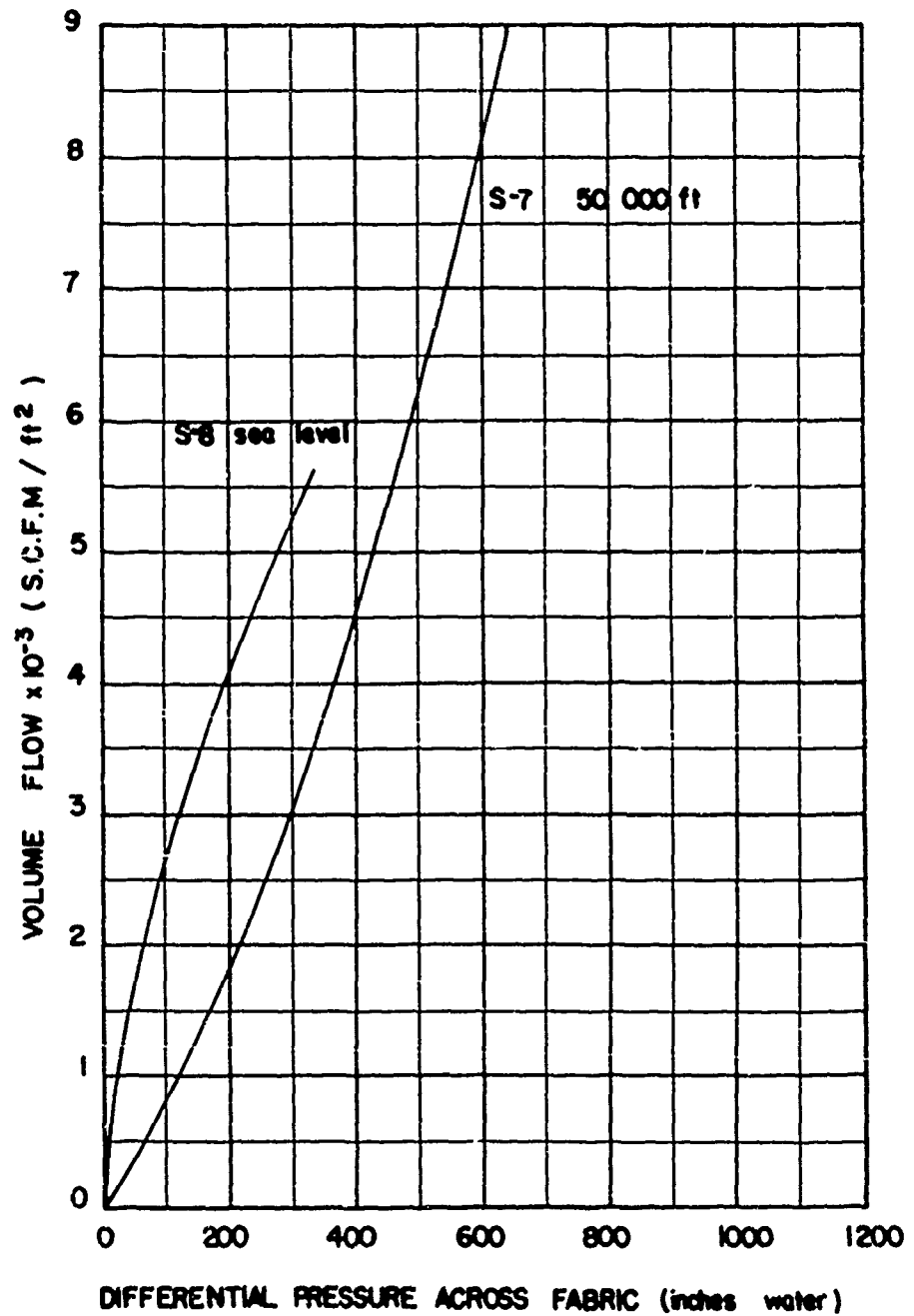
Figure 9. Permeability of Fabric S-7, S-8

S — 3 : MIL— C — 7350 B   Type I.
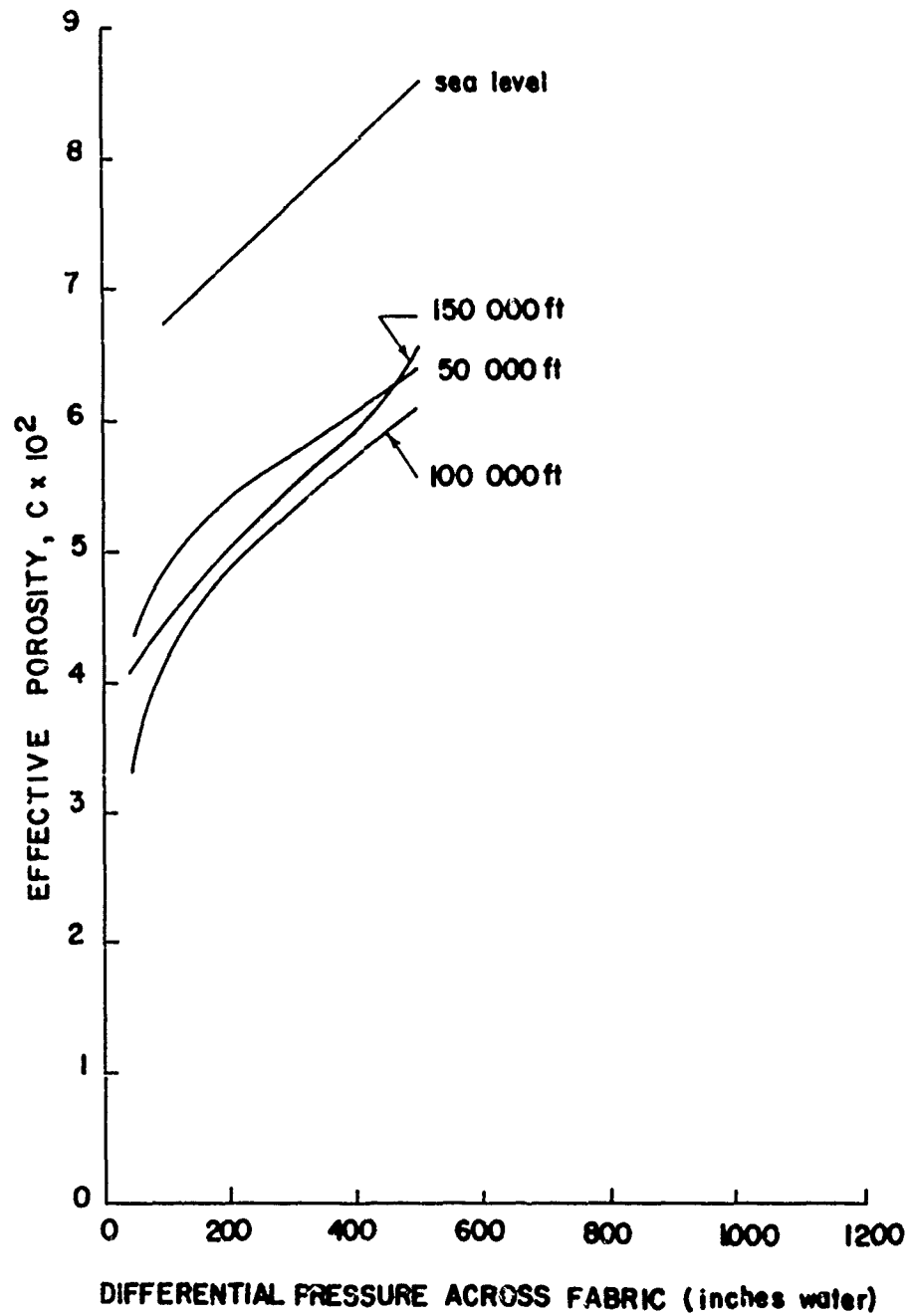
Figure 10.   Effective Porosity of Fabric S—3.

S-6 : MIL- C - 8021 B   Type II.
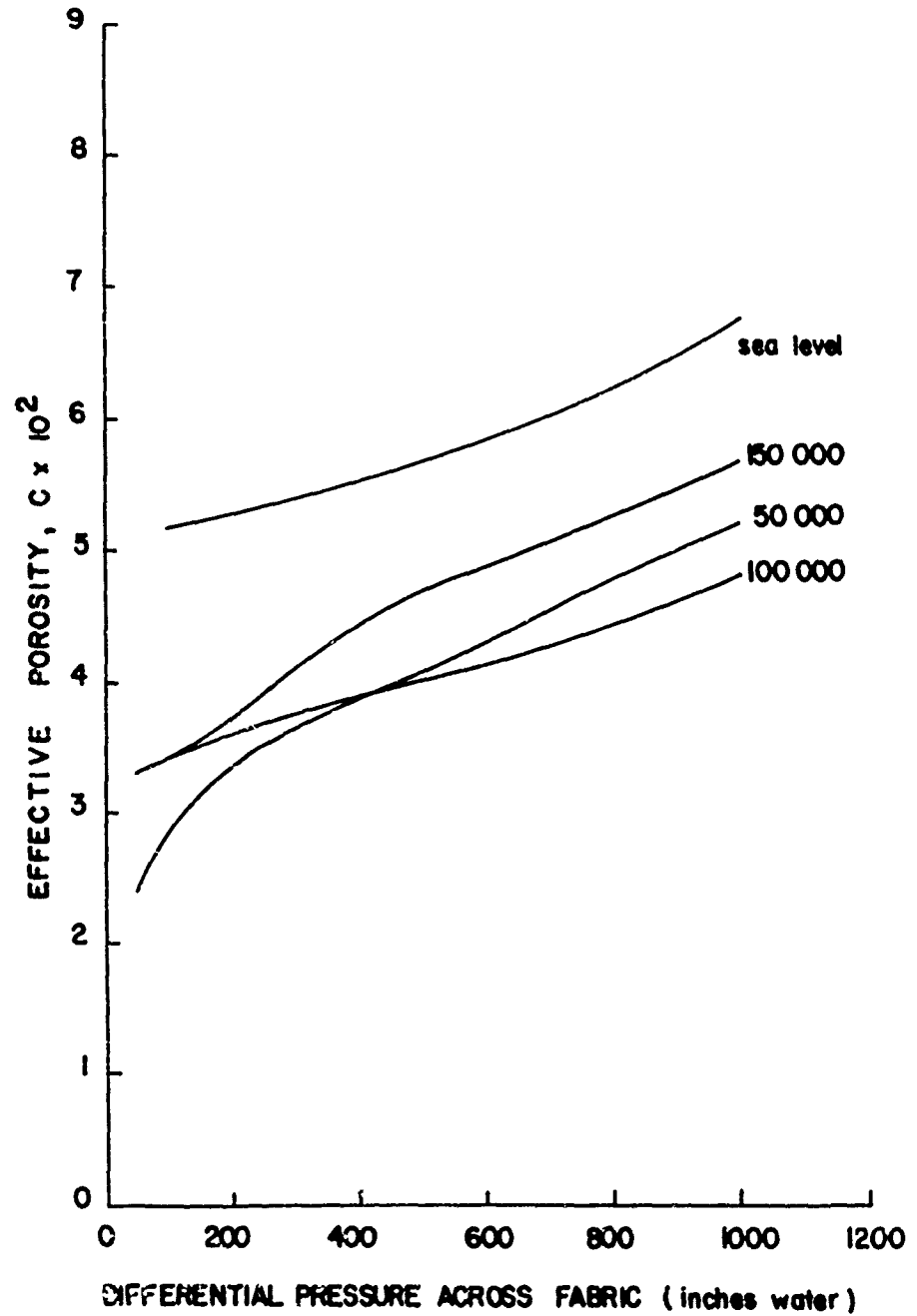
Figure 11. Effective Porosity of Fabric S-6.
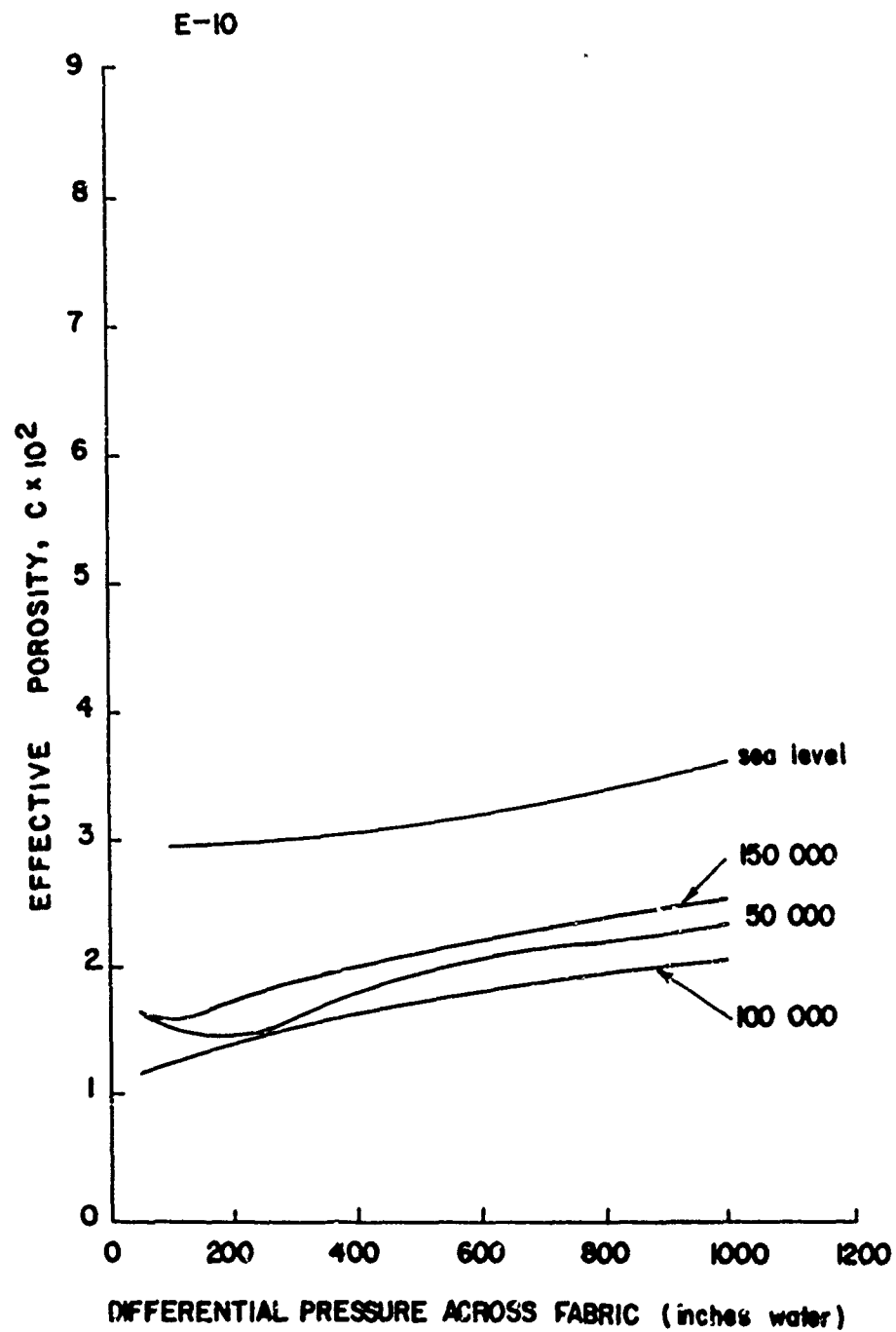
Figure 12. Effective Porosity of Fabric E-10.

Figure 6 shows the experimental data for Fabric S3. The curves
shown are for altitudes of sea level, 50,000, 100,000 and 150,000 ft.
At all altitudes the flow rate increases steadily as the pressure
drop across the fabric is increased. At a Δp of 500 inches water
and sea level conditions, the flow rate through the sample is about
10,000 SCFM/ft^2, while for altitudes between 50,000 to 150,000 ft.
the flow rate has decreased to about 4400 SCFM/ft^2. The individual
mean curves representing the flow rates at 50,000, 100,000, and 150,
000 ft are grouped about an average mean curve with $\pm$ 10% or less at
all values of Δp. At a given value of Δp, the flow rate is highest
for an altitude of 50,000 ft and lowest for an altitude of 100,000 ft.
The original data show very little scatter and the data for 100,000
and 150,000 ft are practically coincident. It will be shown later that
the curves for the three highest altitudes should be very close together,
but should also show decreasing flow rate with increasing altitude.

Figure 7 shows the experimental data for Fabric S6. At all alti-
tudes the flow rate increases with increasing Δp. At a Δp of 500
inches water and sea level conditions, the flow rate through the sample
is about 7500 SCFM/ft^2, while for the three highest altitudes the av-
erage flow rate is about 4300 SCFM/ft^2. Again, as in Fig. 6 an average
mean curve could be placed through the mean curves for 50,000, 100,000,
and 150,000 ft with a deviation of $\pm$ 10% at all values of Δp. At a
given value of Δp, the flow rate is highest for the 150,000 ft data
and lowest for the 50,000 ft data. The actual experimental data for
two samples at 50,000 ft scatter within $\pm$ 3% about the mean curve
shown in Fig. 7, while the data for two samples at 100,000 ft scatter
within $\pm$6% about the mean curve. The data for these altitudes are
practically coincident as indicated by Fig. 7 and as would be seen
from a plot of the actual data. At 150,000 ft only one sample was tested
and the data were only about 3% higher than the data from one of the
samples used at 100,000 ft. This indicates that the mean curve for
150,000 ft may have been closer to curves for 50,000 and 100,000 ft
if more samples had been used. These facts also suggest that due to
the variability of the geometric porosity of fabric samples, it is
difficult to measure accurately the influence of altitude on flow
rate once the altitude becomes sufficiently high. This is true since
the pressure ahead of the fabric is controlled by Δp and not by the
pressure behind the fabric once the altitude conditions have reduced
the pressure behind the fabric to a very low value.

Figure 8 shows the experimental data for Fabric E10. At a Δp
of 500 inches water and sea level conditions, the flow rate through
the sample is about 4250 SCFM/ft^2, while for the three highest altitudes
the average flow rate is about 1900 SCFM/ft^2. At a given value of Δp,

the flow rate is highest for the 150,000 ft data and lowest for the 50,000 ft data. It is interesting to review the actual data for each altitude. The data for the single sample tested at 50,000 ft were coincident with the data for one of the two samples tested at 100,000 ft, while the mean curves for the data of two samples at 150,000 ft was practically coincident with the data for the other sample tested at 100,000 ft. Once again, it appears that one should not take each mean curve for an individual altitude as seriously as a mean curve representing all the data for the three highest altitudes.

The flow rate data for Fabrics S3, S6 and E10 follow the expected trend of highest flow rate (at a given $\triangle$ p) for Fabric S3, and lowest flow rate for Fabric E10, since Fabric S3 has the highest geometric porosity and Fabric E10 the lowest.

Figure 9 shows the experimental data for Fabrics S7 and S8. During the early stages of this research program a fabric was received from the Textiles Branch, WADC, and labelled as S7. The samples of S7 were distributed among the various test units engaged in this research. As a result of the disagreement evidenced in the data from various test instruments a closer check of the original samples representing the S7 lot was made. It was found that different pieces contained within the lot had different fabric constructions and, in addition, the material did not conform to the material specifications for Fabric S7. Accordingly, additional material was requested. Some of this new material, which was labelled S8, arrived in time for inclusion in certain phases of the test program, but it was not possible to run the complete set of tests on Fabric S8. The experimental data for sea level tests on Fabric S8 and for tests on Fabric S7 at 50,000 ft are shown in Fig. 9. Since only these data are available for fabrics S7 and S8, the results for these fabrics will not be discussed further.

Figures 10, 11 and 12 show the experimental data for Fabrics S3, S6 and E10, respectively, in terms of effective porosity versus pressure drop across the fabric. The curves were calculated from the data of Figs. 6, 7, and 8, respectively, and the necessary values of p_1 which may be determined from $\triangle$ p, p_2 (at each altitude) and the air temperature of 70°F. For all fabrics, the values of effective porosity at sea level conditions are greater than those at the higher altitudes. In general, the variation of C with altitude (at a given $\triangle$ p) is the same as the variation of flow rate with altitude shown in Figs. 6, 7 and 8. For a given altitude, the effective porosity tends to increase with increasing $\triangle$ p. The values of effective porosity are in good agreement with values reported by Heinrich (12)

Heinrich (12) found that C decreases continuously with increase in altitude (at a given Δ p) between sea level and 60,000 ft. The variation of C with altitude shown in Figs. 10, 11 and 12 does not correspond to any regular variation with altitude. This can be explained by the fact that the measurement of changes of flow rate with altitude between sea level and 60,000 are larger and less affected by variation of sample geometric porosity than between 50,000 and 150,000 ft.

An actual comparison of geometric porosities from this report and Heinrich (12) can be made in the case of Fabric S6. At sea level conditions and a Δp of about 30 inches water, Heinrich reports a value of C of about 0.039 while Fig. 11 shows a value of C of about 0.05 at a Δ p of 50 inches water and sea level conditions. At 60,000 ft and an Δp of about 6 inches water, Heinrich reports a value of C of about 0.029 while Fig. 11 shows a value of about 0.030 at about 50 inches water and the high altitudes.

Analysis of Flow Through Fabrics at High Altitudes

It would be very useful to be able to predict the mass flow rate of air through a fabric for a given pressure ratio or difference across the fabric, and for various pressures behind the fabric which simulate the use of the fabric at various altitudes. An estimate of this flow rate could probably be made using the usual nozzle and orifice flow equations if the actual flow area of the fabric could be predicted. However, this flow area is a rather complex function of the pressure difference across the fabric, temperature of the fabric, loading rate on the fabric, etc., and, therefore, accurate predictions are difficult to make.

The next best situation is one in which the large amount of flow rate-pressure drop data which has been taken with sea-level pressure behind the fabric can be used to predict results for higher altitudes. If these sea-level data are to be used in such a fashion then a suitable theoretical model must be found to describe the flow through the fabric. Since the pressure ratios across the fabric will be very large at high altitudes, such a theoretical model must necessarily involve certain aspects of compressible fluid mechanics.

This section describes a possible theoretical model based on the assumption that the characteristics of the flow through the fabric are similar to those of isentropic flow of air, through a nozzle. Certain characteristics of the nozzle flow are reviewed, and the necessary restriction which must be made for using these characteristics for the fabric flow are discussed. Finally, a method is described for predicting the flow-rate-pressure drop characteristics of a fabric used

WADC 59-374

at a high altitude from similar data taken with sea-level pressure behind the fabric.

Isentropic Nozzle Flow

Figure 13 shows a simple converging nozzle into which air flows at a stagnation state 1 where the velocity v_1, is practically zero and the stagnation pressure and temperature are p_1 and T_1, respectively. The air passes through the nozzle, leaves the nozzle at the exit section e and enters a region where the pressure p_2 is either equal to or less than the static pressure at section e, namely p_e. (The pressure p_2 would correspond to the pressure maintained behind a fabric to simulate a particular altitude). For purposes of analyzing the results of this research program, it is necessary to derive an expression for the mass flow rate per unit area at section e. The following assumptions will be made concerning the flow through the nozzle.

1. The flow is steady.
2. The flow is one-dimensional, i.e., at a given section in the nozzle the state of the air can be adequately described by a single value for the velocity, temperature, etc.
3. The flow is adiabatic or there is no heat transfer between the air in the nozzle and the surroundings.
4. The flow is frictionless. Any frictional or viscous effects due to the wall are confined to the thin boundary layer near the wall. From assumptions 3 and 4 it follows that the flow is isentropic.
5. Air is a perfect gas with an equation of state given by (Eq.12) and constant values of the specific heats at constant pressure and constant volume.

The analysis is as follows:

Conservation of Mass-Continuity Equation

$$w = \rho_e A_e v_e \tag{10}$$

First Law of Thermodynamics-Steady Flow Energy Equation and perfect Gas Assumption.

$$v_e^2 = 2g_o J c_p (T_1 - T_e) \tag{11}$$

Perfect Gass Assumption

$$P_e = \rho_e R T_e \tag{12}$$
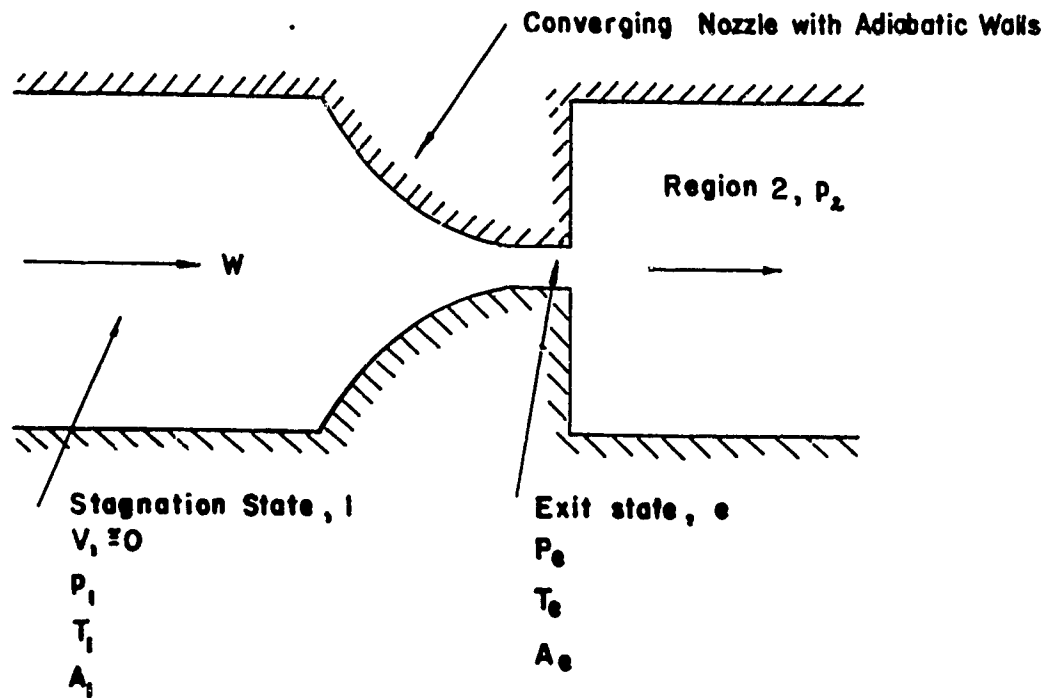
Figure 13.   Flow Through a Converging   Nozzle

Second Law of Thermodynamics and Perfect Gas Assumption

$$\frac{P_1}{P_e} = \left(\frac{\rho_1}{\rho_e}\right)^{k} \tag{13}$$

Combining Equations 10, 11, 12 and 13 yields the following Equation for the mass flow rate per unit area.

$$\left(\frac{W}{A_e}\right) = \frac{P_1}{\sqrt{T_1}} \sqrt{\frac{2g_e}{R}\frac{k}{(k-1)}} \left(\frac{P_e}{P_1}\right)^{\frac{1}{k}} \sqrt{1-\left(\frac{P_e}{P_1}\right)^{\frac{k-1}{k}}} \tag{14}$$

Before applying equation 14 over the pressure ratio, p_e/p_1 range from one to zero, it is necessary to consider the compressible flow aspects of the nozzle operation. Consider a case where the nozzle inlet conditions are held constant at

$$P_1 = 759'' \; H_2O \; abs.$$
$$T_1 = 530° \; R \; abs.$$

and the back pressure p_2 is varied as follows: For values of p_2 close to p_1 a certain flow rate and velocity will be established at e and the flow at e will be subsonic, i.e., v_e will be much lower than the velocity of sound, a at section e. This is equivalent to a Mach number at e, M_e of practically zero since

$$M_e \equiv \frac{v_e}{a_e} \tag{15}$$

The stream lines at e will be almost straight as the air jet enters region 2 and, consequently, p_e and p_2 will be equal. Since p_1, p_e and p_2 are only slightly different the flow will be almost incompressible and under the assumptions made Bernoulli's equation should be valid, or

$$\frac{W}{A_e} = \sqrt{2g_e \rho (P_1-P_e)} = \frac{\rho_1}{\sqrt{T_1}} \sqrt{\frac{2g_e}{R}} \sqrt{1-\frac{P_e}{P_1}} \tag{16}$$

The assumption of incompressible flow is usually made for Mach numbers up to about 0.2. For $M_e = 0.20$, the value of p_e/p_1 is 0.973 and if this value is used in Equations 14 and 16 it is found that the mass flows per unit area for these equations differ by about 1.5 percent. At $p_e/p_1 = 0.70$ (corresponding to $M_e = 0.73$) the two equations give values which differ by about 22 percent. Actually the use of Equation 14 is equivalent to using the expansion factor in the usual nozzle or orifice equation. As p_2 is lowered, both v_e and M_e increase until

the air leaves section e at the velocity of sound (or $M_e = 1.0$).
The value of p_e/p_1 at which this occurs is called the critical
pressure ratio p_e^*/p_1, and it can be shown to be

$$\frac{p_e^*}{p_1} = \left(\frac{2}{k+1}\right)^{\frac{k}{k-1}} \qquad (17)$$

For air $k = 1.4$ and

$$\frac{p_e^*}{p_1} = 0.528 \qquad (18)$$

Up to this value of p_2, the values of p_e and p_2 are still the same
since the jet has straight streamlines and is subsonic. Also, w/A_e
shown in Fig. 14, and at the critical pressure ratio, for the case
selected, w/A_e, is about 5540 lbm/min-ft^2. Now if p_2 is reduced beyond
405 inch H_2O abs. (corresponding to p_e^*/p_1, the values of M_e, p_e, and
w/A_e will not change, and the nozzle is said to be "choked".^{e} The sim-
ple explanation for this phenomenon is that since the air at e is
travelling at the velocity of sound, any change of p_2 cannot influence
the flow in the nozzle since the pressure pulse which results when
p_2 is changed also travels at the velocity of sound and, therefore,
cannot be propagated up-stream into the nozzle. Thus, for values
of p_2/p_1 less than the critical pressure ratio, w/A_e, M_e, p_e/p, re-
main constant. The difference between p_e and p_2 take place by a
modification of the flow pattern outside the nozzle in region 2.
For values of p_2/p_1 equal to or less than the critical pressure ratio,
the mass flow per unit area is fixed from Equation 14 by inserting
the critical pressure ratio. For this case, Equation 14 becomes

$$\left(\frac{w}{A_e}\right)^* = \frac{p}{\sqrt{T_1}} \sqrt{\frac{2g_o}{R}\frac{k}{k-1}} \cdot \sqrt{2^{\frac{2}{k-1}}(k-1)\left(\frac{1}{k+1}\right)^{\frac{k+1}{k-1}}} \qquad (19)$$

The equation has been left in this form since it will be used later
to predict mass flow per unit area for fabrics at high altitude from
similar sea-level data, although Equation 19 can be simplified to

$$\left(\frac{w}{A_e}\right)^* = \frac{p}{\sqrt{T_1}} \sqrt{\frac{g_o k}{R}\left(\frac{2}{k+1}\right)^{\frac{k+1}{k-1}}} \qquad (20)$$

The operating characteristics of the nozzle are summarized in
Table 3 for the two ranges of p_2/p_1. The results are given for $k = 1.4$,

WADC TR 59-374

Figure 14.   Flow Characteristics of a Converging Nozzle
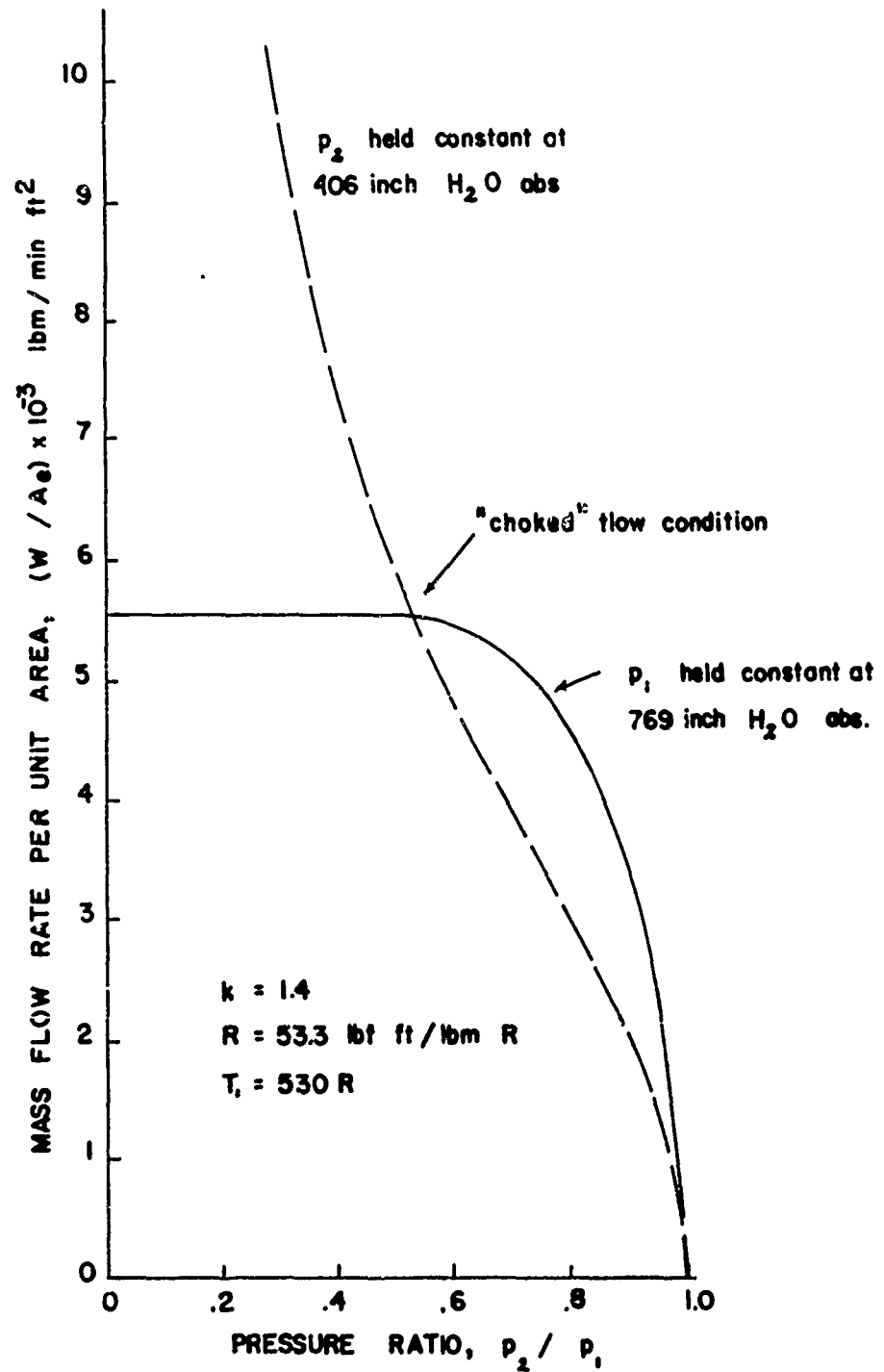
TABLE 3

OPERATING CHARACTERISTICS OF CONVERGING NOZZLE

p_2/p_1	> 0.528	< 0.528
p_e/p_2	= 1	> 1
M_e	< 1	1
w/A_e	Equation 14	Equation 19 or 20

It is worthwhile to mention another means of operating the nozzle which corresponds to the usual method whereby data on the mass flow per unit through a fabric are obtained. In this case, the back pressure p_2 is held constant and the inlet pressure p_1 is increased in order to reduce the pressure ratio, p_2/p_1. As in the previous case w/A_e, M_e, v_e increase as p_2/p_1 is reduced, while p_e remains equal to p_2. When the critical pressure ratio is reached and further reductions in p_2/p_1 are made, M_e and p_e/p_1 remain constant at 1.0 and 0.528 respectively while w/A_e and p_e continue to increase. The increase in w/A_e and p_e arise from the fact that p_1 is being increased with p_2 held constant, whereas in the former case p_1 was held constant as p_2 was decreased. The mass flow per unit area curve for a case in which:

$$p_2 = 406'' \; H_2O \; abs.$$

$$T_1 = 530^\circ \; R$$

is also shown in Fig. 14. The point where the curves cross is arbitrary and can be adjusted by selecting new values of p_2 and p_1 for the two cases.

Since most data on fabrics are presented in terms of flow per unit area versus pressure drop across the fabric, rather than pressure ratio across the fabric, the curves of Fig. 14 are replotted in Fig. 15 versus pressure difference, Δp. The curve for the case where p_1 is held constant at 769 inch H_2O abs., does not extend beyond a pressure drop of 769 inch H_2O abs., since p_2 goes to zero at this point. The only major difference between the curves of Figs. 14 and 15 occurs for the case where $p_2 = 406$ inch H_2O abs. Beyond the critical pressure ratio in Fig. 14, the mass flow per unit area increases hyperbolically with p_2/p_1 whereas in Fig. 15 w/A_e increases linearly with the pressure difference after the
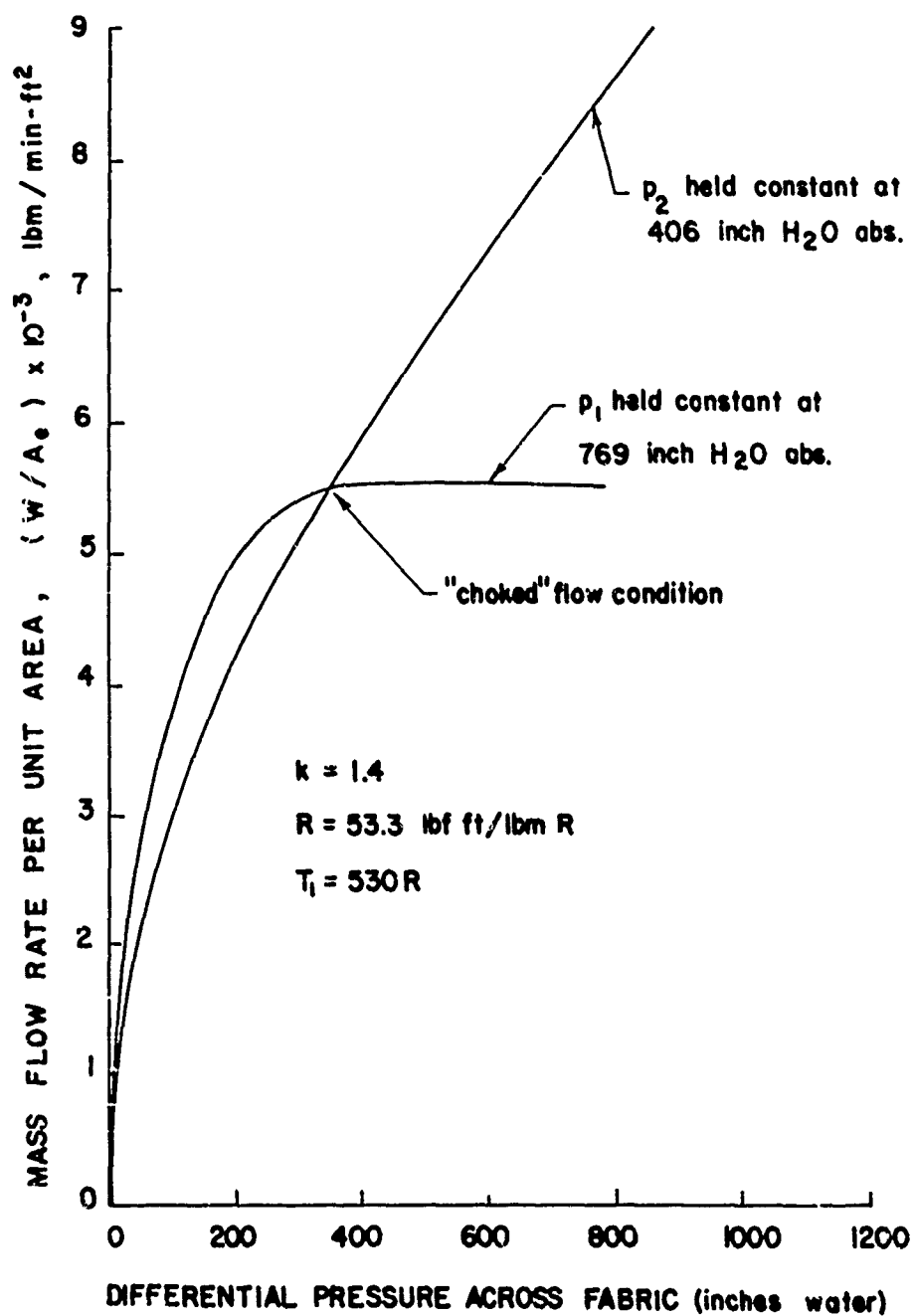
Figure 15. Flow Characteristics of a Converging Nozzle

pressure difference corresponding to the critical pressure ratio has been exceeded.

Finally, Fig. 16 shows w/A_e vs. pressure difference for a nozzle which is operated with various constant values of p_2. The uppermost curve for $p_2 = 760$ mm Hg. abs. (sea-level) pressure is the same curve as shown in Fig. 15. The mass flow per unit area increases as the pressure difference is increased or the pressure ratio is decreased, according to Equation 14. At a pressure difference of 363 inch H_2O, the critical pressure ratio is reached and the flow becomes choked. Beyond a pressure difference of 363" H_2O the flow remains choked and the mass flow per unit area increases linearly with pressure difference. Curves are also shown for values of p_2 of 100, 76 and 7.6 mm Hg. abs. These values of p correspond to altitudes of about 50,000, 100,000 and 150,000 ft. respectively. The curve for p_2 of 7.6 mm Hg. abs. represents to a very small error all values of p_2 less than 7.6 mm Hg. abs. The locus of points which represent the choked condition is also shown and is a straight line since Equation 20 can be written in terms of the pressure difference as follows:

$$\frac{W}{A} * = K_2 (p_1 - p_2) + K_3 p_2 \qquad (21)$$

where K_2 is a constant. The most striking feature of this locus is that for any value of p_2 less than 100 mm Hg. abs. any pressure difference greater than 50 inch H_2O will cause the nozzle (or fabric) to operate under choked flow conditions. The relatively close spacing of the curves for values of p_2 of 100 mm Hg and less indicates that extremely accurate flow measurements would be required in order to define curves of different p_2. As mentioned earlier, the variation of the geometric porosity of a fabric could lead to changes in the locations of these curves even when accurate flow measurements are made. It is also of interest to note the curves of Fig. 16 for p_2 lower than 100 mm Hg. abs. are grouped together within about ± 3 percent. This close spacing of curves for the fabrics at 50,000, 100,000 and 150,000 feet can also be seen in Figs. 6, 7 and 8.

Nozzle Flow Analogy for Flow Through Fabrics

In order to apply the results of the preceding section to predict the mass flow per unit area for a fabric used at a high altitude from the similar data taken at sea-level conditions, it is necessary to form a theoretical model of the flow through a fabric. Fig. 17 shows the model for the flow through the fabric. The sketch is intended to indicate also the apparatus which is used to
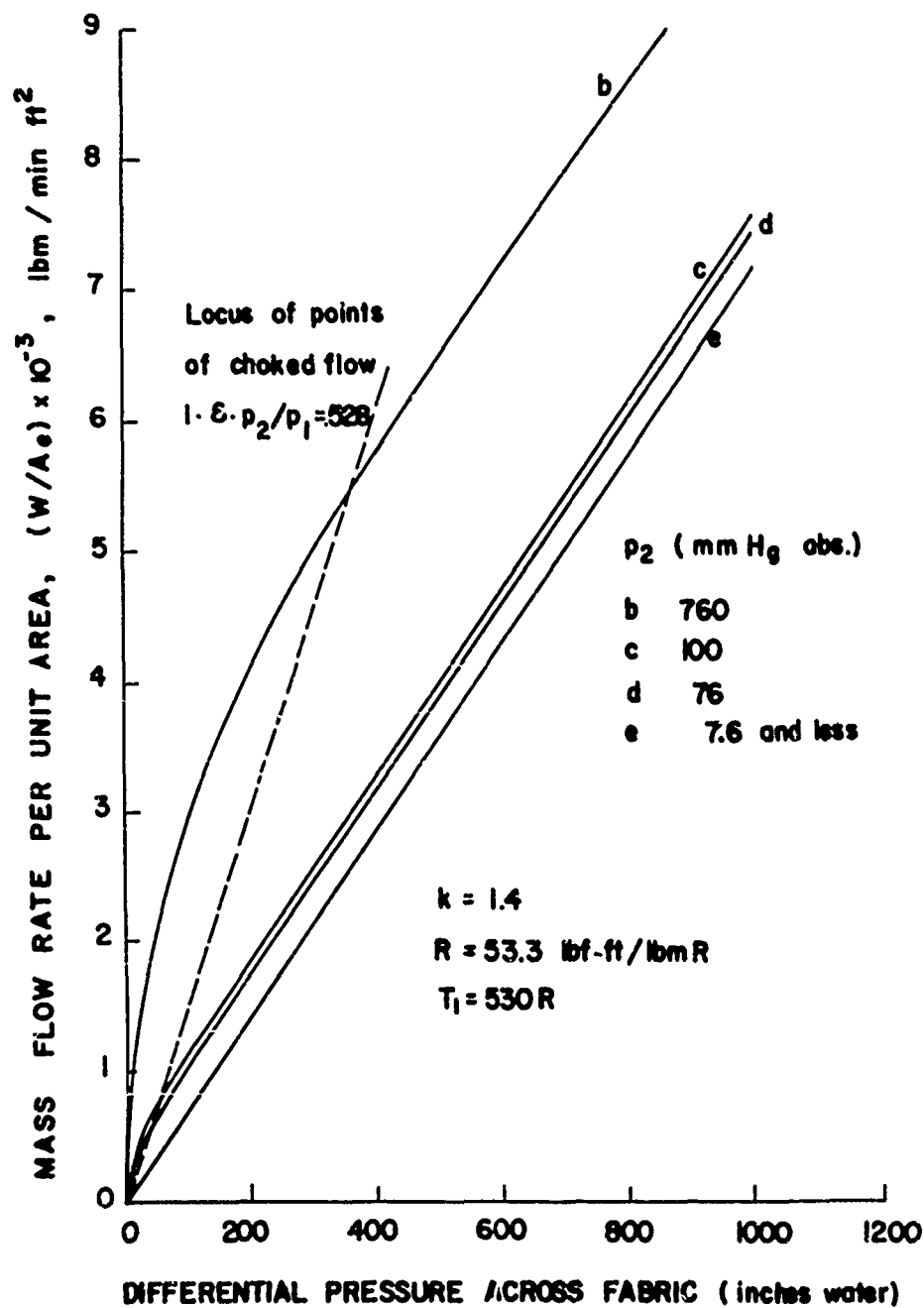
Figure 16. Effect of Altitude on Flow Charecteristics of Converging Nozzle.

WADC TR 59-374

36
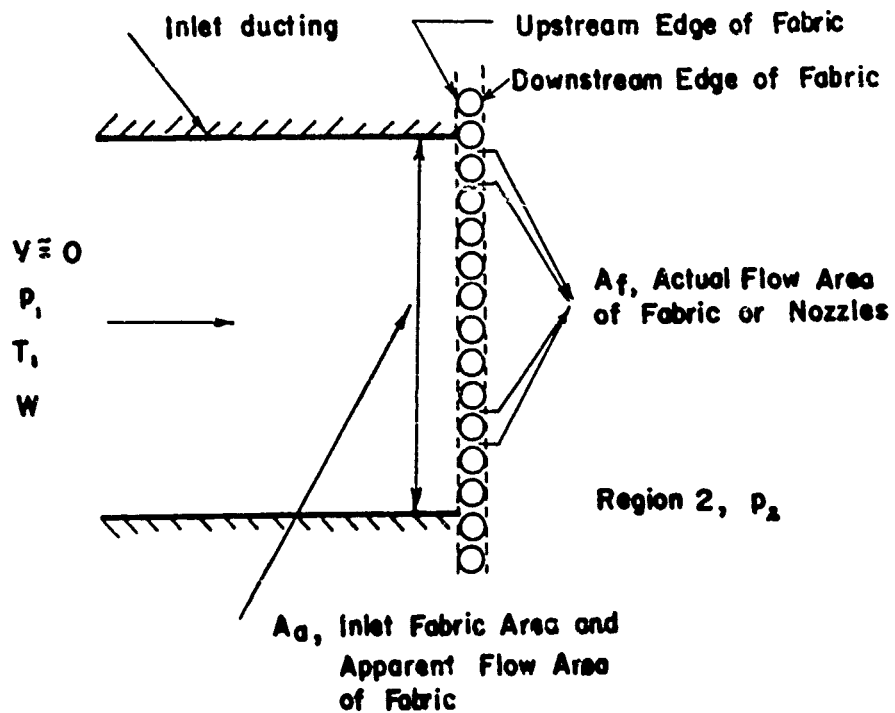
Figure 17. Nozzle Flow Analogy for Flow Through
a Fabric

measure the flow rate through the fabric. The air approaches a
sample of the fabric through the inlet ducting at the inlet state 1.
A certain area of the fabric is exposed to the flow and this is the
apparent area of the fabric through which the flow passes, A_a. The
passages through the fabric are assumed to have flow characteristics
similar to isentropic nozzle flow characteristics. The flow exhausts
from the downstream edge of the fabric into a region maintained at
a pressure p_2. The downstream edge of the fabric corresponds to the
exit area of the nozzle in the preceding section. Physically, the
actual exit area of the passages through the fabric will be some-
where back inside the fabric. Also, the passages do not have the
area A_a available for flow but some actual flow area, A_f. For
fabrics the percent free flow area, A_f/A_a, or geometric porosity is
between 5 and 15 percent.

The assumption of isentropic flow through the fabric may seem
to be a poor one since the passages are very small. However, a
calculation of a Reynolds number based on passage diameter of 0.010
inches will show that at the choked flow condition and an inlet
pressure of 50 inch H_2O abs, and an inlet temperature of $530^\circ F$ abs.
The Reynolds number is about 450. Although this is not a high
Reynolds number, it is not of such magnitude that one would expect
large viscous flow effects in view of the fact that the passages
are very short. This Reynolds number would increase linearly with
the inlet pressure so that at an inlet pressure of 500 in. H_2O abs,
the Reynolds number would be 4500. This assumption of isentropic
flow in the fabric should not be interpreted as meaning that there
is no pressure loss for the flow through the entire fabric. This
is obviously not true since the air jets mix upon leaving the fa-
bric with a resulting loss in stagnation pressure. The assumption
of isentropic flow simply means that the loss of stagnation pres-
sure for the flow inside the fabric is assumed to be small.

Consider the situation where data on the flow rate per unit
area for a fabric have been obtained with a high pressure behind
the fabric and it is now desired to predict the flow rate per
unit area when this pressure is reduced to simulate operation at
a higher altitude. Before describing a method in detail whereby
these predictions can be made some restrictions will be discussed
which must be observed for the flow through the fabric which do
not apply to the nozzle. When the nozzle equations are used for
the fabric, the exit area of the nozzle, A_e should be replaced by
the actual flow area of the fabric A_f. However, since A_f is un-
known the experimental results are usually based on the apparent
area of the fabric, A_a. The use of this apparent area

will cause the usual shapes of the flow per unit area curves for nozzle flow to be modified in the case of fabrics. However, it is possible to predict these modifications in advance.

First, consider where the flow through the fabric should be choked if there is a valid analogy between nozzle flow and fabric flow. If p_2 is fixed by altitude conditions then there is a critical value of the pressure difference for which the flow through the fabric should become choked. Let this critical pressure difference be Δp *. The value Δp * can be found from the identity

$$\Delta p^* = p_1 \frac{\left(1 - \frac{p_2^*}{p_1}\right)}{\left(\frac{p_2^*}{p_1}\right)}$$

(22)

For air (k = 1.4), the critical pressure ratio, p_2^*/p_1, is 0.528. Substituting this value in Equation (22) yields

$$\Delta p^* = 0.895 \, p_2$$

(23)

Table 4 shows values of Δp^* as a function of altitude.

TABLE 4

VARIATION OF CRITICAL PRESSURE DIFFERENCE WITH ALTITUDE

Altitude (feet)	Critical Pressure Difference (inches H_2O)
Sea-level	363
50,000	41.5
100,000	3.84
150,000	0.516

For a choked nozzle, the quantity $w\sqrt{T_1}/A_e p_1$ will become constant at a value fixed by Equation (20). For air (k = 1.4, R = 53.3, ft-lbf/lbm-R, g_o = 32.174 lbm ft/lbf sec^2) Equation (20) yields

$$w\sqrt{T_1}/A_e p_1 = 0.532 \; \text{lbm-R}^{1/2}/\text{sec lbf}$$

(24)

WADC TR 59-374

If T_1 is fixed at 70°F, as in these experiments, then Equation (24) becomes

$$W/A_n p_1 = 38.6 \; lbm/min \; ft^2 \; cm \; Hg \; abs. \tag{25}$$

For the nozzle, if $W/A_n p_1$ is plotted against Δp, the points for all values of p_2 (or altitude) and for all values of Δp, greater than Δp^* should fall on a single horizontal line having a value of 38.6 lbm/min ft^2 cm Hg abs. If the analogy between choked nozzle flow and choked fabric flow is true, then a plot of $W/A_f p_1$ versus Δp should be identical with the plot for the nozzle. However, a plot of $W/A_a p_1$ versus Δp will show a different shaped curve than those just mentioned. It is possible to predict the shape of the $W/A_a p_1$ vs Δp curve if a few simplifying assumptions are made concerning the behavior of A_f during testing.

In general, A_f will depend on

1. The pressure difference across the fabric.

2. The temperature of the fabric.

3. The rate at which the pressure difference is applied across the fabric.

4. The loading cycle.

For the usual experimental methods the temperature of the fabric does not vary significantly and the loading cycle is usually a simple one in which the pressure difference is increased slowly from one value to another. Thus, it is reasonable to assume that for this type of experiment

$$A_f = f\left(p_1 - p_2\right) = f\left(\Delta p\right) \tag{26}$$

and that A_f will increase as Δp is increased. For a "stiff" fabric increases in A_f/A_a with increases in Δp will be small, while for a 'soft' fabric increases in A_f/A_a with increases in Δp may be large.

The following identity may be written

$$\frac{W}{A_a p_1} = \frac{W}{A_f p_1} \cdot \frac{A_f}{A_a} \tag{27}$$

The quantity $(W/A_f p_1)$ should have a constant value independent of Δp, while the geometric porosity, A_f/A_a, should be less than

WADC TR 59-374

unity (perhaps in the range from 0.01 to 0.20) and increase with increases in Δp. Since $w/A\,p_1$ is independent of Δp and p_2 and since under the simple assumption of Equation (24), A_f/A_a is independent of p_2, it should follow that $w/A\,p_1$ should be independent of p_2 and dependent on only Δp. Therefore, a plot of the data for all altitudes and for all Δp's greater than Δp^* in the form of $w/A_a p_1$ versus Δp, should show a single curve which increases as Δp increases. The values of $w/A\,p_1$ should be less than 38.6 lbm/min ft^2 Hg. abs. and dependent on the geometric porosity of the fabric.

In order to test this prediction, the actual experimental data for Fabrics S3, S5, and E10 have been plotted in the above form and are shown in Figures 18, 19, and 20 respectively. The quantity $w/A_a p_1$ will be called the choked flow coefficient. For Fabric S3 (Fig. 18) this coefficient has an average value of 2.50 $\pm 10\%$ at a Δp of 50 inches H_2O and at a Δp of 500 inches H_2O., the value has increased to $4.62 \pm 5\%$. For Fabric S5, the coefficient is $2.39 \pm 20\%$ at 100 inches H_2O, and increases to $4.05 \pm 11\%$ at 1000 inches H_2O. For Fabric E10, the coefficient is $1.1 \pm 20\%$ at 150 inches H_2O, and increases to $1.95 \pm 10\%$ at 1000 inches H_2O. As predicted earlier, Figs. 18, 19 and 20 show values of the choked flow coefficient which are less than 38.6 lbm/min ft^2 cm Hg abs. and values which increase as Δp increases. However, the maximum and minimum values of the choked flow coefficient, which vary $\pm 20\%$ about the mean, must be viewed somewhat critically in terms of supporting or disclaiming the nozzle flow analogy for fabric flow. A close inspection of the data for a single fabric sample taken at a single altitude will reveal that there is very little experimental scatter. The data form a single rather smooth curve. The spread of the data for various samples seems to be more a function of the sample than the altitude. This is very important because the entire choked nozzle flow analogy leads to the conclusion that the entire choked flow coefficient should depend on Δp and be independent of p_2 (or altitude). Further inspection of Figs. 18, 19 and 20 will show that the data for one sample at 100,000 feet will coincide with the data for another sample at 50,000 feet, while data from another sample at 100,000 feet will coincide with data from another sample at 150,000 feet. This point was mentioned earlier in the discussion of Figs. 6, 7, and 8. Based on these observations, it would appear that the prediction that all the choked flow coefficient data should fall on a single curve is not wrong because the nozzle flow analogy is incorrect but more likely because of variation in the geometric porosity of the fabric samples. Variations of geometric porosity between fabric
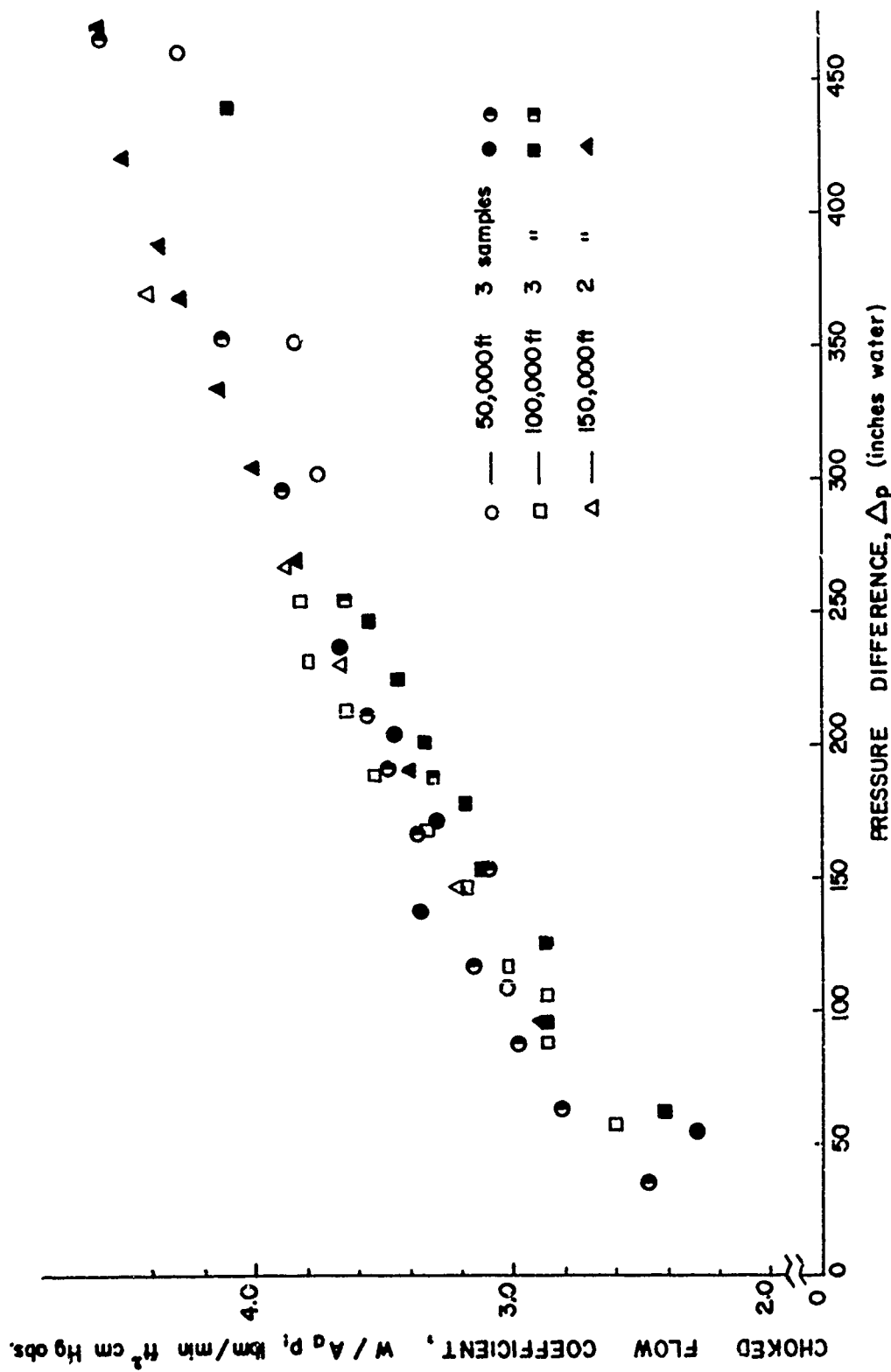
Figure 18. Choked Flow Coefficient for Fabric. S-3
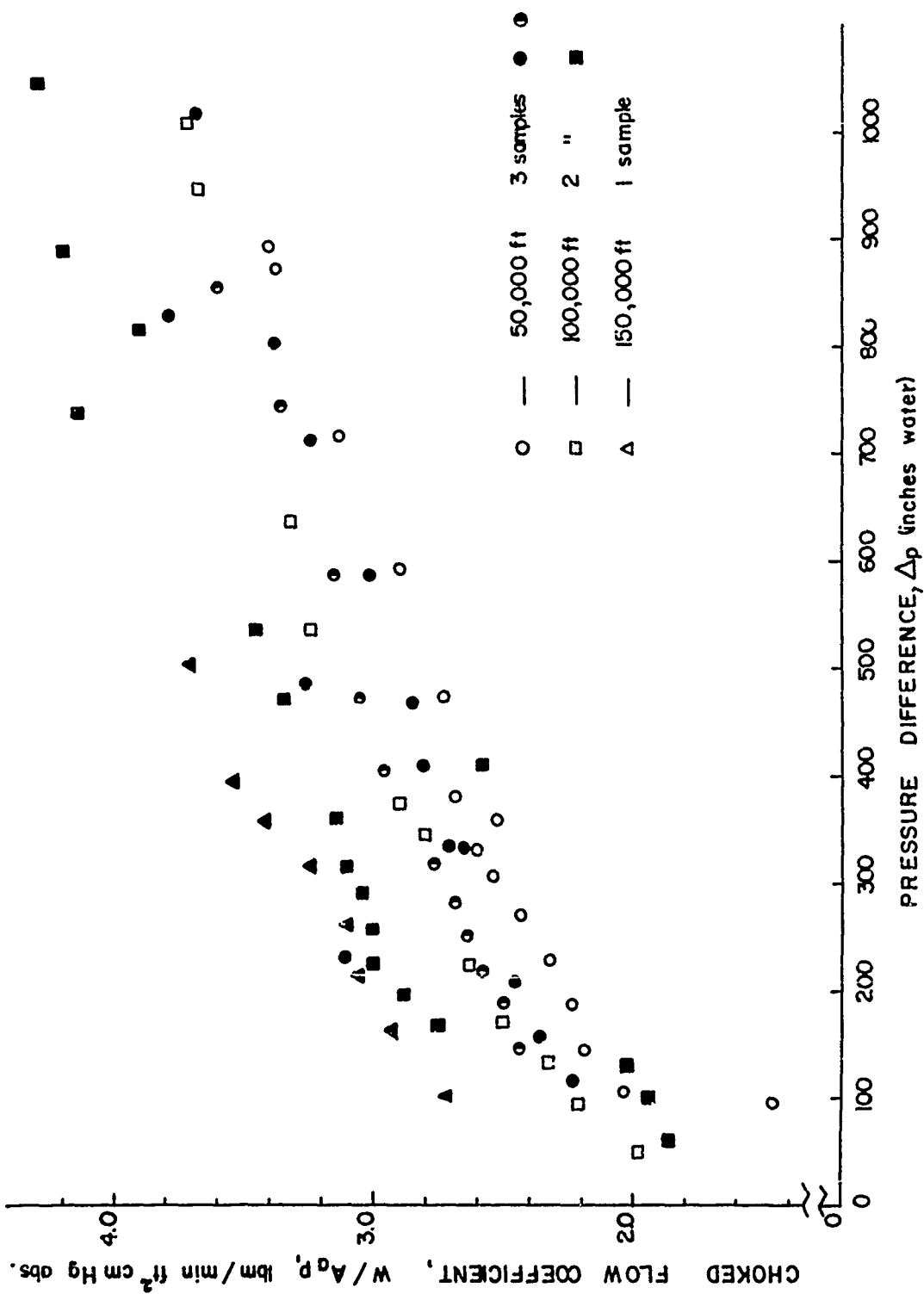
Figure 19 . Choked Flow Coefficient for Fabric. S-6
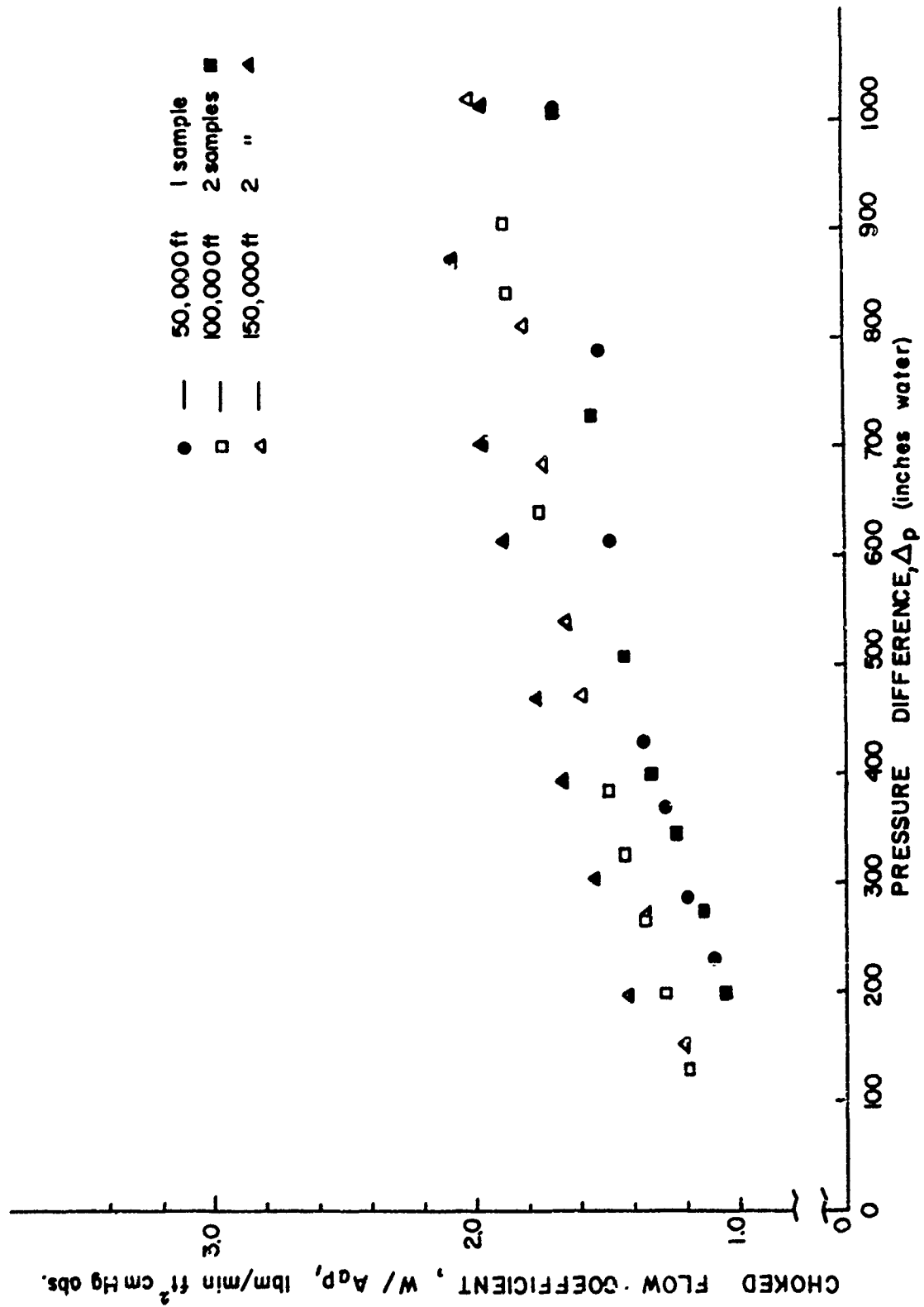
Figure 20. Choked Flow Coefficient for Fabric. E-10

samples taken from different lots of fabric or even from the same
lot may run as high as 20%.

The results shown in Figs. 18, 19, and 20 can be used to
estimate the geometric porosity of the fabric, since Equation (27)
may be rewritten as

$$\frac{A_f}{A_a} = \frac{W/A_a P_1}{W/A_f P_1} \tag{28}$$

Theoretically $W/A_f P_1$ should be 38.6 lbm/min ft^2 cm Hg abs.
assuming that choked flow conditions exist in the fabric. Table
5 summarizes these calculations.

It is interesting to note that the sea-level data for all
three fabrics have also been correlated using the choked flow co-
efficient. The data for sea-level and 150,000 feet represent a
variation in p_2 of 760 to 1.

TABLE 5

GEOMETRIC POROSITIES OF FABRICS

Fabric	Δp inch $H_2 0$	$w/A_a p_1$ *	A_f/A_a
S3	50	2.50	0.065
	500	4.62	0.12
S6	100	2.39	0.062
	1000	4.05	0.105
E10	150	1.1	0.029
	1000	1.95	0.051

* Dimensions - lbm/min ft^2 cm Hg abs.

These values of the geometric porosity are in the usual range
for these fabrics.

In Fig. 21 the curve marked "H" might represent the data taken
with a high pressure (perhaps corresponding to sea-level pressure)

WADC TR 59-374
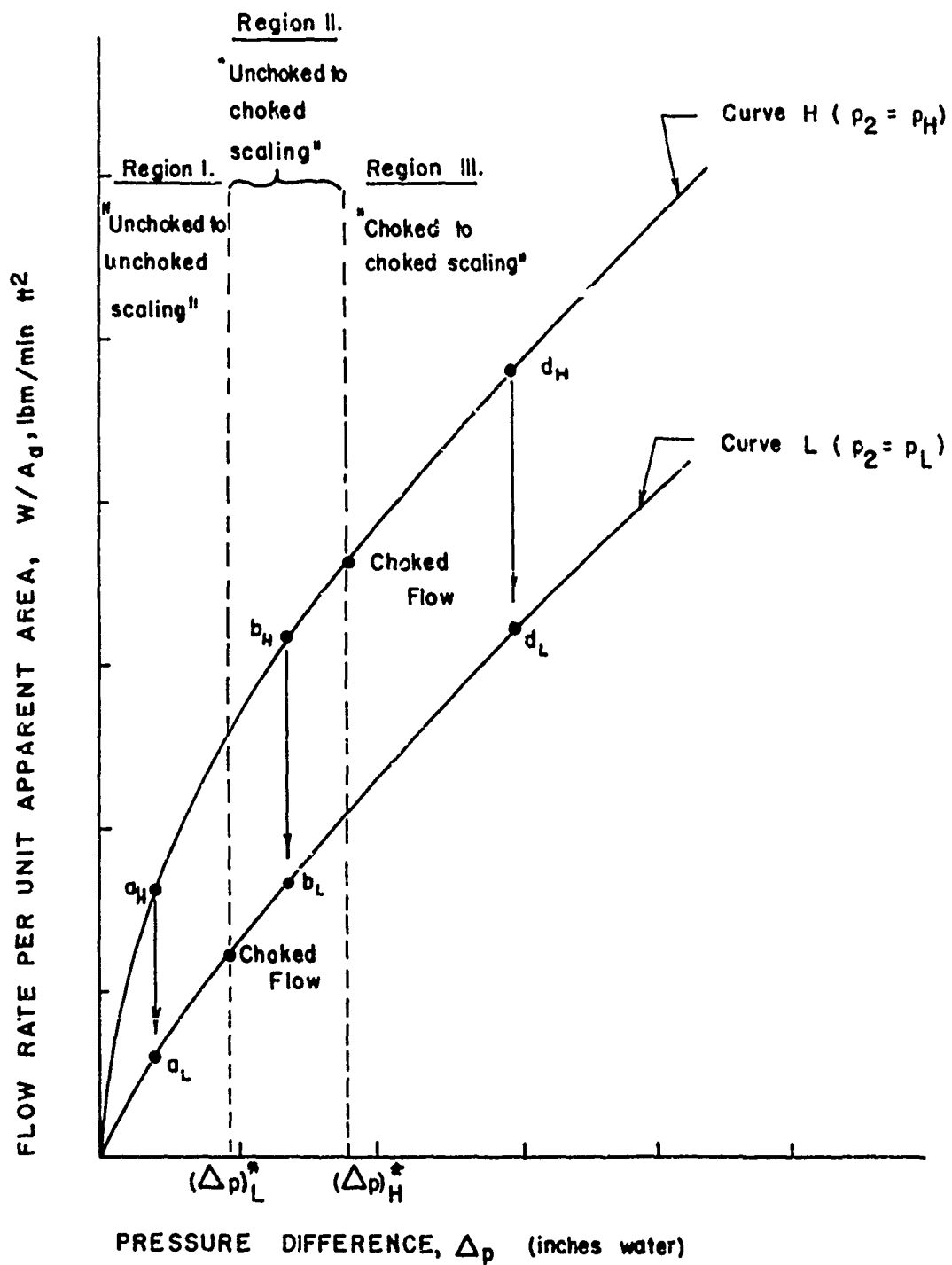
Figure 21. Predection of High Altitude Flow Rates from Sea Level Data

behind the fabric. It is desired to predict the curve marked "L" which will represent the data for a lower pressure behind the fabric (or a higher altitude). The first step in predicting curve "L" is to locate the values of the critical pressure difference which correspond to the critical pressure ratio or choked flow for the two values of p_2, namely, p_H and p_L. These critical pressure differences can be calculated from Equation (23).

Once these two values $\Delta p_H *$ and $\Delta p_L *$ have been determined, vertical lines can be erected at the corresponding values of Δp This construction immediately divides the graph into three regions.

Region I: The use of point a_H on the "H" curve to calculate point a_L on the "L" curve involves the use of mass flow per unit area data taken under unchoked flow conditions with $p_2 = p_H$ to predict a mass flow per unit area under unchoked flow conditions with $p_2 = p_L$. This will be termed "unchoked to unchoked scaling."

Region II: The use of point b_H on the "H" curve to calculate point b_L on the "L" curve involves the use of mass flow per unit area data taken under unchoked flow conditions with $p_2 = p_H$ to predict a mass flow per unit area under choked flow conditions with $p_2 = p_L$. This will be termed "unchoked to choked scaling."

Region III: The use of point d_H on the "H" curve to calculate point d_L on the "L" curve involves the use of mass flow per unit area data taken under choked flow conditions with $p_2 = p_H$ to predict a mass flow per unit area under choked flow conditions with $p_2 = p_L$. This will be termed "choked to choked scaling."

It is very important to note that the scaling from the "H" curve to the "L" curve is only done at the same Δp . The reason for this can be seen by using Equation (27) as follows:

$$\frac{\left(\frac{w}{A_a}\right)_H}{\left(\frac{w}{A_a}\right)_L} = \frac{\left(\frac{w}{A_f}\right)_H}{\left(\frac{w}{A_f}\right)_L} \cdot \frac{\left(\frac{A_f}{A_a}\right)_H}{\left(\frac{A_f}{A_a}\right)_L} \tag{29}$$

It is assumed that the mass flow per unit <u>actual</u> flow area w/A_f is controlled by the isentropic flow equations whereas the geometric porosity A_f/A_a is controlled by Δp according to Equation (26). Thus, at the same Δp the ratio $(A_f/A_a)_H/(A_f/A_a)_L$ should be unity and, therefore, the mass flow per unit apparent flow area can also be scaled using the isentropic flow equations. If Δp is not the same, then the ratio $(A_f/A_a)_H/(A_f/A_a)_L$ is not known

The scaling equations for the various regions can be written down immediately from the section on isentropic nozzle flow.

Region I: "Unchoked to Unchoked Scaling."

From Equation (14) it follows:

$$\frac{\left(\frac{W}{A_e}\right)_L}{\left(\frac{W}{A_e}\right)_H} = \frac{(P_1)_L}{(P_1)_H} \cdot \frac{\left(\frac{P_2}{P_1}\right)_L^{\frac{1}{k}}}{\left(\frac{P_2}{P_1}\right)_H^{\frac{1}{k}}} \cdot \frac{\sqrt{1-\left(\frac{P_2}{P_1}\right)_L^{\frac{k-1}{k}}}}{\sqrt{1-\left(\frac{P_2}{P_1}\right)_H^{\frac{k-1}{k}}}} \tag{30}$$

Region II: 'Unchoked to Choked Scaling."

From Equations (14) and (19) it follows:

$$\frac{\left(\frac{W}{A_e}\right)_L}{\left(\frac{W}{A_e}\right)_H} = \frac{(P_1)_L}{(P_1)_H} \cdot \frac{\sqrt{2^{\frac{2}{k-1}}(k-1)\left(\frac{1}{k+1}\right)^{\frac{k+1}{k-1}}}}{\left(\frac{P_2}{P_1}\right)_H^{\frac{1}{k}}\sqrt{1-\left(\frac{P_2}{P_1}\right)_H^{\frac{k-1}{k}}}} \tag{31}$$

For k = 1.4 Equation (31) becomes

$$\frac{\left(\frac{W}{A_e}\right)_L}{\left(\frac{W}{A_e}\right)_H} = \frac{(P_1)_L}{(P_1)_H} \cdot \frac{0.2588}{\left(\frac{P_2}{P_1}\right)_H^{\frac{1}{k}}\sqrt{1-\left(\frac{P_2}{P_1}\right)_H^{\frac{k-1}{k}}}} \tag{32}$$

The quantity appearing below the 0.2588 is tabulated for k = 1.4 in Table 25 of reference (16).

Region III: "Choked to Choked Scaling."

From Equation (20) it follows:

$$\frac{\left(\frac{W}{A_e}\right)_L}{\left(\frac{W}{A_e}\right)_H} = \frac{(P_1)_L}{(P_1)_H} \tag{33}$$

Equations (30), (32), and (33) were applied to the sea-level
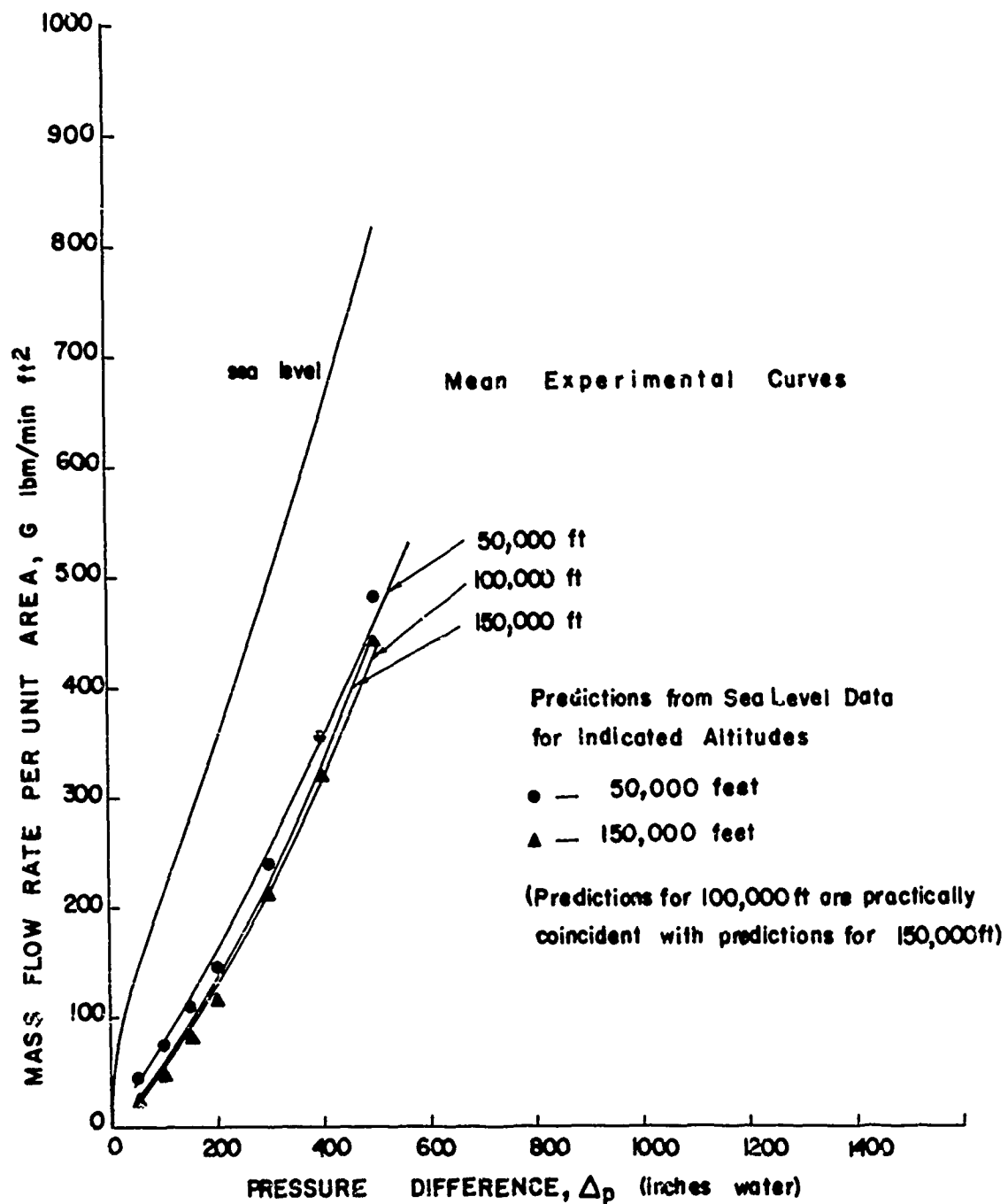
Figure 22.   Predicted and Measured Flow Rates for Fabric. S-3
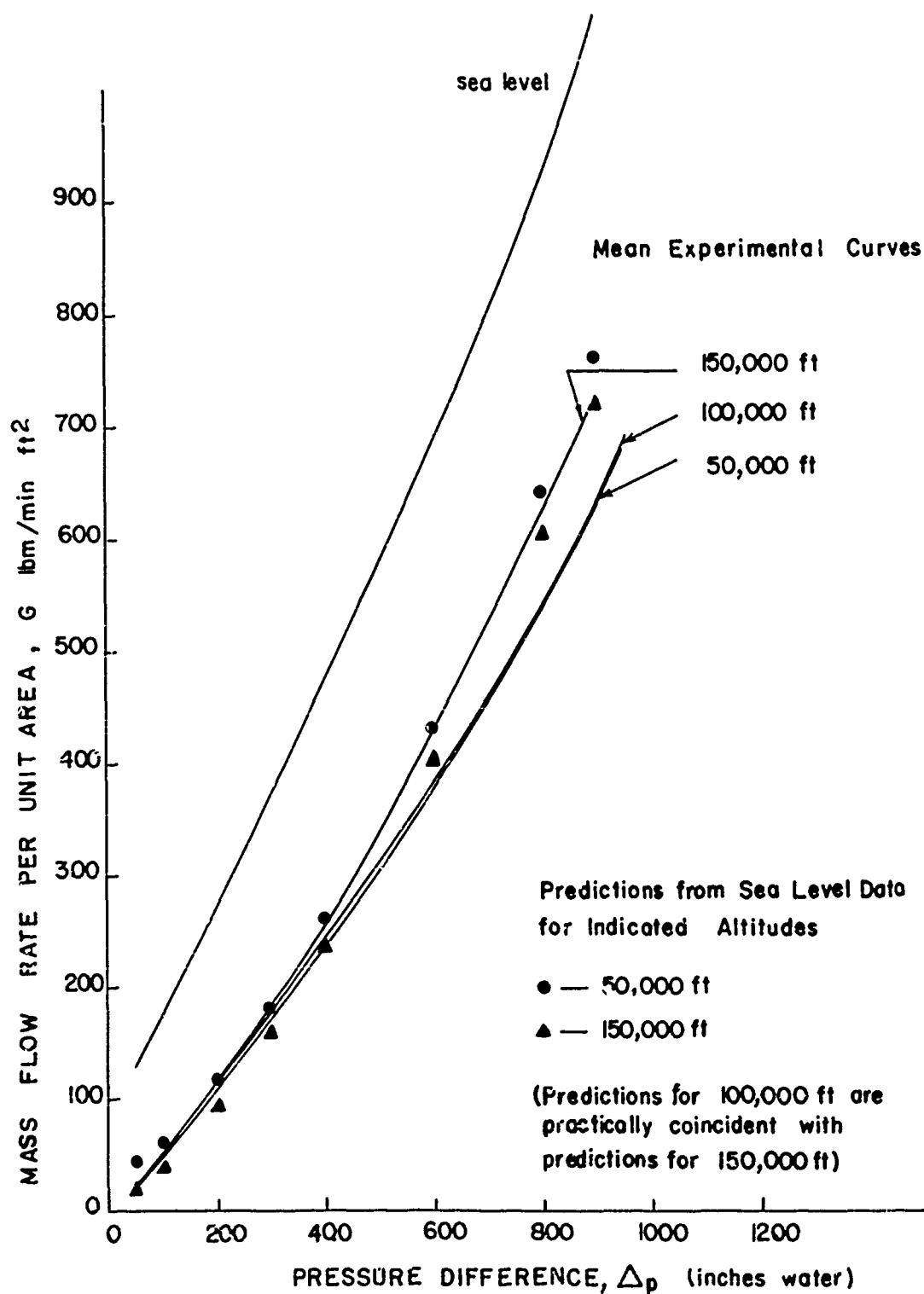
Figure 23.   Predicted and Measured Flow Rates for Fabric. S--6
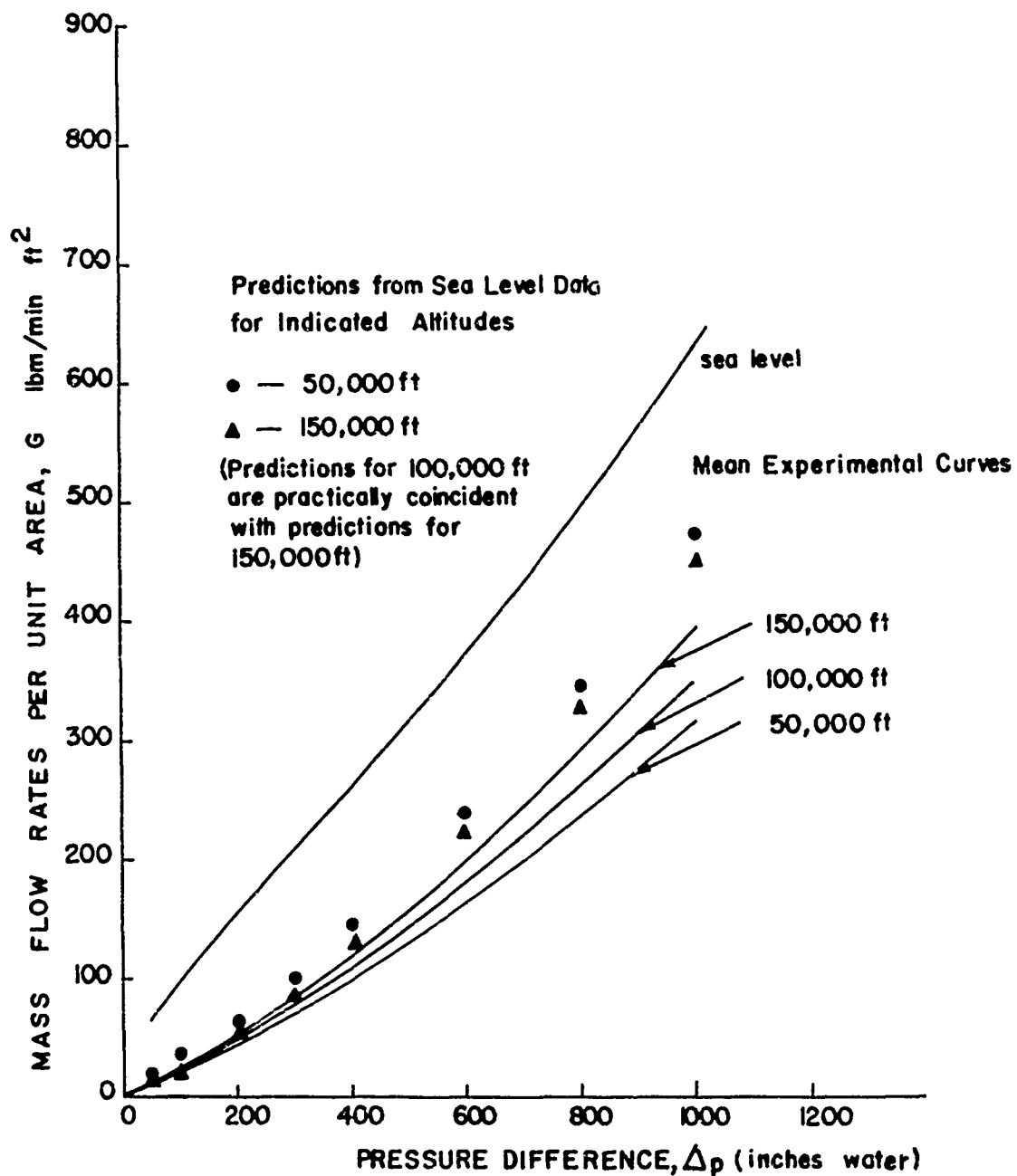
Figure 24. Predicted and Measured Flow Rates for Fabric. E-10

WADC TR 59-374

51

flow rate data of reference (3) for fabrics S3, S6, and E10, and predictions were made of the flow rates through the fabrics at altitudes of 50,000, 100,000 and 150,000 feet. Figures 22, 23, and 24 show the measured mass flow rates per unit area for Fabrics S3, S6, and E10 taken at 50,000, 100,000, and 150,000 feet and the predicted values using the sea-level data.

The agreement between the mean experimental curves and the predicted curves for Fabrics S3 and S6 is excellent. The predicted curves are practically coincident with the mean curves for Fabric S3 and are about 10% higher for Fabric S6 at the higher values of Δp . The method of prediction works very well both in cases where choked flow sea-level data are used to predict choked flow high altitude data and in cases where unchoked flow sea-level data are used to predict choked flow high altitude data.

The agreement between the mean experimental curves and predicted curves for Fabric E10 is not as good as for Fabrics S3 and S6. At values of Δp of 1000 inches water, the predicted curves are as much as 30% higher than the experimental curves. A great deal of scatter was found in the sea-level data for Fabric E10 so that the reason for the large discrepancy between the curves is not clear. Further experimental work should be done on this fabric.

From the foregoing comparison between the prediction based on the nozzle flow analogy and the measured data it appears that flow rate data taken at sea-level conditions can be used to accurately predict flow rate data at high altitude conditions. This method has been verified for cases where the pressure difference across the fabric is rather large, greater than 100 inches water, but additional careful experimental work should be done for cases where small pressure differentials are encountered i.e. about 10 inches water.

II CLOTH GEOMETRY AND AIR FLOW

Introduction

The assumption that parachute cloth behaves as a rigid screen woven of uniformly round wire monofilaments has been a useful step in aerodynamic treatments of the flow of air through textile materials. Even with this gross simplification numerous mechanisms of flow must be postulated to explain the experimental flow results reported in the literature. With the best of these postulations the flow resistance of parachute cloths at higher pressure differentials is less than that predicted by fluid theory and it is customary to attribute such higher apparent permeabilities to the opening of the fabric pores under stress.

Definition of the pore geometry in an unstressed woven cloth is in itself a difficult if not impossible task. Peirce (13) who established the first general theory of fabric structure, called the geometry of a pore 'weird'. One grasps the significance of this comment in viewing the successive cross-sections of the simplest of pores, that belonging to a completely balanced plain weave (14). This together with the three other types of intersections which allow for an infinite variety of weaves and patterns, provide even greater range in pore geometry. Further, if the usual parameters of cloth geometry are altered in a given weave the distortion of a single pore can quickly vitiate any generalizations one might draw in treating the balanced weave.

A first step in making the balanced, plain-weave, monofilament screen model more realistic was to account for the four types of pores which are found in various textile weaves. It has been shown that each of these pores, for a given projected area, has a different minimum cross sectional area (taken in the fabric plane).(14). Experiments with models of these four pore types show that the ratio of minimum jet area, at a Reynolds number of 400, to minimum pore area is relatively constant. It is suggested that for the models tested (with diameter/spacing ratios of .33 - .36), the minimum pore area may serve as the best parameter for estimating the effective pore area of fabrics, regardless of their weave structure and be useful in treatment of fabric pores as orifices (15).

Unfortunately, the minimum cross sectional areas of the different pores change with stress application, and it may be expected that different pore types will change different amounts, depending on the degree of interlacing, the initial crimp and the ratio of stresses developed in warp and filling.

WADC TR 59-374

The first attempt to account for the changes in pore size with the stresses set up by applying significant pressure drop across the fabric was reported by Klein et al (10). Here the changes in fabric dimensions were noted under various test conditions and were allocated to the measured projected pore dimensions. In addition, light transmission measurements made during airflow tests were correlated with free area measurements taken under the microscope. Thus, stress-strain adjustments of geometric porosity were made in calculating discharge coefficients for various fabrics under different pressure drops. But for many fabrics - of relatively low porosities (½ or less as contrasted to Penner's porosity of 4/9's) the discharge coefficients calculated on the basis of projected area measurements - both at rest and under stress, did not agree with experimental values. It remained to take into account the inclination of pore axes to the normal vector of the fabric plane.

Klein et al, (11) proposed that the effective orifice area is not dictated by the projected pore area, but rather by the area of a surface generated by lines connecting closest points of two adjacent warp (or filling) yarns. This area is calculated by single area integration along one set of yarns and forms a warped sheet such as that obtained by twisting a thin ribbon through 25° to 50°. By using measurements of fabric extension under test conditions and fabric light penetrability under stress, the change in effective pore area can then be calculated. This area value was then used in calculating the Reynolds number for a given flow rate. From an empirically determined relationship of projected area discharge coefficients and Reynolds number, Klein then determined the projected area discharge coefficient and finally the effective 'twisted' area discharge coefficient for fabrics. The 'twisted area' discharge coefficient thus calculated was observed to be in agreement with the measured discharge coefficient for selected fabrics of low porosity.

Viewing this development of our knowledge of airflow through textile structures, one becomes aware of the importance of having information relating to the geometry of the cloth and the change in this geometry with the stresses of parachute usage. Development of such information was the goal of the second part of this research at M.I.T. Part II of this report presents the work carried out in the Textile Division to evaluate geometric effects, stress-strain behavior under biaxial tensile conditions, alterations in pore geometry resulting from applied stresses, and the influence of prestress on air flow behavior of selected fabrics.

WADC TR 59-374

Directional Effects

During high pressure drop air permeability studies of Fabric E9 of W.A.D.C. TR-57-443 (600 lb/in Dacron cloth), it was noted that the air stream did not issue normal to the cloth but seemed to be diverted considerably to one side. Such behavior is not found in the case of wire screens, and had not been noticed before for other fabrics. Closer examination revealed the following differences between wire-screens and fabrics, pointing up possible reasons for the effect. First, wire screens are rigid in the usual pressure ranges of interest but conventional parachute fabrics deform under the slightest pressure difference. Therefore, the incident flow need not be everywhere normal to the plane of the fabric. Second, a study of the geometry of woven cloth shows an infinite number of ways that orifices can be formed. Differences in orifice orientation, shape, size and length, over and above the normal statistical variation cannot only occur from fabric to fabric, but in the same specimen.

The problem of 'directional' behavior of a fabric can be formulated in the following questions. What types of fabric show a directional effect of flow? Under what conditions of flow does this effect take place? For a given fabric construction what are the variables that affect the overall airstream deflection? What mechanisms determine the degree of deflection in a given material?

The 'directional' phase of the program has given partial answers to the above questions and has brought out some significant results. Fabrics S3, S6, S8 have been studied and in addition Fabrics E6 and E9 of W.A.D.C. TR 57-443. The fabric construction details are available in Appendix I of this report.

Equipment for Directional Studies:

The permeometer used for the study of directional effect of airflow has been described in WADC TR 57-443. The modifications necessary to take quantitative angle measurements are described below:

Two pieces of aluminum channel, 1½x4' and 4'' long, were bolted to the base plate (See Fig. 25.1), such that the plane of the large flat surface of air channel was in one case parallel to the warp yarns and in the other to the filling yarns. The indicating element was a very fine nylon fiber, 2' long, which was attached to a stiff copper wire stretched across two screws. The wire formed one diagonal of the 4 inch square formed by the fabric inside the jaws and was 1 3/8'' from the undeformed specimen.

Two special film protractors were prepared by inking half circles of polar coordinate graph paper and photographing them. These were pasted

Figure 25.1. Directional Indicator on Permeometer

sample

filling

warp

indicating fiber

filling mirror

warp mirror
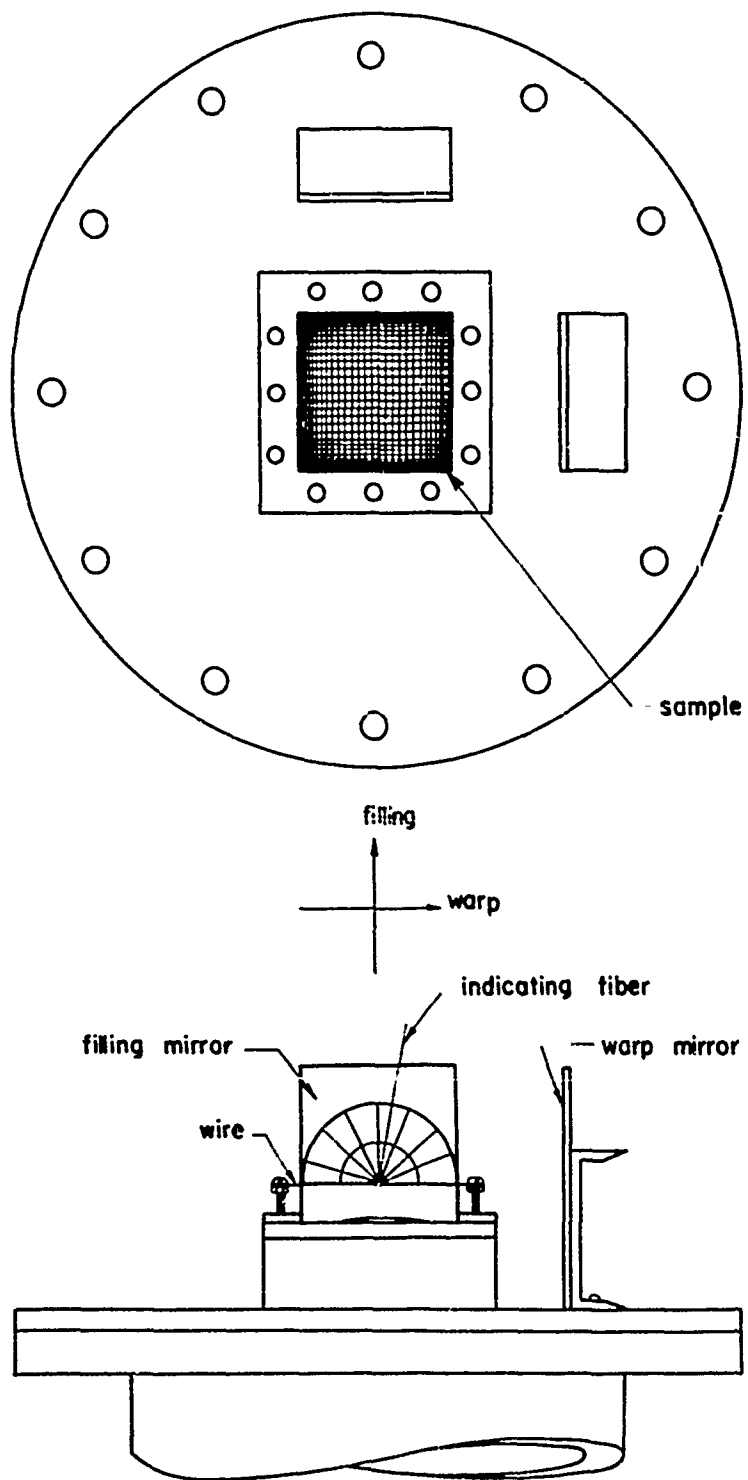
wire

on 4" x 6" mirrors, and the mirrors lined up on the channels such that the base of the semi-circular protractor was coincident with the stiff copper wires, center to center, without parallax. The mirrors were then taped into place. The distance between the edge of the jaws and the mirrors is not critical, but in the present equipment was equal to 2". The mirrors were set up so that (referring to Fig. 25.1), a projection of the 'warp plane angle' would be obtained on the filling mirror and vice versa. The error in the angle measurement was $\pm 2°$ mainly due to slight flutter of the indicating fiber.

Analysis of Directional Flow Data

It is necessary because of the three dimensional nature of the fabric cum flow system, to pick a reference system of coordinates (Fig. 25.2a). The face of the fabric is arbitrarily taken as that side which is concealed in the roll as supplied by WADC. The fabric visible on the outside of this roll is taken as the fabric reverse side. The warp positive direction goes into the roll, and the filling direction is chosen as positive in the direction determined by rotation of the warp counterclockwise through $\pi/2$ as viewed in the face plane of the fabric.

On the reverse side it is seen that the warp positive directions match, but the filling direction originally chosen as positive, reverses itself if the warp is rotated counterclockwise, in the plane of this side. For reasons specified below, we change the convention of filling positive direction for the reverse side. The reason for this becomes clear if we consider Figure 25.2b. The line AOA' is a line in space through a fabric plane. It can be seen that OA' is in the first quadrant of the face plane, but if we can change convention for the reverse plane the line AOA' will be in the first quadrant in both face and reverse planes and the trigonometric functions would retain the same sign. Thus an inconsistency in flow deviations would immediately become apparent.

Referring to Figure 25.2c which is a head-on view of the fabric and mirror system, the indicator fiber is shown in each of the four directions it could assume in a directional flow experiment. The 'warp plane angle' (β) is the angle made by the projection of the fiber on the warp mirror with the projection of the duct axis on that mirror. The filling plane angle (α) is the angle made by the projection of the indicator fiber on the filling mirror with the corresponding projection of the airduct axis. Now β is considered positive,

WADC TR 59-374

Figure 25.2. Fabric Airstream Orientation Scheme

in Figures 25.2c(2) and 25.2c(3) and negative in Figures 25.2c(1) and c(4). At the same time, α is positive in Figure 25.2c(1) and c(2); negative in c(3) and c(4).

The final form of the data has been reported with reference to a spherical coordinate system (Figure 25.2d). If the indicating fiber makes angles β, α with the warp and filling mirrors shown as ZON' and ZOP' respectively, then these can be transformed into the latitude angle ϕ and the azimuth angle by means of the relationships

$$\tan \phi = \sqrt{\tan^2 \alpha + \tan^2 \beta}$$

$$\tan \theta = \tan \beta / \tan \alpha$$

From these equations it is clear that we cannot distinguish between conditions 25.2c(1) and c(3) or between c(2) and c(4) if the parameters ϕ and θ are used to characterize the flow. Additional information taken from the α and β signs must be used to designate the deflection quadrant.

Experimental Procedure and Exploratory Work:

The experimental procedure was similar to taking measurements on permeability with one exception. Precautions were taken to ensure that the approach flow was normal to the fabric and that the backing diaphragm was mounted centrally when clamping the fabric. Initially, the following factors were investigated:

1. degree of clamping
2. effect on angles of rotation of the specimen in its own plane through $\tau/2$.
3. consistency of angles with respect to the flow being incident on the face or on the reverse.
4. effect of area of flow on the angles; due to the clamping device this would mainly be an effect of different stress patterns.
5. flow through the corners.

The specimen fabrics for the initial probing studies were the same ones that had been used for WADC TR 57-443, specifically fabric E9. The final data is reported in terms of freshly cut samples carefully marked and chosen so as to be contiguous to those used in other tests reported at this time. Findings of our exploratory tests are cited below:

1. The degree of clamping did not affect the angles. The clamping was not varied quantitatively, and therefore, not

WADC TR 59-374

reproducibly. But a wide difference in tautness of the fabric specimen did not seem to change the directional flow.

2. When the fabric was rotated through 90° in its own plane, the directional flow consistently followed this change.

3. The consistency of angles is discussed in conjunction with the final data.

4. The effect of area of flow on the angles. In one case the flow was allowed to take place through the central 1 (one) square inch of the fabric. In the other the flow was allowed to take place without any backing dental rubber diaphragm whatsoever. The change was remarkable. There was almost three times as much deflection in the latter as in the former.

5. Flow through the corners. The fabric was backed up by a diaphragm that had an opening of 1 square inch in the center of one specimen quadrant for each experiment. All four quadrants were thus investigated. This experiment was carried out because it was noticed that when the fabric was completely open (15 sq.in) the flow seemed to be concentrated in half the area available to flow. The results of these qualitative tests indicated that the flow in each quadrant generally agreed with the expected combined directional effects of the local fabric inclination and the inherent deflectional characteristics of the cloth pores.

Discussion of Results:

The deflection angle data are presented in tabular form in Tables 6, 7, 8, and the flow data are presented in graphical form in Figure 25. Table 5 contains the experimental results on S3, S8, and S6 of the current contract which are detailed in Appendix I, Table 10.

DIRECTIONAL EFFECTS IN AIR FLOW MEASUREMENTS

TABLE 6

Orifice diameter: 1.40"   Temperature (Room): 75°F.

Sample description	Mounting method	Run	Pressure drop across fabric inches water	$\beta°$	$\alpha°$	$\varnothing°$	$\theta°$	Quadrant
S-8	F	1	53.5	3	3	4.55	45	1
		2	107.0	3	3	4.55	45	1
S-3	F	1	33.7	2	2	2.71	45	1
		2	63.7	2	2	2.71	45	1
S-6	F	1	80.3	3	3	4.55	45	1
		2	133.8	6	3	6.70	63.42	1
E-6	F	1	107.0	12	0	12.00	90.00	1
		2	311.9	10	2	10.20	78.80	1
		3	530.7	8	2	8.23	76.03	1
		4	841.5	6	10	6.07	80.83	1
E-6	R	1	100.5	6	6	8.43	45.	1
		2	287.3	6	6	8.43	45	1

*F - Face exposed to atm. pressure, Flow incident to reverse
 R - Reverse exposed to atm. pressure, Flow incident to face

WADC TR 59-374

DIRECTIONAL EFFECTS IN AIR FLOW MEASUREMENTS

TABLE 7

Orifice diameter: 1 40"   Temperature (Room): 75°F

Sample description	Mounting method	Run	Pressure drop across fabric inches water	Pressure drop across orifice	$\beta°$	$\alpha°$	$\phi°$	$\theta°$	Quadrant
E-9₁	F	1	42.26	1.7	6	-4	7.183	-56.36	2
		2	24.90	2.7	8	-6	9.933	-53 23	2
		3.	110.20	3.6	6	-4	7.183	-56.36	2
		4	143.40	4.8	6	-4	7.183	-56.36	2
		5	204.90	6.3	6	-4	7.183	-56.36	2
E-9₂	R	1	21.40	0.8	-10	-10	13.93	45.00	3
		2	54.03	1.75	-14	-8	13.97	60.60	3
		3	80.78	2.5	-14	-8	13.97	60.60	3
		4	128.40	3.8	-10	-8	13.97	60.60	3
		5	156.80	4.5	-14	-4	14.50	74 38	3
		6	222.02	6.2	-16	-6	16.97	69 83	3
		7	370.20	9.7	-14	-4	14 50	74.38	3
E-9₃	F	1	71.69	2.7	6	-4	7.183	-33 63	2
		2	133.80	4.5	10	-4	10.73	-21.63	2
		3	177.10	5 7	10	-6	11.60	-30 80	2
		4	217.20	6.9	10	-6	11.60	-30.80	2
		5	528.00		10	-6	11.60	-30.80	2

*F - Face exposed to atm. pressure, Flow incident to reverse
R - Reverse exposed to atm. pressure, Flow incident to face

DIRECTIONAL EFFECTS IN AIR FLOW MEASUREMENTS

TABLE 8

Orifice diameter: 1.40"   Temperature (Room) 75°F

Sample description	Mounting method *	Pressure drop across fabric inches water	$\beta°$	$\alpha°$	$\phi°$	$\theta°$	Quadrant
E-9	F	46.5	35	25	40.05	56.33	1
		74.9	25	25	33.40	45.00	1
		112.9	25	20	30.63	52.03	1
		214.0	20	10	22.00	64 15	1

* F - Face exposed to atm. pressure; Flow incident to reverse

R - Reverse exposed to atm. pressure; Flow incident to face.
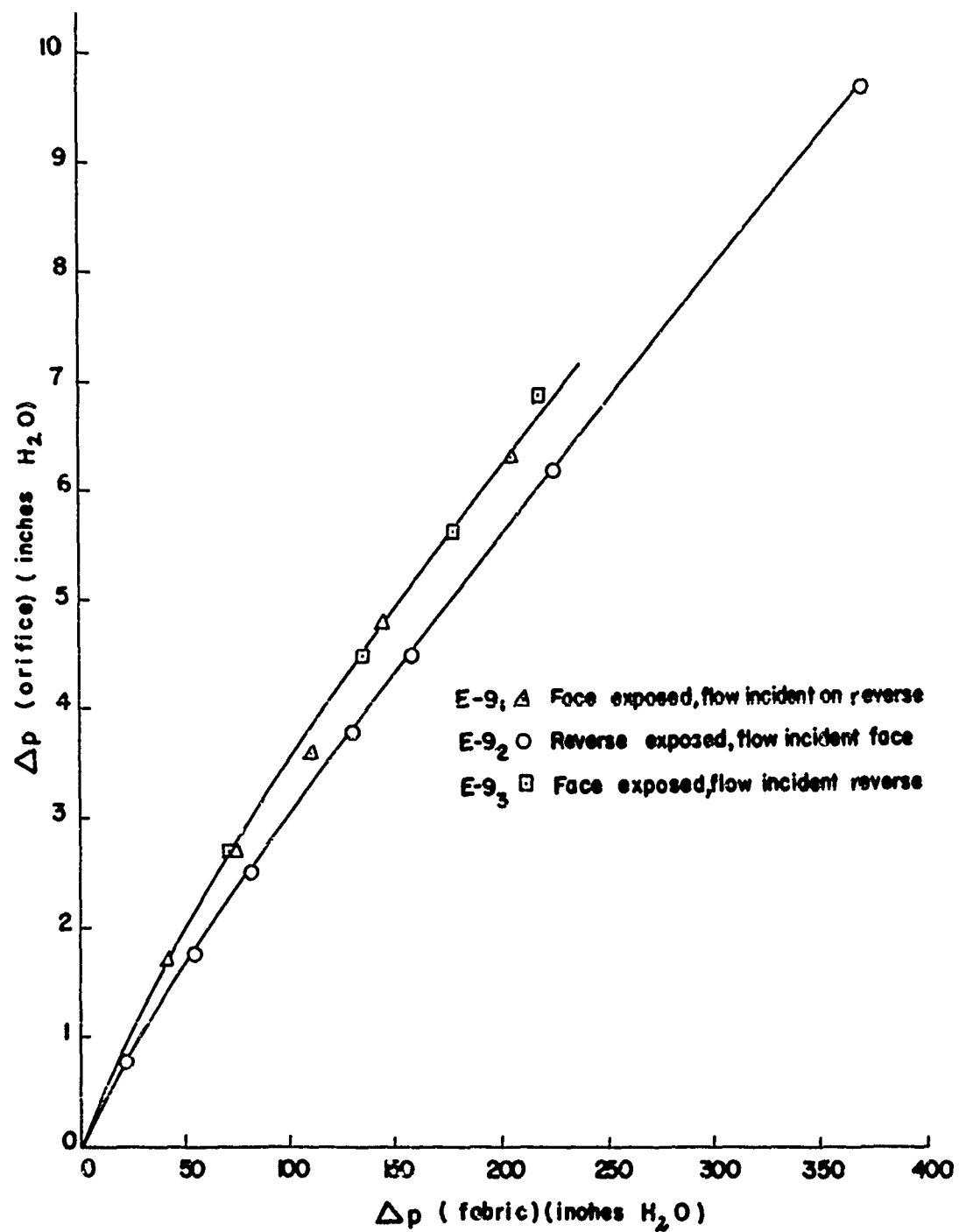
Figure 26. Directional Effects on Fabric E-9

and of Fabric E6 of WADC TR 57-443. Tables 7 and 8 were obtained from studies on Fabric E9 of the same report, the former being data taken with flow only through the central 1(one) square inch and the latter being data taken with flow through all sixteen square inches held by the jaws. Samples $E9_1$, and $E9_2$ were fresh samples; $E9_3$ had been used in WADC TR 57-443.[1] The discussion will treat the questions posed by the general formulation of the airflow problem before a study of Fabric E9 which showed the most effect, is undertaken.

1.   What types of fabrics show a directional effect of flow? The data of Tables 6 and 7 would indicate that all fabrics show a slight effect, though in the case of Fabric S3 the effect is within the limits of experimental uncertainty ($\pm 2^{\circ}$ in the measurement of α and β). Compare the yarn specifications of the various fabrics; it is obvious that the directional effect increases as denier and thickness increases. (See Appendix I). Confining attention to Fabrics S3, S8, and S6 the deflection angles are approximately the same whereas Fabric E6 shows considerably more deflection than the other three. Thus the data would indicate that the effect is present only after a minimum yarn diameter is reached or a minimum fabric thickness or pore length is attained.

2.   Under what conditions of flow does this effect take place? In general, the effect of varying pressure drop across the specimen did not affect the angles for experiments in which only 1 square inch was exposed. However, Fabric E9 showed an appreciable change (Table 8) when 16 square inches were exposed.

3.   For a given fabric construction what are the variables that affect the overall airstream deflection: The two different conditions that were tested were consistency of flow being incident on the face and the reverse, and change of area exposed to flow. The data on E6 showed that the stream was not turned around on itself due to pore curvature. But the data on $E9_1$ vs. $E9_2$ showed that the deflection depended on which side was approached by the flow--remembering the coordinate transformation--since this is a very thick parachute material, the channel could be considerably curved inside. E9 showed a different deviation than $E9_2$. Since the former was an extensively cycled sample, the difference may be due to a change in the viscoelastic properties of the yarns. This difference however, was not reflected by the permeability data of Figure 26. On this graph the orifice pressure drop is plotted against the fabric pressure drop to determine the

difference in permeability. It is seen that depending on which
side is exposed to the flow, the permeability varies, and the
difference is 6.5% at Δp (fabric) = 200". The effect is not a
very large one but it is consistent with the differences in
deviational characteristics of the two sides.

Table 8 shows the most significant finding of this study, namely,
that depending on the stress conditions imposed on the fabric
the orifices can assume different configurations. For in the
case of Fabric E9 exposed to air only over an area of uniform
stress concentrations (1" square at the centre-data of Table 7)
the angle was never more than 17° and had become constant with
further changes in (fabric), whereas in the completely open case
the angle was as high as 40° and decreasing with increasing hy-
drostatic pressure. In the latter case the fabric progressively
closer to the jaws and away from the center, experience stresses
continuously departing from biaxial uniformity, until at the
very edge of the jaw only the yarns normal to the edges are
stressed. The data shows that as the hydrostatic pressure is in-
creased the effect of this nonuniformity on the directional
effect decreases.

Summary of Results: The practical application of the results
of this study to parachute design is not self evident, but a
few general results may now be stated:

1. The deviation of an airstream by a parachute
fabric is directly proportional to thickness. Correspondingly,
thicker fabrics show different airflow characteristics
depending on whichever side is presented to the stream.

2. Parachute fabrics can be made to divert the stream
by imposing different stress patterns on the two different
axes. This conclusion was reached on the present per-
meometer set-up and would have to be checked on different
jaw configurations for confirmation.

Further comments on those aspects of pore shape which lead to
airstream deflection will be presented in the detailed section
on fabric geometry.

WADC TR 59-374

66

Prestress Airflow Studies

It has been fully recognized that stresses imposed by a pressure drop across a textile fabric in an airflow test lead to enlargement of the cloth pores. If the stresses applied to the fabric are independent of the pressure drop, or at least are dependent on another variable besides pressure drop, we may expect that the geometric porosity will not be a univalued function of pressure drop. Likewise, air permeability will not be a univalued function of pressure drop.

If the stress in the fabric plane can be held constant during an air flow test the geometric porosity should likewise remain fixed and the air flow can be expressed as a univalued function of the pressure drop at each density. A different univalued relation should exist for each stress level as pictured in Fig. 27. Here we assume a fixed density of air flow. The relationships of Q as a function of Δp alone are marked as curves a,b,c,d,e, and f. In an actual airflow test the pressure drop across the fabric develops fabric stress, so in effect the real Q vs. Δp relationship follows curve a for a short time, then moves to curve b, curve c and so on as shown for curve A. In the absence of stress buildup data, the technologist measures only curve B, Q vs. Δp, or the projection of curve A on the Q vs. Δp plane. The projection of curve A on the σ vs. Δp plane is shown as curve C. Clearly, the curve B of Q vs. Δp is misleading for its height depends entirely on the relationship of σ vs. Δp and the strains which result from the stress level. It will be shown later that the σ vs. Δp curves depend on fabric properties and jaw geometry.

To approximate the pure airflow curves (a,b,c,d,e, and f of Fig. 27) a prestress device has been designed and built for use in the airflow tests of this program. The tensions applied by this device were to approximate the tensions developed across a 4 square fabric specimen subjected to pressure differentials of 3,6,9 and 12 lb/in respectively. In other words, the fabric was allowed to assume the shape and strain it would normally assume under a pressure differential of say, 12 psi in a permeometer; the difference being that this stressed condition was achieved without the introduction of airflow. Then the flow of air was started and the permeability measured.

Equipment

The prestress-airflow permeometer uses the same measurement and control orifices and valves as in WADC TR 57-443. The modification is in the clamping device, which is mounted on the flow-tube.
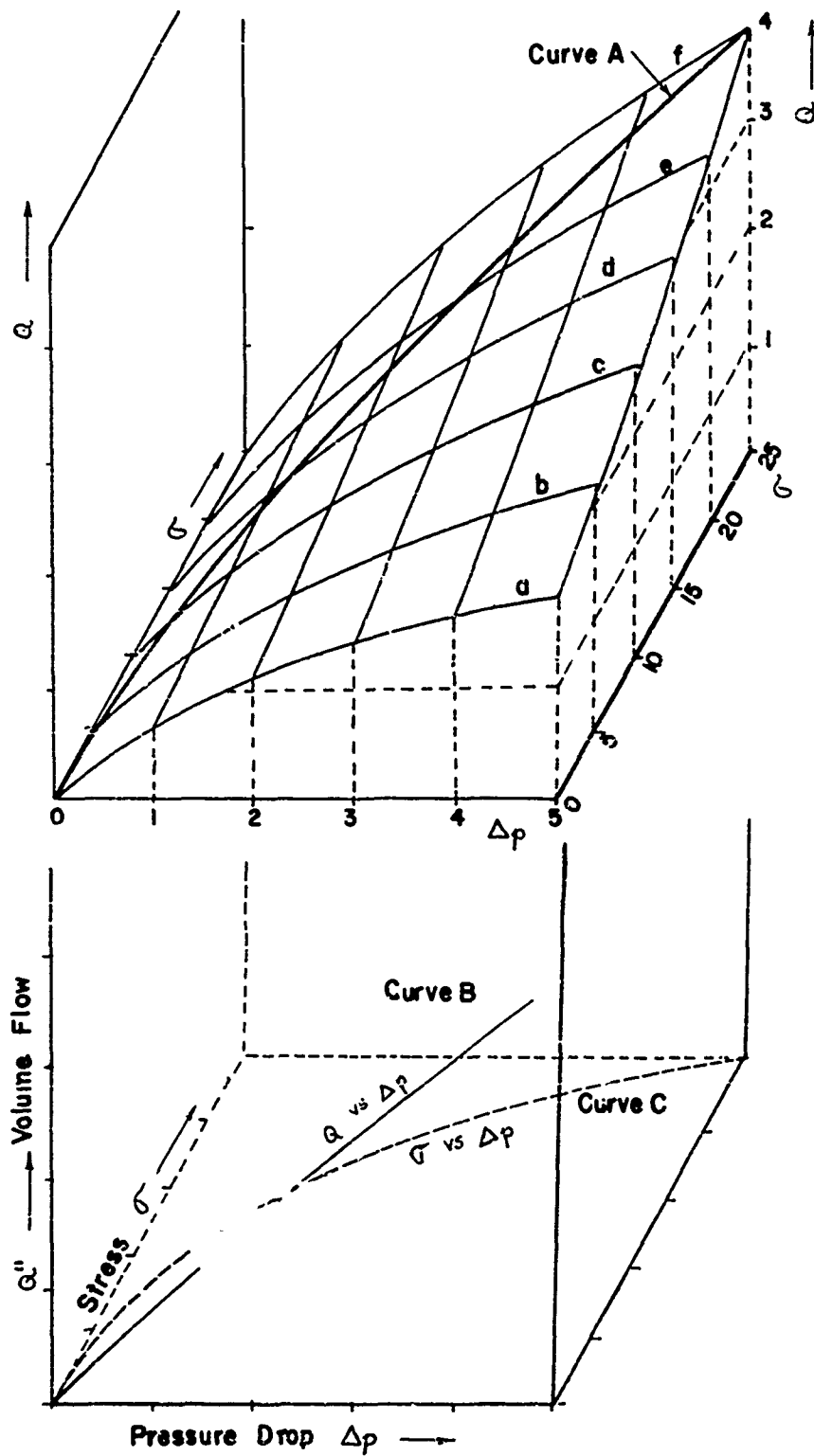
WADC TR 59-374

67

Figure 27.   Permeability as a Function of Pressure Drop and Fabric Stress

Figure (28) is an assembly drawing of the prestress assembly and Figure 29 is a schematic of the pressurizing tubes of the rig. The prestressing device consisted of two major parts, the prestressing chamber and the permeometer flow tube. The prestressing chamber served as a biaxial loading device and the flow tube allowed passage of air and static pressure buildup. The prestress chamber was made up of the jaw frame, jaws, the cloth sample, the flange and the ring. The flow tube was rigidly mounted to the permeometer (WADC TR 57-443) and the prestress unit could slide on its outer surface. The ring had an internal annular groove which carried two inflatable O-rings fabricated from neoprene tubing and copper tees, the vertical legs of the tees being used for the inflation. At the fully inflated state (50 lb/in^2), these tubes prevented the whole prestress assembly from sliding off the end of the permeometer during an experiment. In actual practice, it was found that a piece of rubber adhesive tape between the O-rings and the flow tube helped grip the flow tube more securely. The ring was secured to the jaw plate by means of a threaded flange. To prevent binding of the threads and to facilitate easy machining the ring was made of brass whereas the jaws, jaw plate and flange were made of aluminum. The teflon bushing, inserted between the flange and the flow tube gave a smooth bearing surface with little friction.

The deformable wall of the prestress chamber consisted of the fabric, a fortisan orifice - rubber membrane backing and another thin rubber membrane clamped to the flow tube. The first two elements were prepared the same way as the high pressure permeometer studies and have been described in WADC TR 57-443. Cloth area exposed to flow was a 1" square. The last of these is of prime interest here as it formed the pressure retaining (but not the load retaining) wall of the matrix. It was cut out in the form of a 6" square from a 10-mil rubber sheet. Holes corresponding to the Allen-head screws on the jaw plate and jaws were punched along the sides. A 3/4" diameter hole was punched in the center and the membrane was expanded over and clamped to the flow tube by means of twisted copper wires. A thicker piece of rubber (16 mils) was inserted between the membrane and the wires to prevent tearing. This thicker piece and the copper wires are shown as the clamp in the Fig. 28.

The flow tube was made out of a piece of 1½" standard steel pipe. Its surface was smoothed and polished to facilitate easy travel for the prestress jig. This movement was an essential characteristic of the equipment and the assembly was designed such that at any prestress pressure, it automatically slid back until the tensioned fabric was flush against the flow tube. Once the assembly had attained this state the O-rings could be inflated to

WADC TR 59-374

Figure 28. Assembly of Prestressing Device
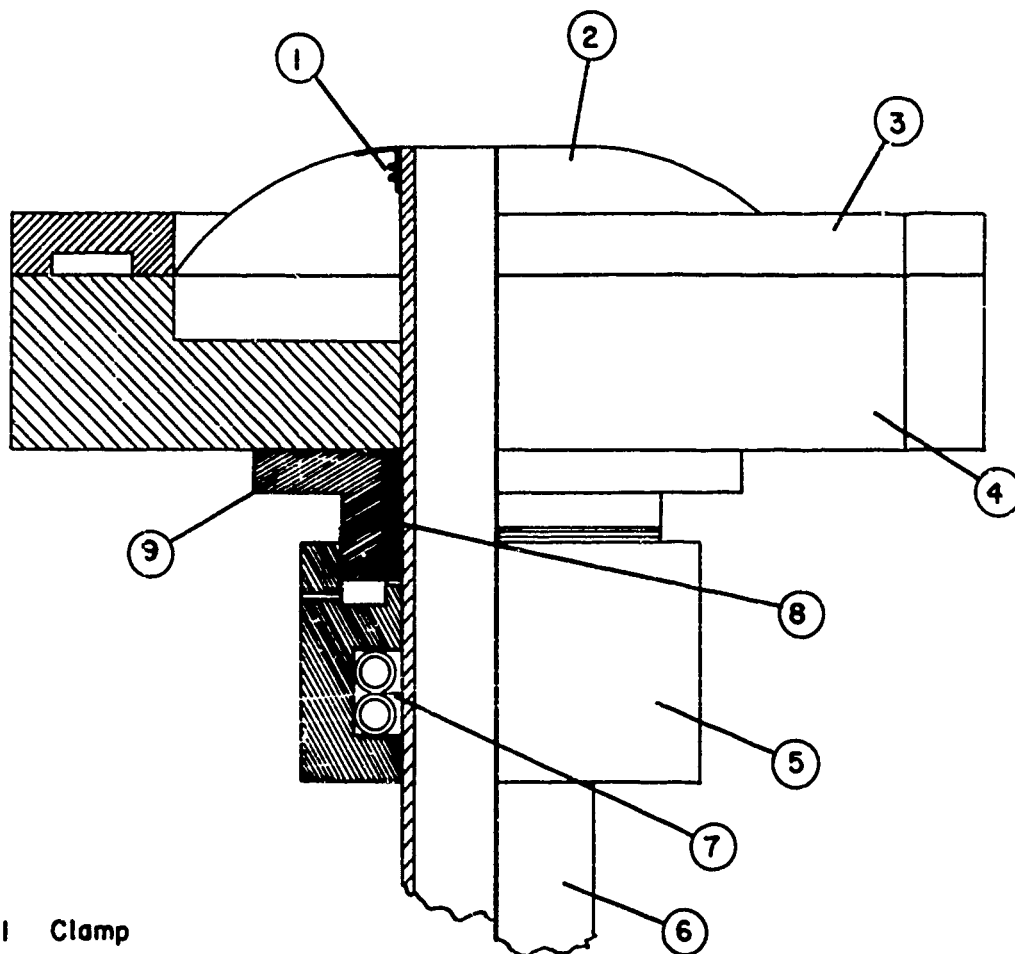
1 Clamp

2 Fabric

3 Jaw

4 Jaw Plate

5 Ring

6 Tubing

7 Rubber Hose

8 Bushing

9 Flange

maintain the assembly rigid, and the fabric tensioned equivalent to the specified pressures during air flow.

To help the assembly slide back during pretensioning as well as to provide a slight clearance for the leakage of air (pressure control in the prestress chamber was easier in such a case), the Teflon bushing and the bore of the jaw plate were machined to within 0.003" of the flow tube. This clearance provided the right amount of leakage along the flow tube and out through 4 holes in the ring to lubricate and to maintain a steady pressure. One of the 4 holes is shown in the Fig. 28.

Fig. 29 is a schematic of the pressure connections used in the assembly. The inflatable O-rings were pressurized from a nitrogen cyclinder as shown, the valving not being critical. However, to pressurize the prestress chamber from the compressor supply line, needle valves were used both for the main and the by-pass. The other connections are self-explanatory. Mercury manometers were used for all pressure measurement, except for orifice pressure drop, where water manometers were used. Fig. 30 shows the prestress device in place on the permeometer. Fig. 31 shows a closeup of the prestress device.

Procedure

A test on a prestressed fabric at a constant prestress level was carried out in three steps 1) sample mounting, 2) sample pre-stressing and 3) flow measurement.

1) Sample mounting: Prior to mounting a cloth sample on the prestressing device, it was translated without rotation to its extreme position on the tube, where it was rigidly held by means of the inflated O-rings, (50 psig). The sample was aligned so that the warp and filling yarns were parallel to the edges and tightened with a small amount of pretension. The pressure on the O-rings was then released and the device pushed back and the movement checked to assume free running.

2) Sample prestressing: After the sample was mounted the prestress pressure line was slowly opened until the required mer-cury column was obtained. The device was secured to the flow tube and then the sample was ready for flow measurements.

3) Flow measurement: Each individually mounted and pre-stressed sample was subjected to a series of increasing pressure differentials at each prestress level. The pressures recorded
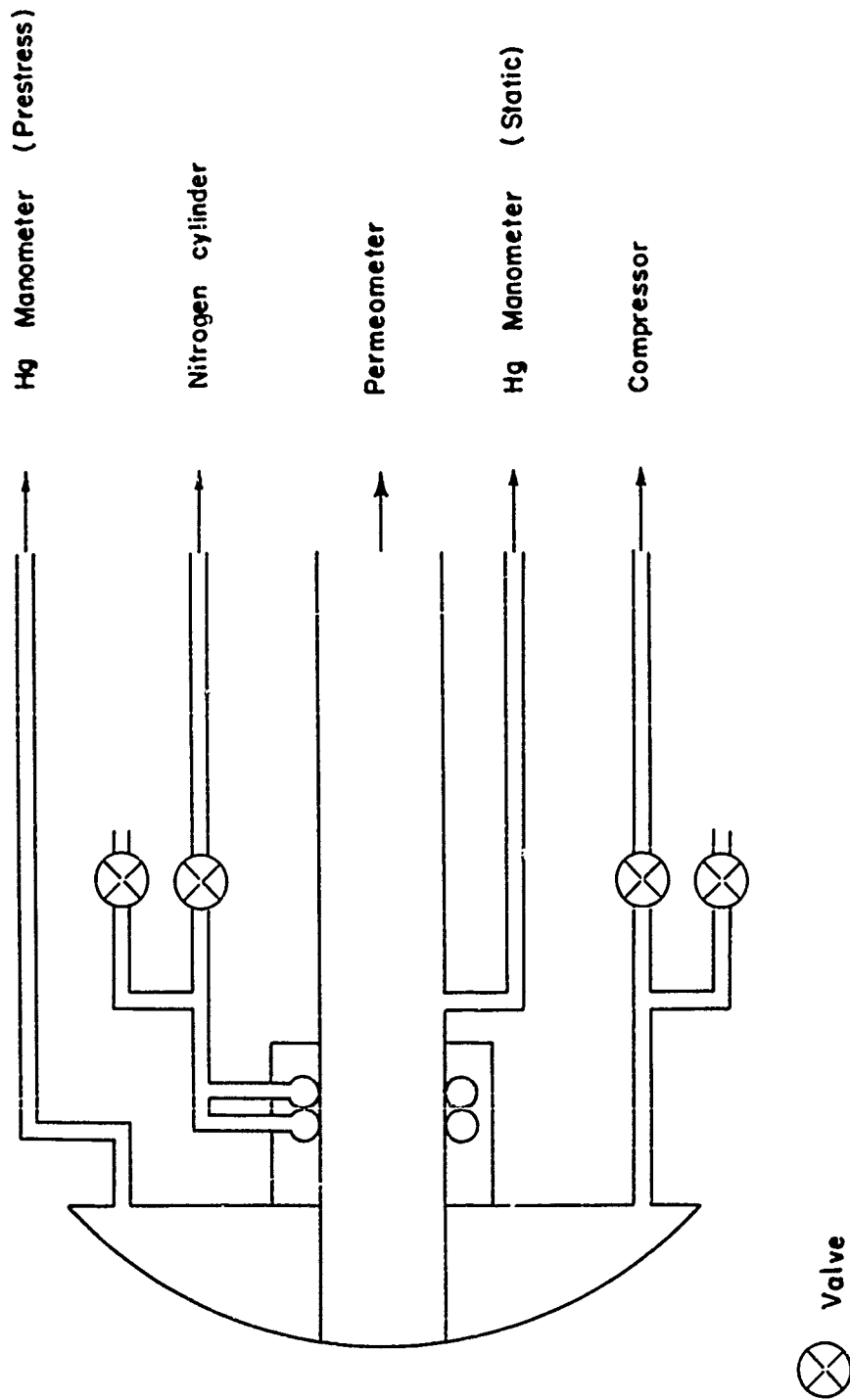
WADC TR 59-374

Hg Manometer (Prestress)

Nitrogen cylinder

Permeometer

Hg Manometer (Static)

Compressor

$\bigotimes$ Valve

Figure 29. Schematic of Prestressing Device
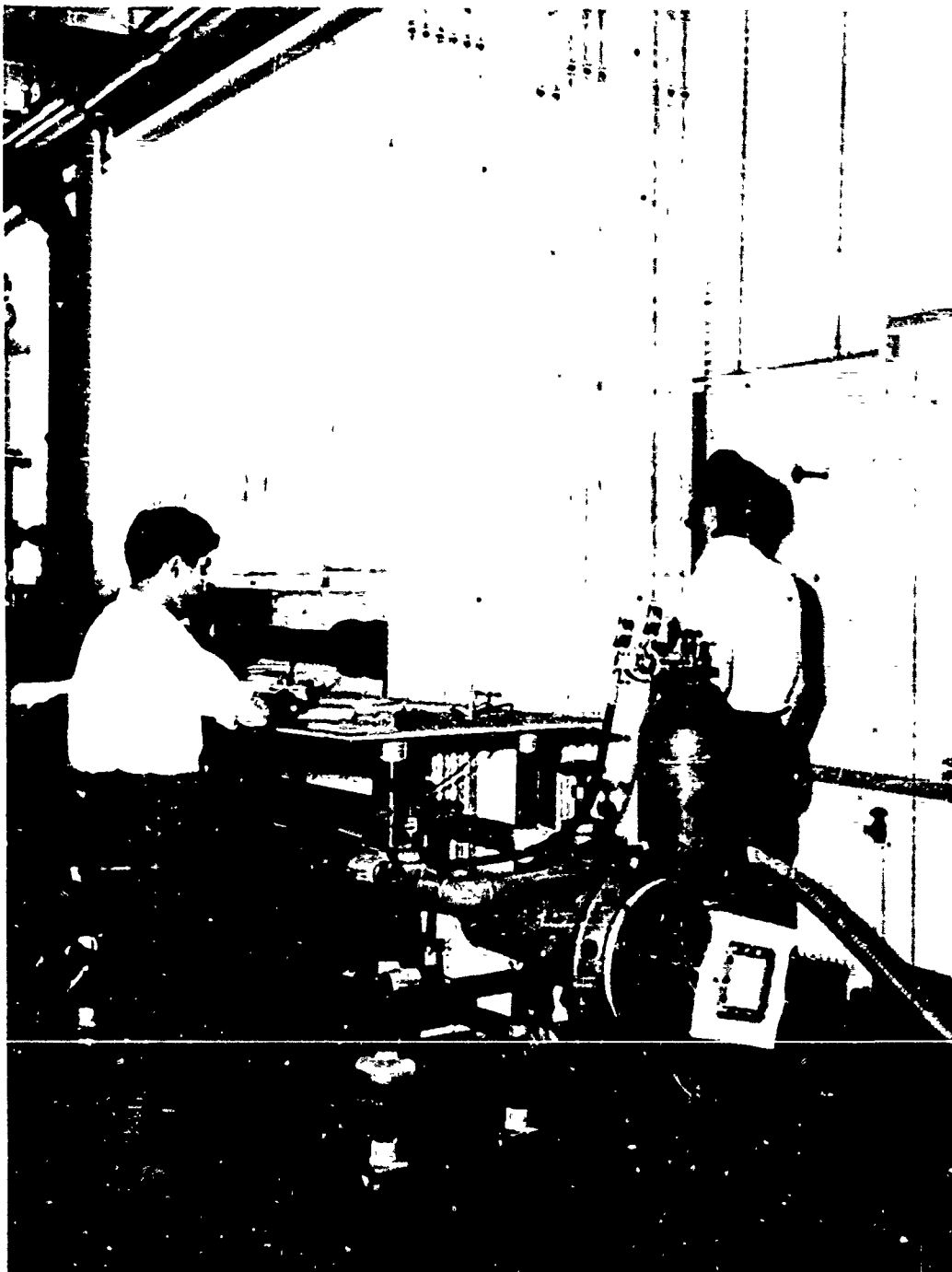
WADC TR 59-374

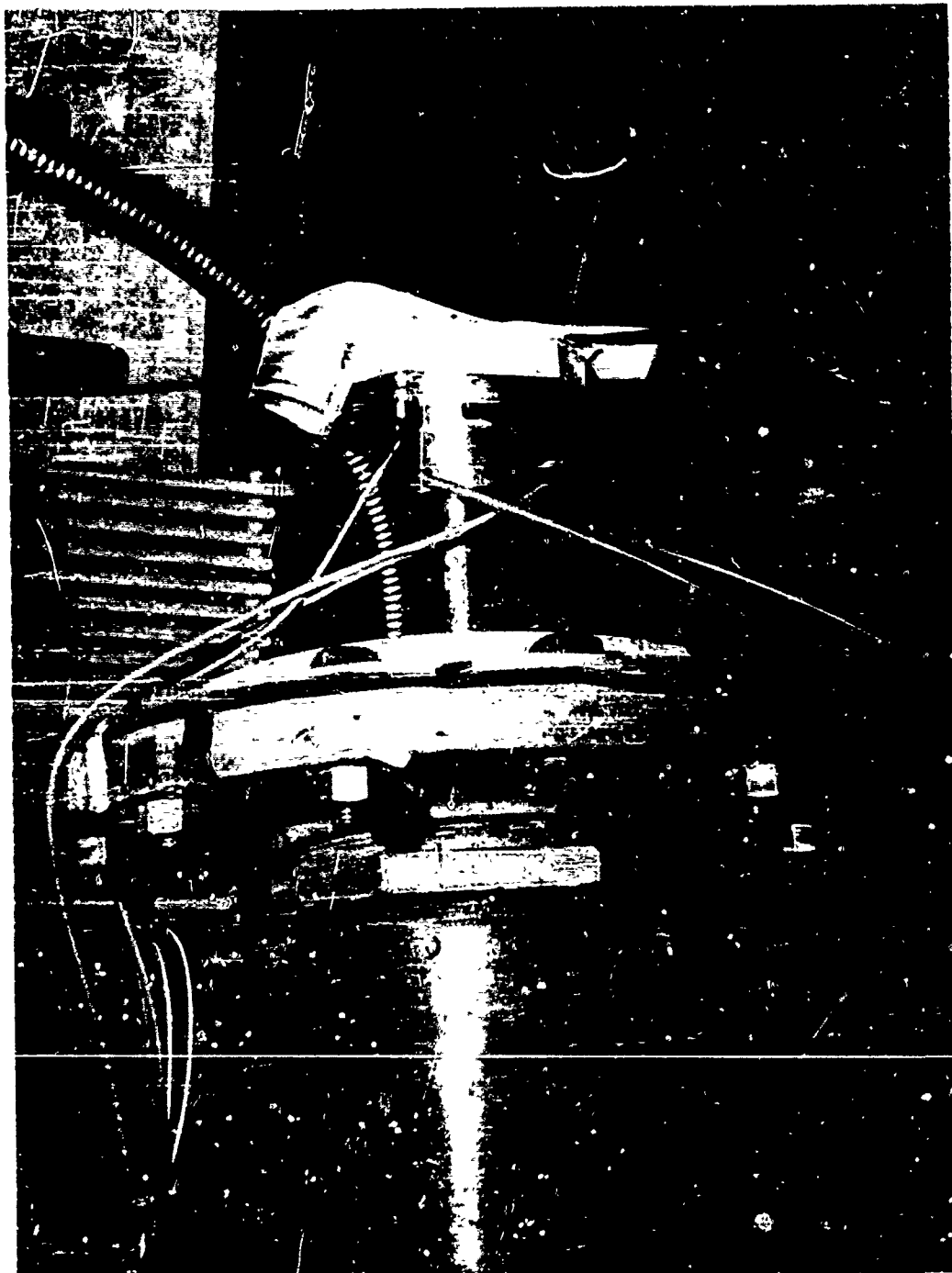FIGURE 30.   PHOTOGRAPH OF PERMEOMETER

WADC TR 59-374

73

FIGURE 31. CLOSE-UP OF PRESTRESSING DEVICE

were 1) fabric differential pressure, 2) differential pressure across orifices and 3) prestress pressure.

Three samples of each of the four fabrics under study were tested at the prestress levels of 3,6,9 and 12 lb/in^2. Flow measurements were taken at differential pressure increments until the prestress pressure was equalled. In inches of water these correspond to 82, 164, 248, and 330 inches respectively. Beyond this point the prestressing does not contribute any more to the fabric configuration and the permeability is the same as would be obtained in standard permeometer tests. Therefore, the permeability values at each prestress level are reported at intervals of differential pressures with the maxima stated above.

Test Results of Prestress Experiments

The test data are reported in Figures 32, 33, 34 and 35 in terms of volume flow versus pressure differential across the fabric. The curves marked 'a' refer to the unprestressed test the curves marked 'b', 'c', 'd', and 'e' refer to the tests run on samples prestressed as noted. In all four figures the 'Volume Flow' is calculated using the current method cited in Table 2 i.e. the quantity Q is plotted not Q'. To permit direct comparison of the results of this set of tests with those reported in WADC TR 57-443 and WADC TR 56-576 for this same permeometer the data must be converted from Q to Q', according to Equation (9) by multiplying by $\sqrt{\rho_i/\rho_s}$. The conversion factors over the range of differential pressures studied are plotted for convenience in Fig. 36.

Discussion of Prestress Data

All prestress permeability curves lie above the zero stress permeability curves for Fabrics S3, S6, S8 and E10. This confirms the general pattern portrayed in Fig. 27. The manner in which curves b,c,d, and e approach curve a in the data of Fabrics S3 and S8 demonstrates the fact that the 'zero prestress' condition does in fact involve fabric stress and the apparent permeability, Q'' is actually a projection of the true permeability curve on the Q vs. Δp plane.

It was observed that the prestress permeabilities showed small variability for tests at low pressure differentials. Here too, the prestressed permeabilities ran from 50 to 100% higher than the

WADC TR 59-374

75

Figure 32. Volume Flow vs. Differential Pressure Sample S-3
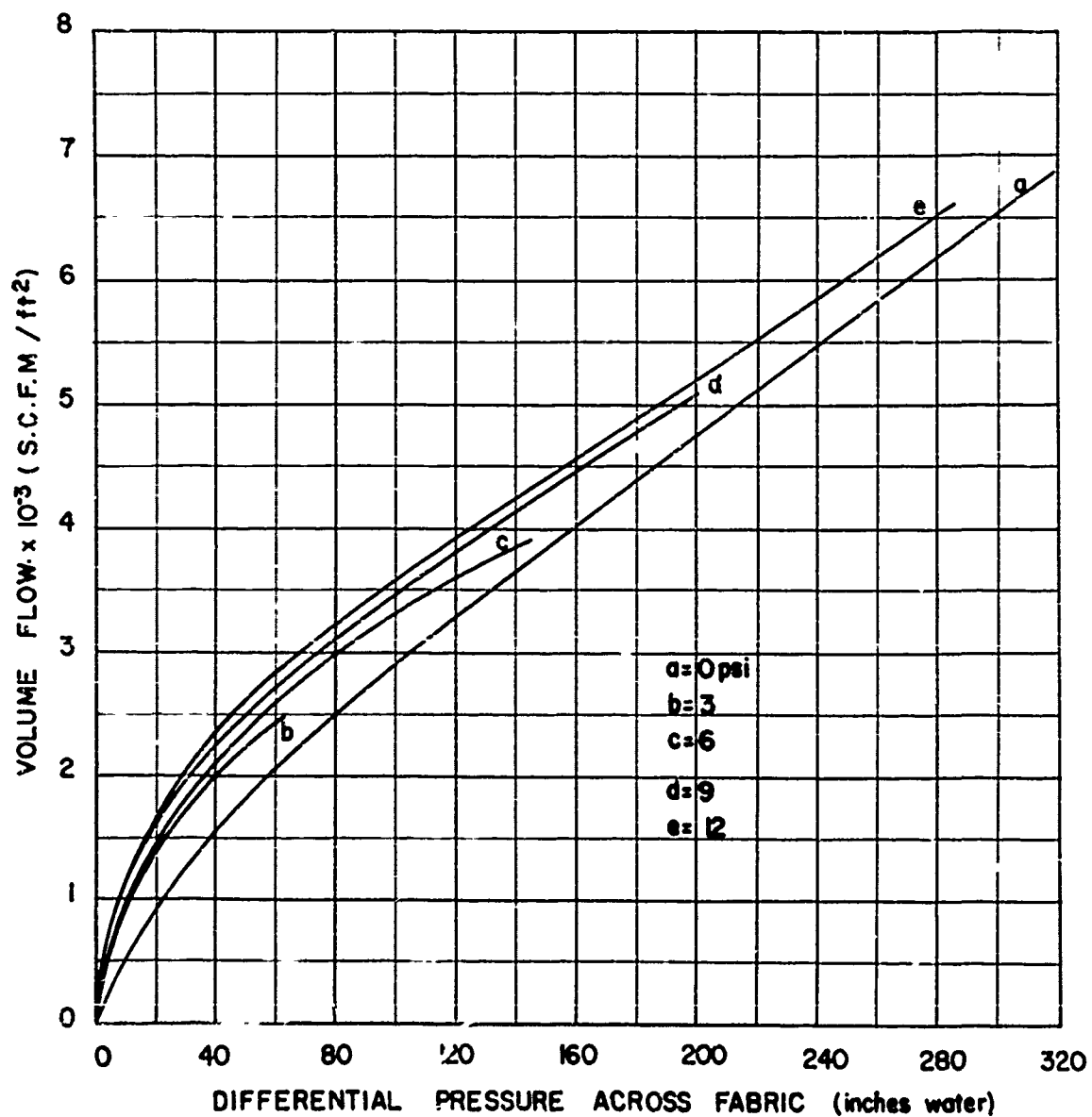
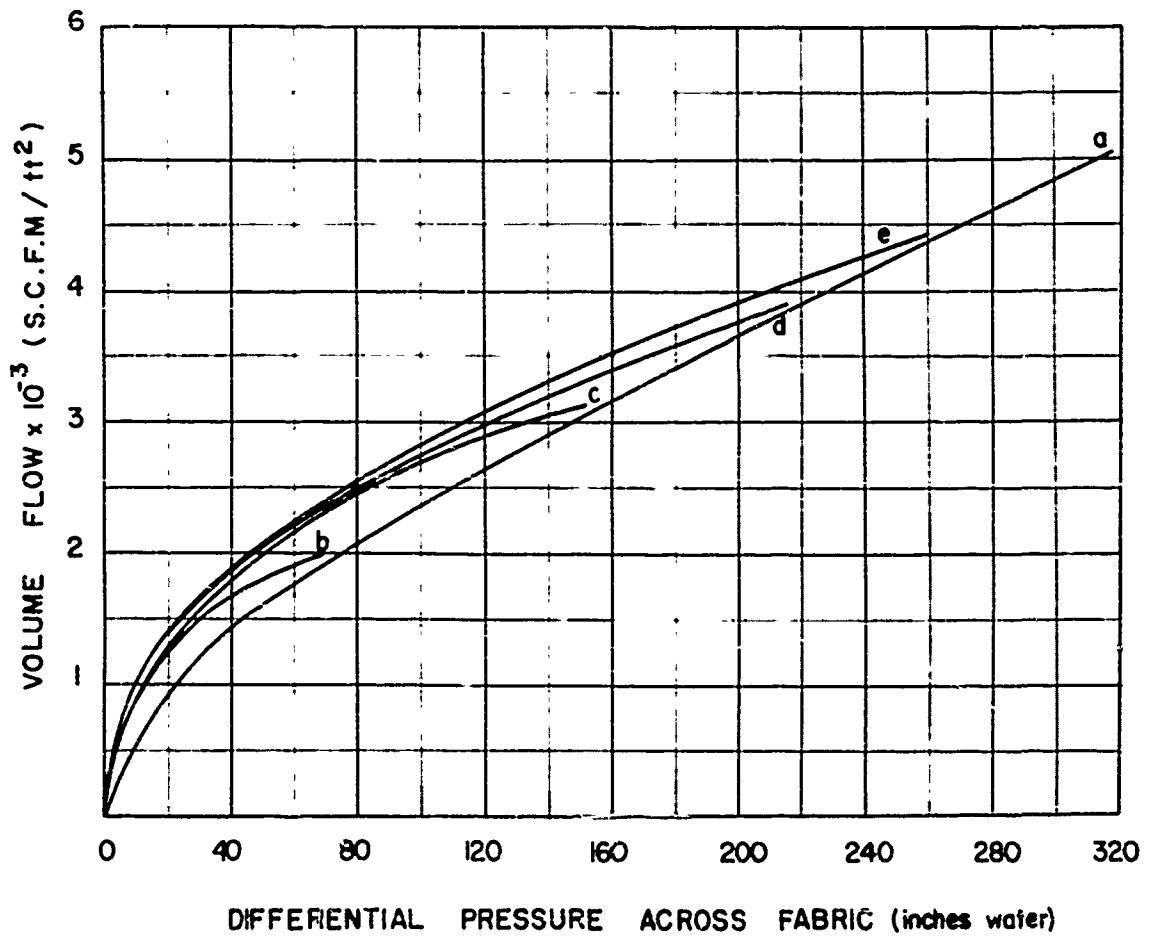Figure 33. Volume Flow vs Differential Pressure. Sample S-6

Prestress: a = 0 psi
b = 3
c = 6
d = 9
e = 12

Figure 34. Volume Flow vs. Differential Pressure. Sample S-8

Prestress: a = 0 psi
            b = 3
            c = 6
            d = 9
            e = 12

WADC TR 59-374

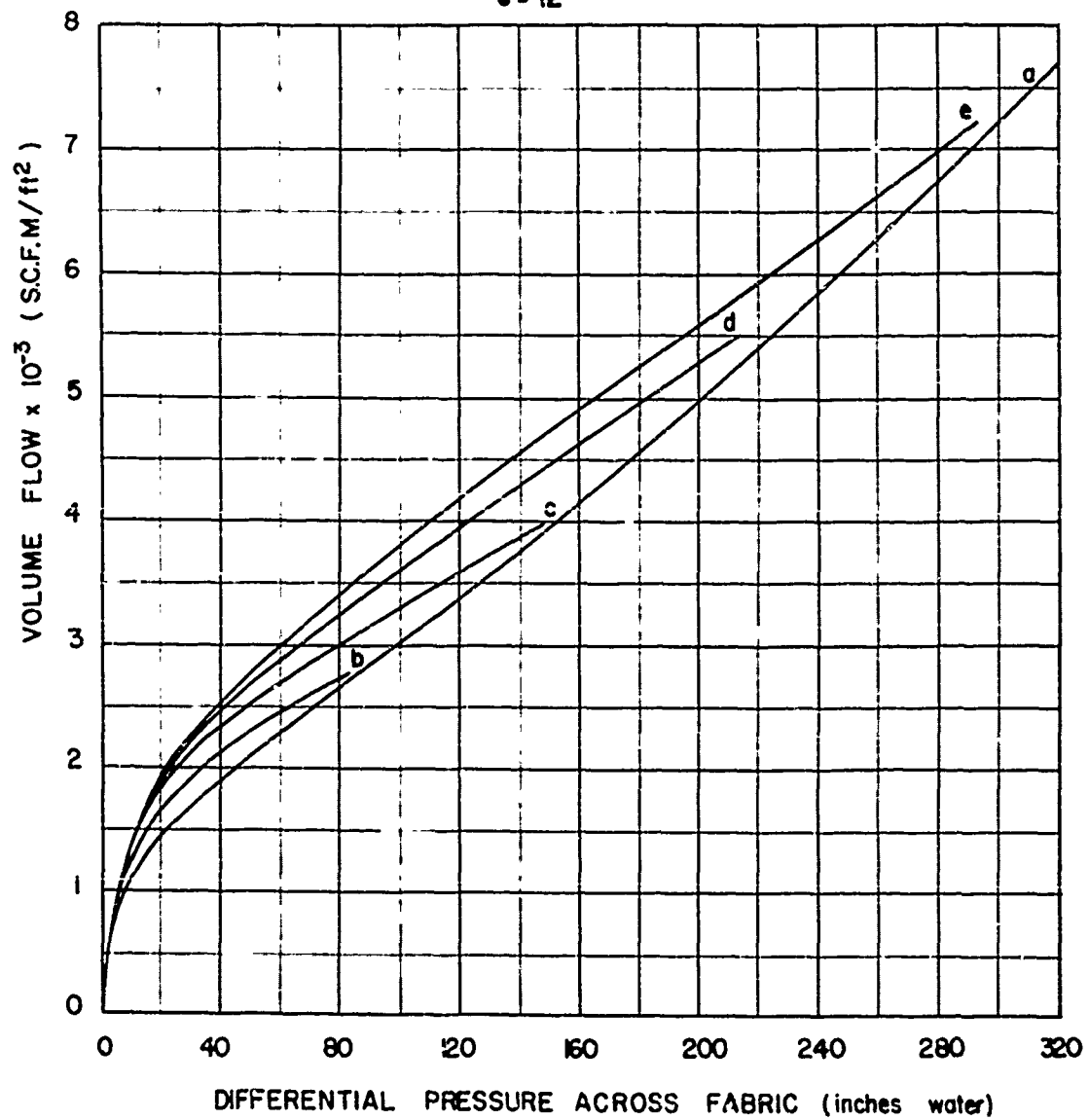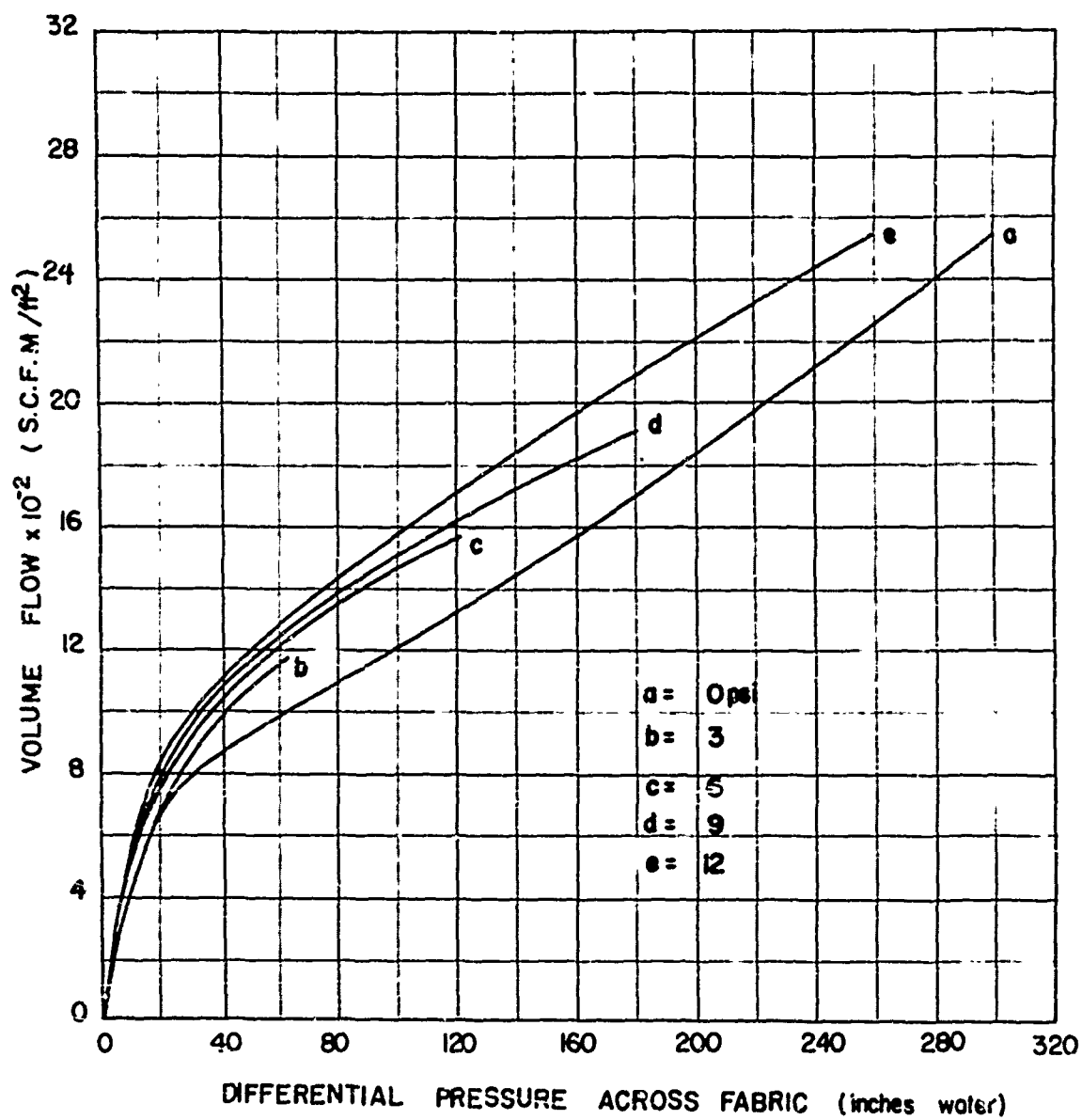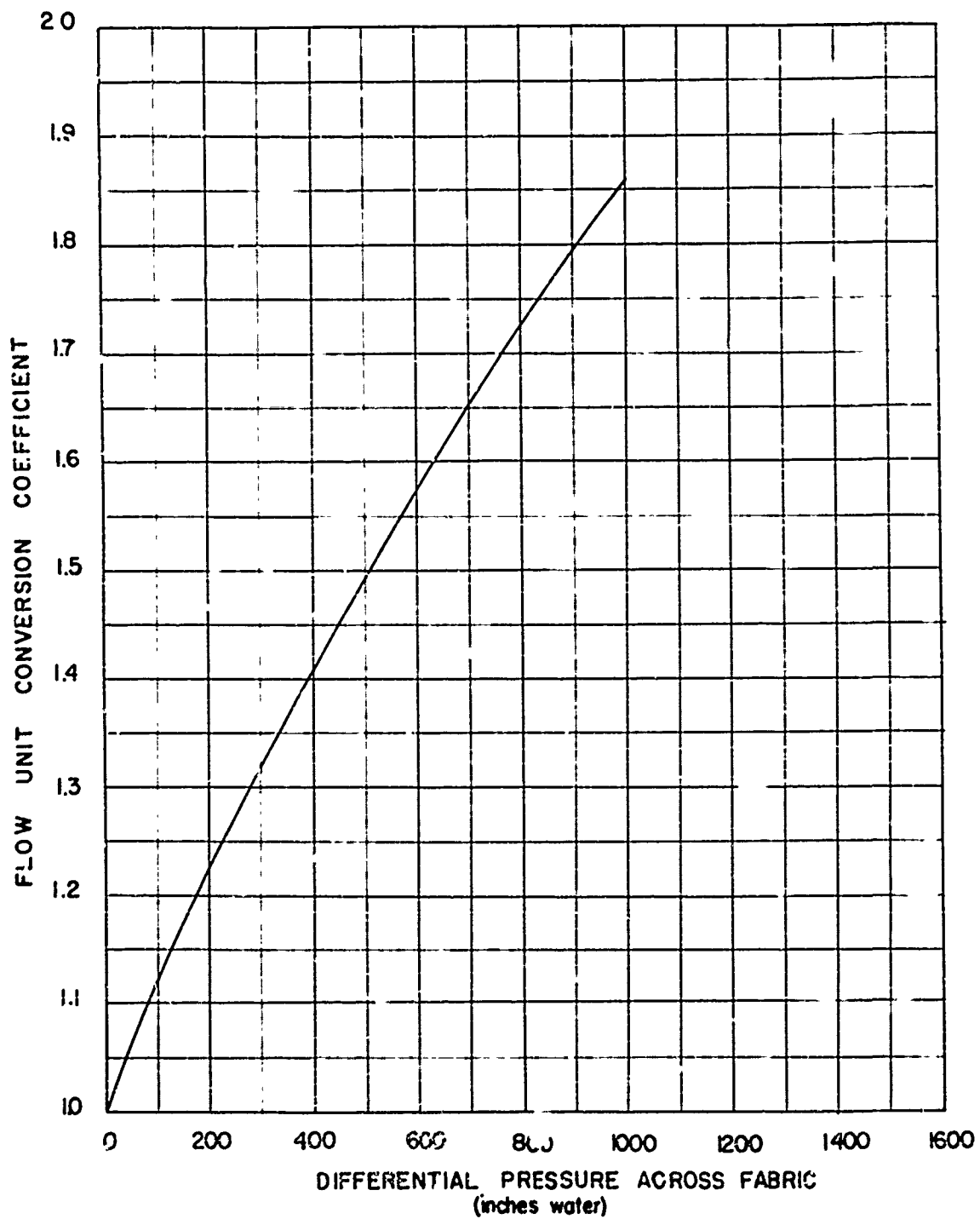Figure 35. Volume Flow vs. Differential Pressure. Sample E-10

Figure 36. Flow Conversion Coefficient vs. Differential Pressure

WADC TR 59-374

80

'unprestressed' values, indicating the importance of local fabric distortions in determining actual air flow behavior. At higher pressure drops the prestress data becomes more erratic and it is questionable whether the last third of each prestress curve has other than heuristic value. Further comment on the prestress permeability behavior of the test fabrics will be reserved for the discussions of cloth geometry and biaxial stress-strain behavior.

Tests on Field Prestressed Specimens (Aged)

The Textile Branch at WADC furnished cloth canopy sections taken from parachutes which had been jumped 6 times and 13 times respectively. The material of the canopies was Fabric S8. Three samples of each 'mechanically aged' group were tested on the permeometer. Flow at differential pressures up to 300 inches in H_2O was measured for the unaged S8, the 6 jumps canopy and the 13 jump canopy. The prestressing device was used without prestress pressures. In Fig. 37, the Volume Flow, Q is plotted against Differential Pressure for all three material states. The data was closely bunched around the average curve (solid line) within bounds of the dotted curves. There was no consistent trend towards an increase in permeability with increasing number of jumps, therefore, the data was simply grouped within the relatively narrow limits of the dotted curves. In short, there is no evidence in the samples tested that 6 and 13 jumps significantly alter the air permeability of the fabric S8.

Figure 37. Volume Flow vs Differential Pressure Sample S-3 (aged)
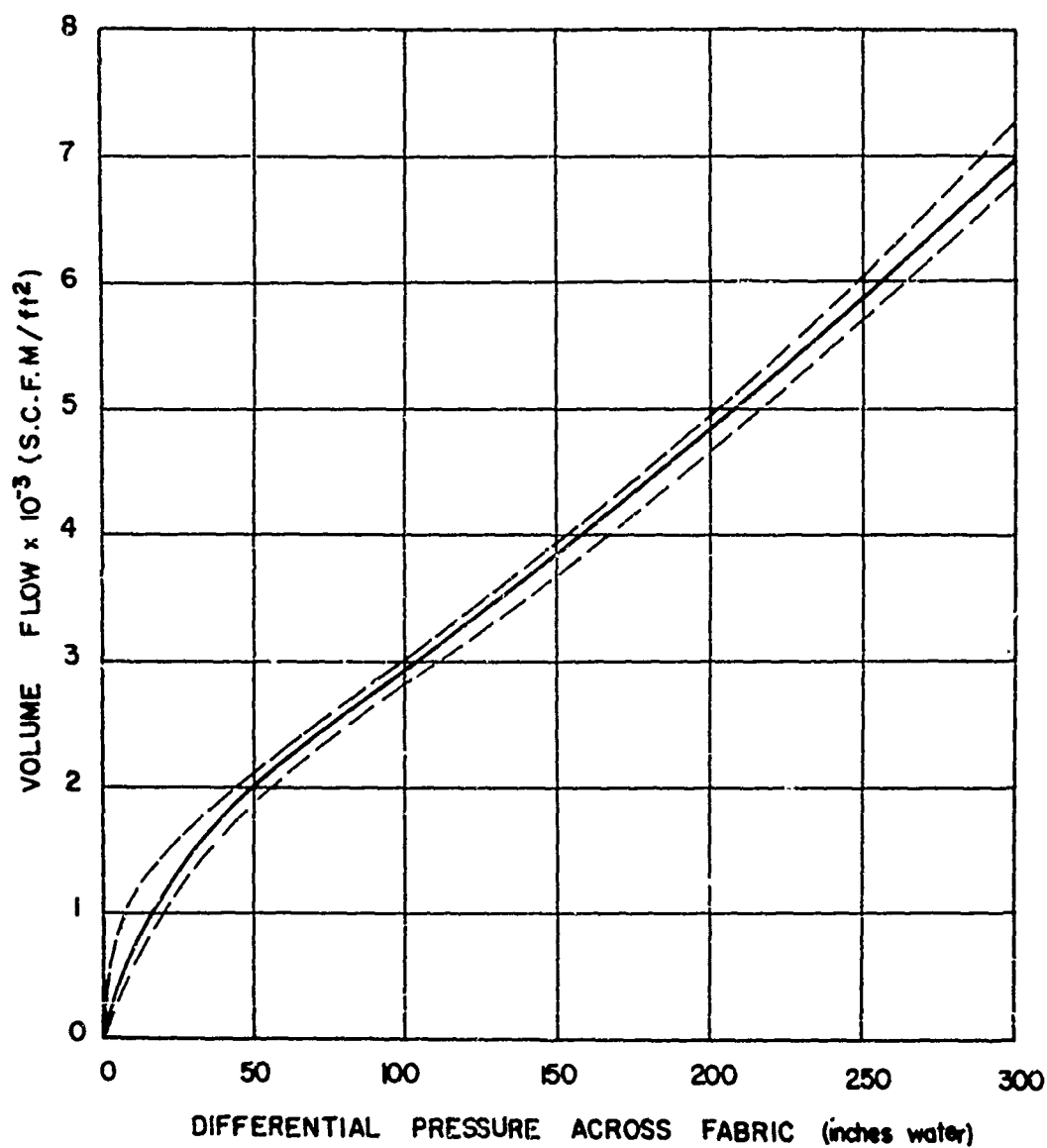
Fabric Stresses During Air Flow Measurements

The build-up of planar stresses in a textile fabric subjected to a pressure drop (exerted normal to the cloth plane) depends on the properties of the material and on the geometry of the specimen jaw. There is no guarantee that stresses in warp and filling yarns will be equal simply because the specimen jaw is either square, or circular. Material specifications list the properties of parachute cloth as balanced in warp and filling directions. But there is no control exerted on the crimp in warp and filling yarns and frequently fabrics balanced in all other aspects, are unbalanced in crimp as a result of weaving tensions or subsequent finishing techniques. Where crimp unbalance exists, the stress build-up in a square jaw (such as that used on the M.I.T. permeometers) differs between warp and fillings.

The build-up of fabric stress will also vary across the specimen in a given jaw with the cloth in the center of the square subjected to a biaxial stress and the cloth at the sides of the square subjected to uniaxial stress. This distribution of stresses was measured and reported in WADC TR 57-443 (3). It was to avoid this varied stress condition that the 'membrane-oriifce' was developed and used to restrict airflow measurements to the biaxially stressed center-square-inch of the fabric specimen.

Measurements of stress build-up at the center of the specimen during airflow were found to duplicate those stresses which developed at the center of a hydrostatically loaded specimen. Thus, by utilizing a full membrane instead of the 'membrane-orifice' both stress build-up and strain measurements could be taken with complete control of the conditions at the center of the specimen.

Once the stress build-up in warp and filling was determined for the hydrostatic condition, together with accompanying strains, it remained to reproduce these same conditions on a more versatile biaxial test unit. Such a unit was designed and constructed in the Textile Division and it permitted application of stress embedding techniques for close internal examination of stressed fabrics. For the fabrics stressed under the hydrostatic condition only surface photographs and measurements were possible. For the stress-embedded case, cross-sectional photographs were possible and permitted a three dimensional view of pore and yarn distortion under stress conditions corresponding to actual loading in the permeometer.

This section presents the results of hydrostatically induced stress-strain measurements and mechanically induced biaxial-stress tests.

WADC TR 59-374

Hydrostatic Tests

Test Apparatus. The equipment used in the static tests consisted of jaws, pressure system, strain gage recorder, and photographic equipment.

The jaws used for the tester are similar to those described earlier in WADC TR 57-443 and are equipped with strain gage lead cells, mounted on split jaw sections lying in two orthogonal directions, as well as initial angle measuring devices. In the case of the present test, the jaw assembly has been removed from the permeometer and has been mounted in a closed pressure system test stand (see Fig. 38). A thin rubber membrane (.010 thick) has been mounted across the entire face and provides complete sealing between pressure system and fabric. Because of the low modulus of the thin membrane the load is effectively taken up by the fabric sample itself.

The pressure system consists of a nitrogen tank reduction and control valves, associated connection levers, and a mercury manometer capable of a 36 psig. range. The output of the split jaw load cells was fed into a two channel Sanborn recorder enabling continual observation of fabric load development due to pressure change, fabric relaxation and creep. A Hasselblad, 1000 F. single lens reflex was used with 6 mm close up rings enabling 1:1 reproduction of 1" gage lengths in both warp and fill direction. A darkroom enlarger was used to further magnify the negatives enabling total magnification of 6X.

Test Procedure. A square 9" x9" was cut and correctly marked for type and thread direction. A template was used to outline mounting holes which were then burned in with the use of a soldering iron (this method produces fusing of the dacron or nylon material surrounding the hole and strengthens the mounting area). Orthogonal lines in warp and fill direction were drawn to indicate the center of the test section. Black plastic adhesive tape was cut in small strips and attached to the sample so as to provide well defined one inch gage lengths at the center of the sample. A small piece of graph paper indicating sample number and warp direction was rubber cemented near the center of the sample. This graph paper served as identification and calibration for all subsequent strain measurement made from the enlarged negatives.

The sample was centered over the rubber membrane and the jaws were secured. Care was taken to keep the warp and fill directions in line with the split jaw edges, while at the same time removing all slack from the sample. Although no pre-tension device is used
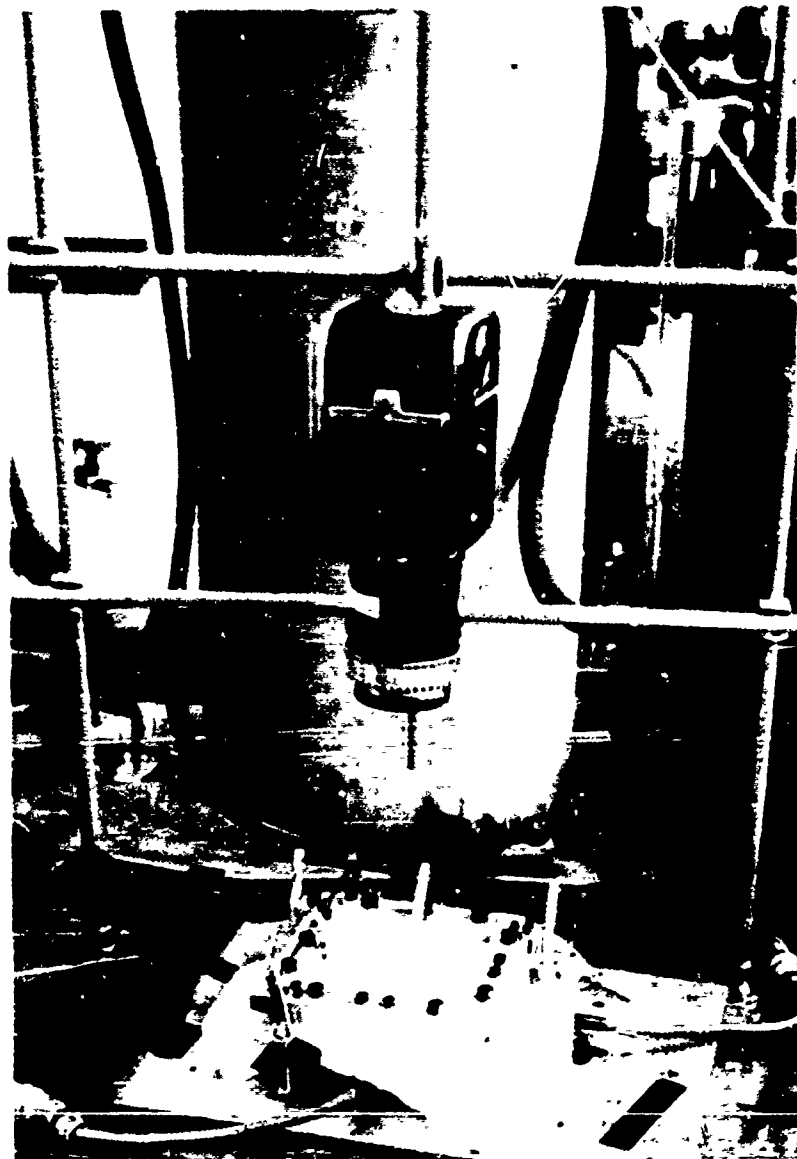
WADC TR 59-374

84

FIGURE 38.   CLOSED PRESSURE SYSTEM
TEST

WADC TR 59-374

in mounting. operator experience soon permitted fairly uniform loading technique. Once the sample was mounted, the angle measuring device was set at the zero position. This device was slightly pretensioned with the use of soft elastic thread. In the final mounted position, a 4" x 4' area is exposed to air pressure. The actual procedure follows:

1. Initial gage lengths were photographed in both an unmounted and mounted position.

2. The Sanborn recorder was balanced, calibrated, and a correct scale chosen.

3. The system was pressurized and the fabric was allowed to relax until the Sanborn indicated a constant load in both warp and fill directions.

4. At this point, pressure, center deflection and angle measurements were recorded. In addition a strain photograph was taken.

This entire procedure was then repeated at a series of increased pressure levels. In all cases data was taken at 3, 6, 9 and 12 p.s.i.g., and in addition at varied points up to the breaking load of the particular sample.

Test Program and Results. The four different fabrics tested over a wide range of pressures were:

Test	M.I.T. Code	Figure No.	MIL Spec
1	S6	39, 40	MIL C-8021A T2
2	E10	41, 42	
3	S3	43, 44	MIL C-7350B T1
4 (a)	S8	45, 46	MIL C-25174 T2
(b)	S80A.1	47, 48 WADC	Code 27-20-78
(c)	S80A2	49, 50 WADC	Code 27-20-76

In the case of tests 1, 2, 3, and 4a the samples were new. Samples 4b and 4c were identical to 4a but came from sections of parachutes that had been jumped 13 and 6 times respectively. In all cases at least three samples were tested of each type of fabric. In some instances further tests were performed to provide additional information.

WADC TR 59-374
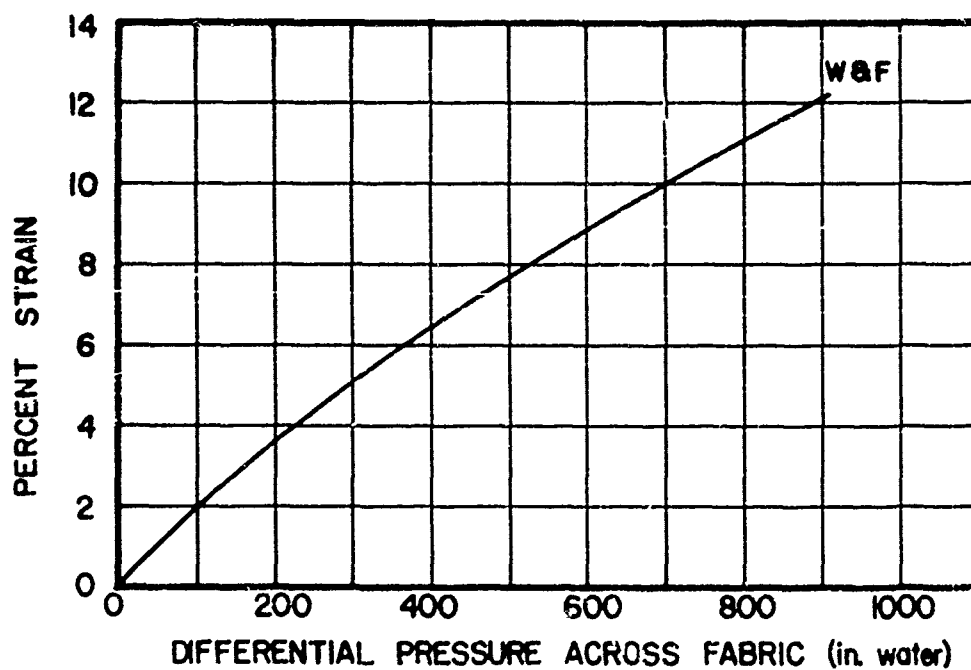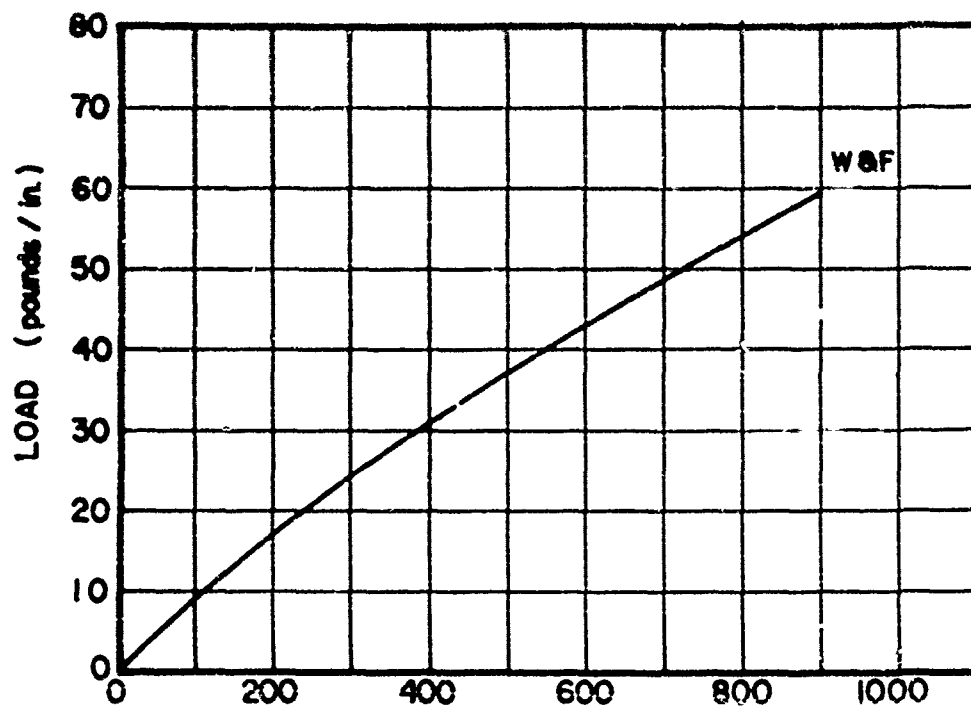
SAMPLE: S-6

Figure 39. Load and Strain vs. Pressure. S-6.

WADC TR 59-374
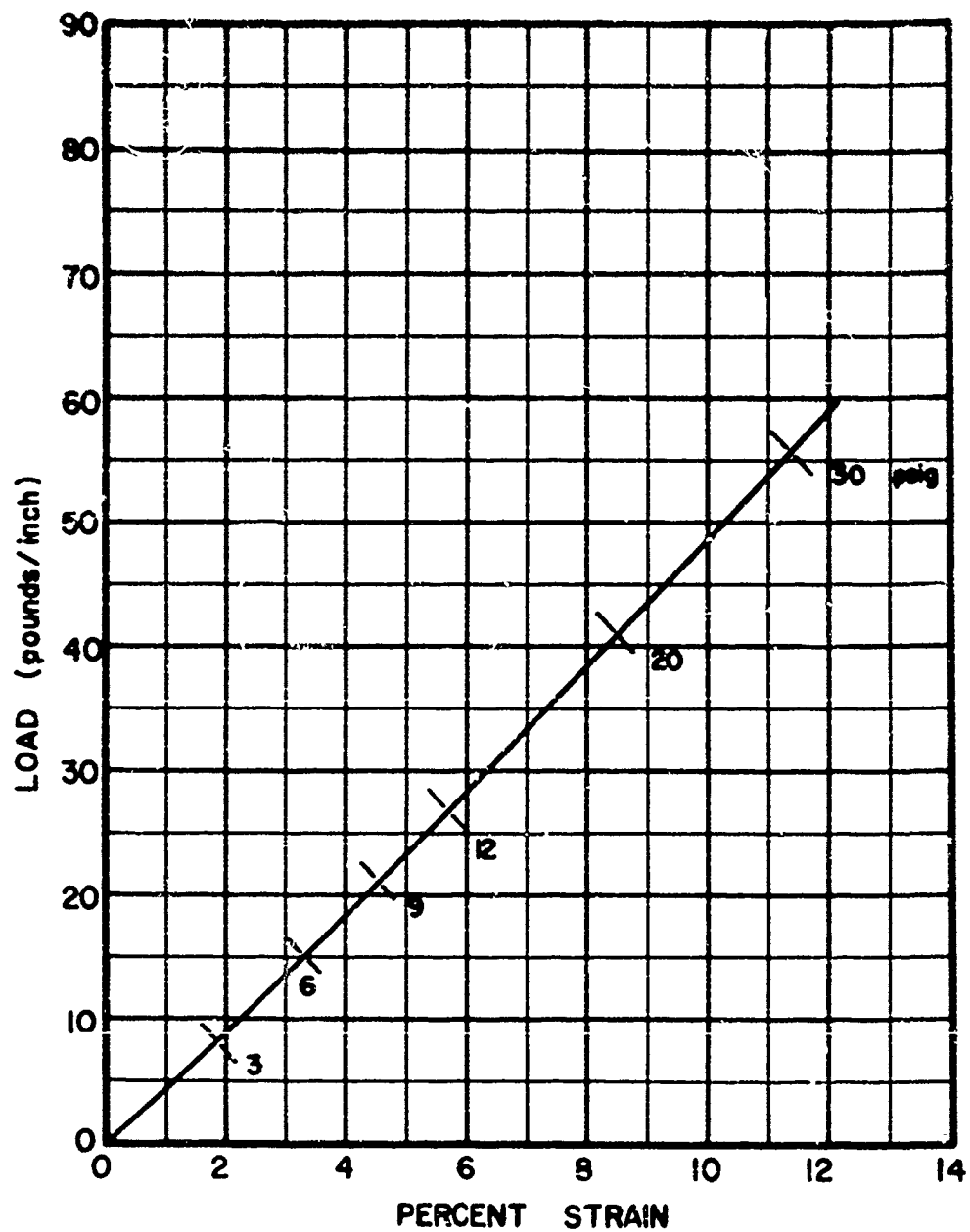
Figure 40. Load vs. Strain. S-6
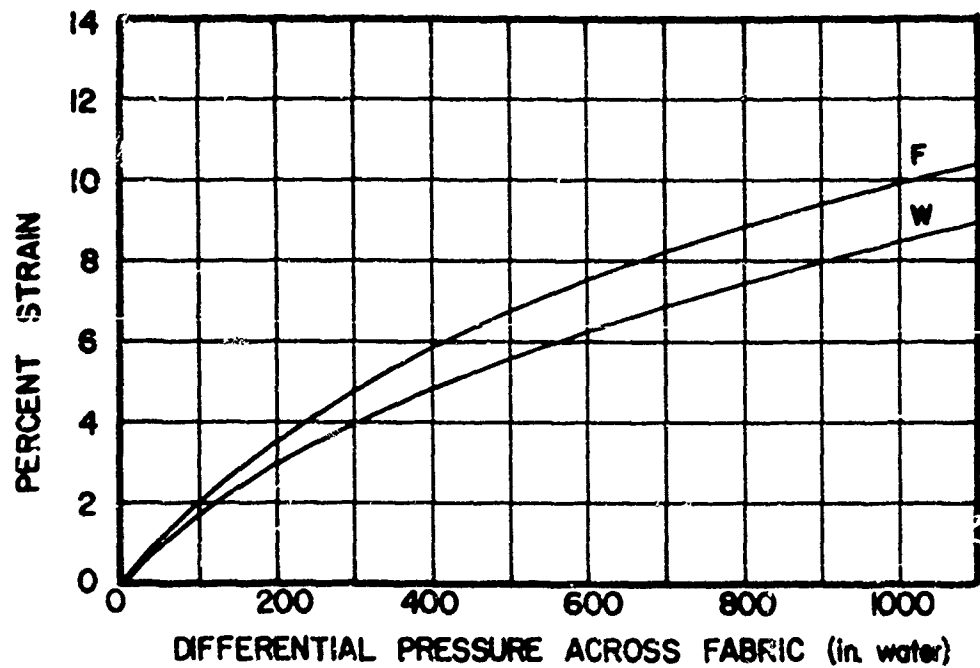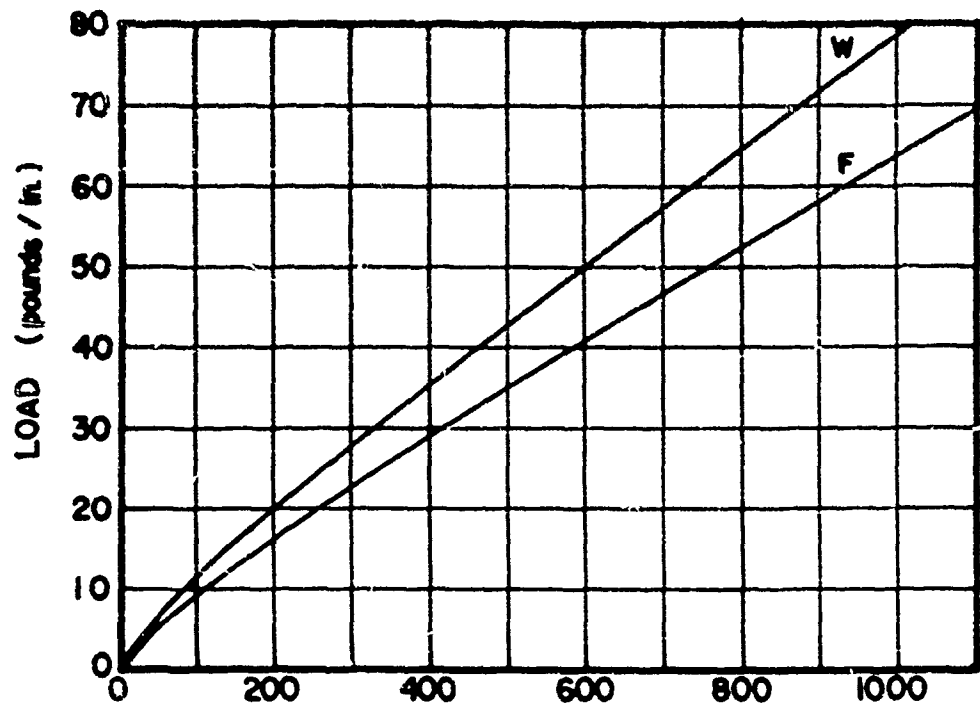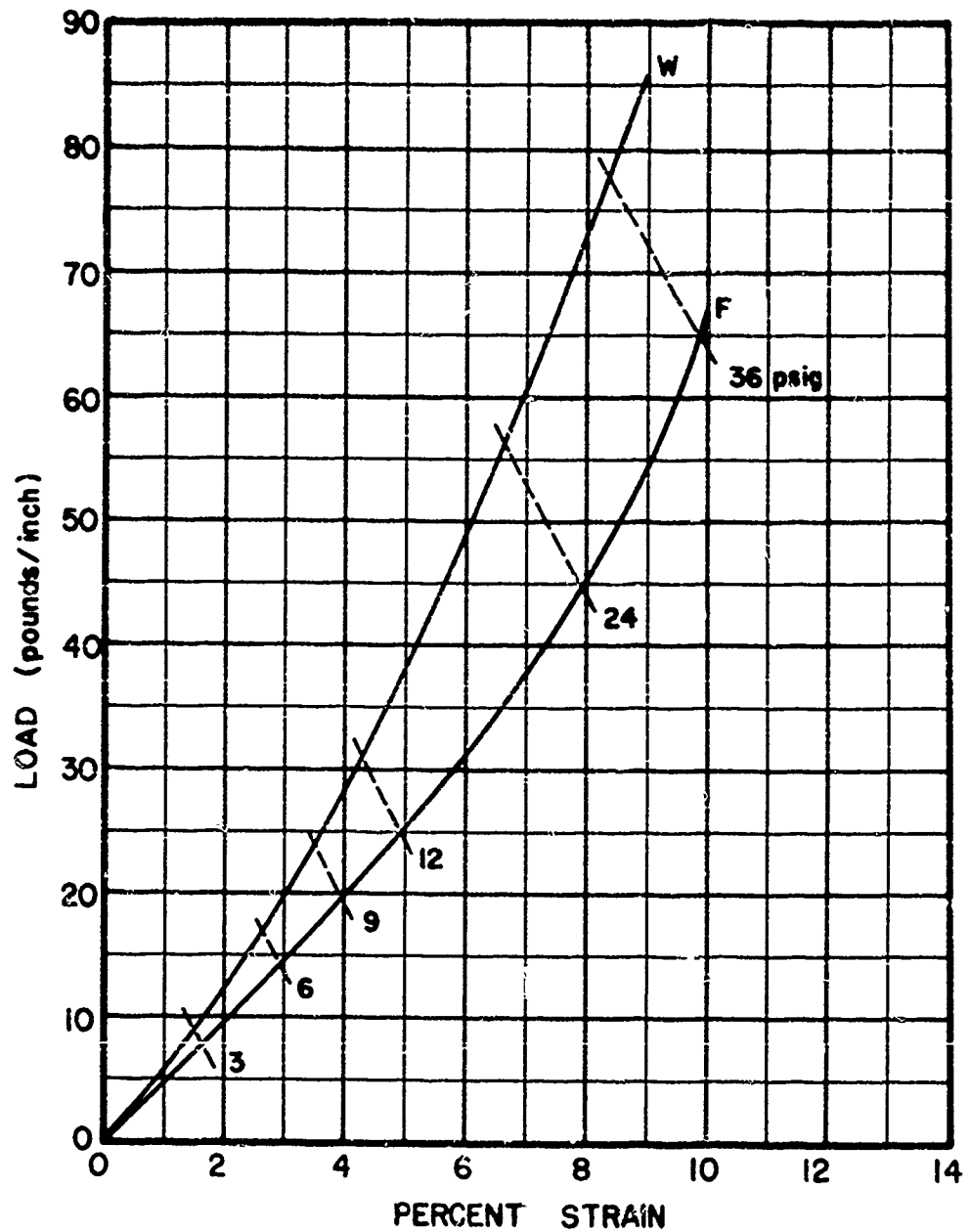
Figure 41. Load and Strain vs. Pressure. E-10

WADC TR 59-374

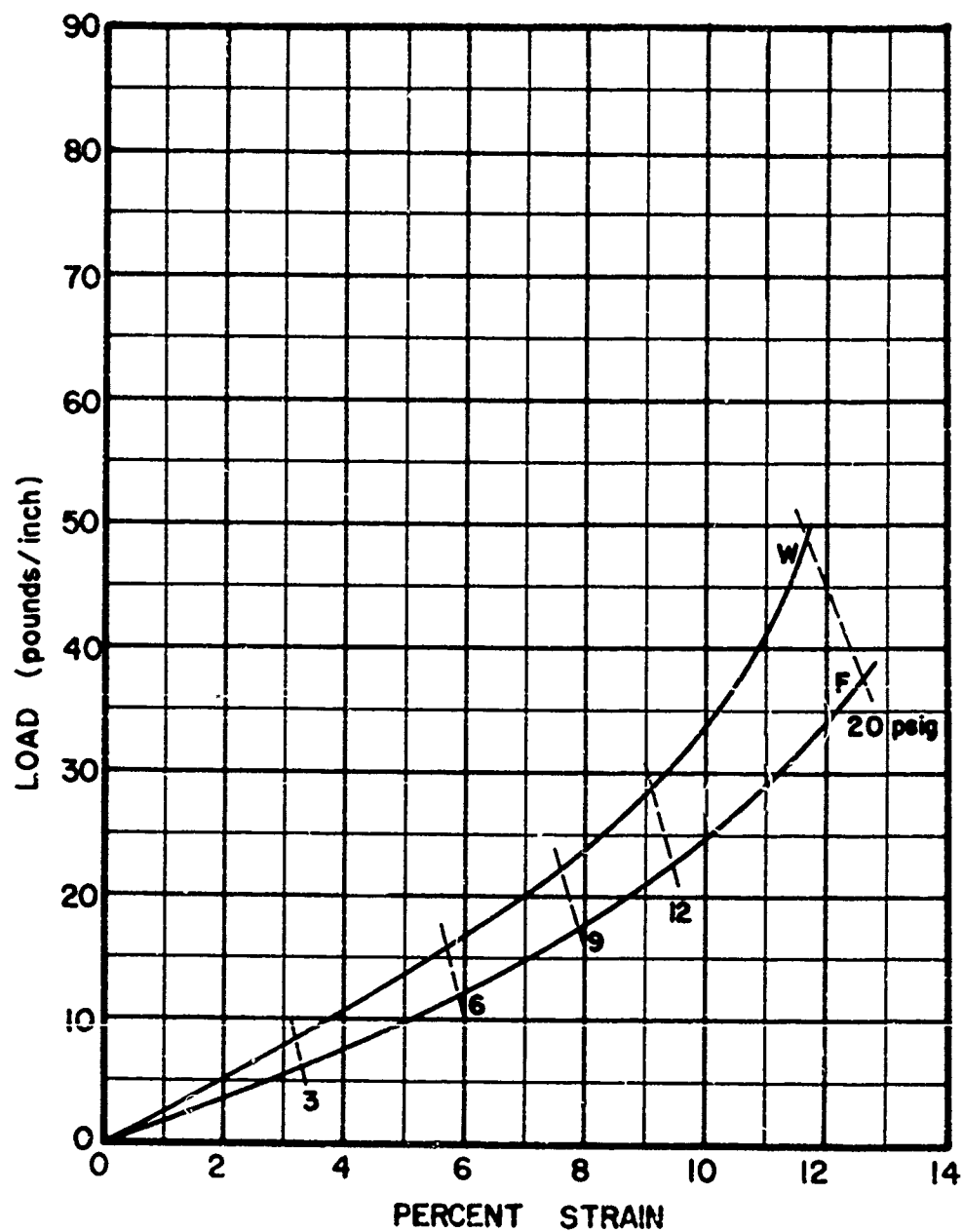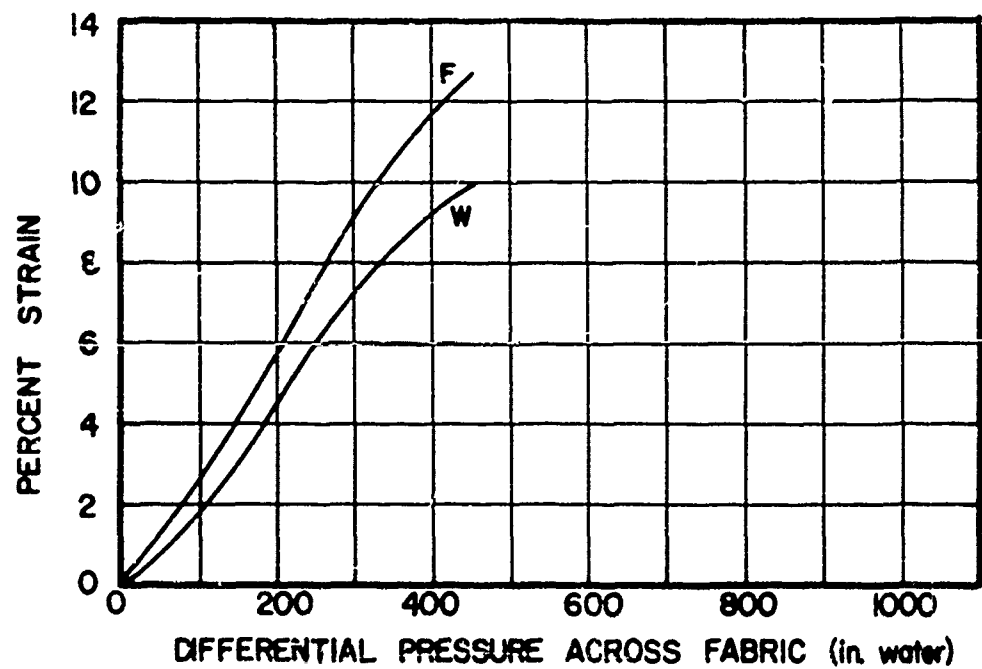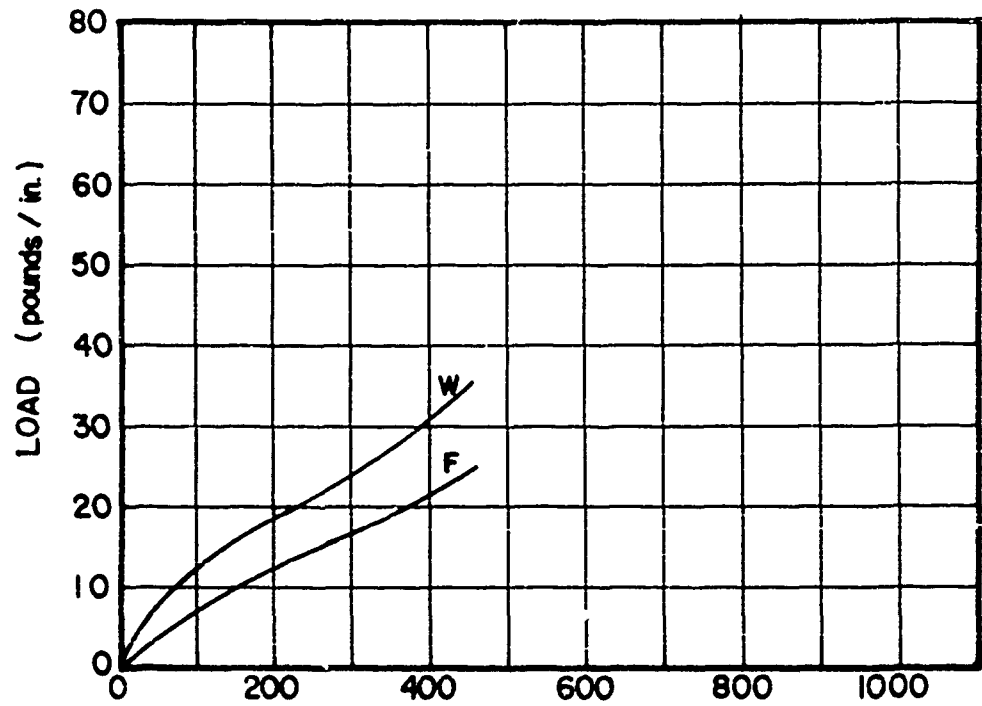Figure 42. Load vs Strain. E-10
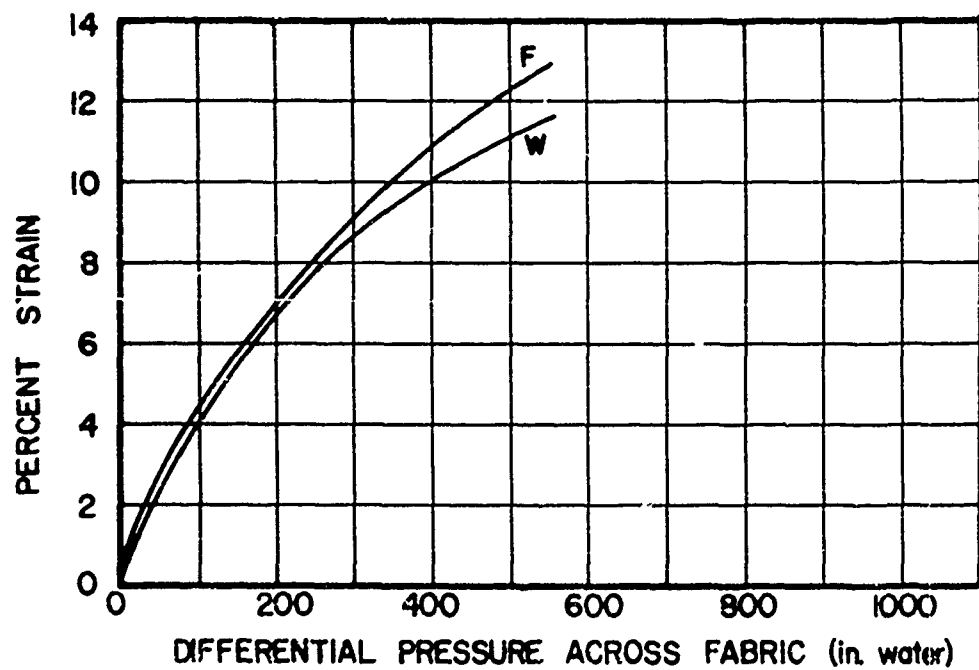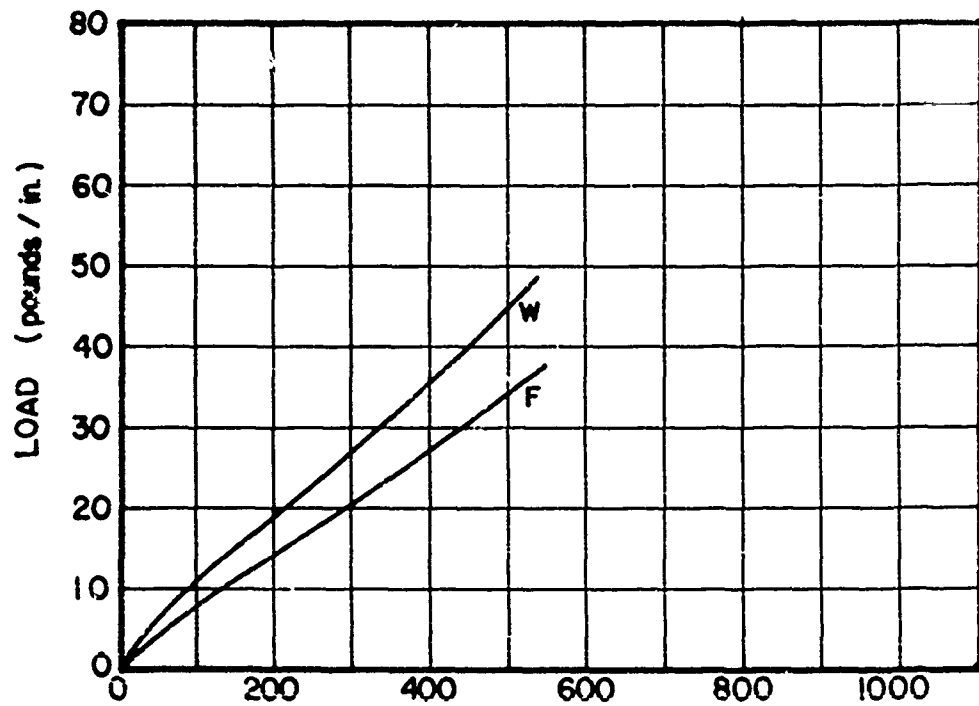
Figure 43. Load and Strain vs. Pressure. S-3

Figure 44. Load vs Strain. S-3

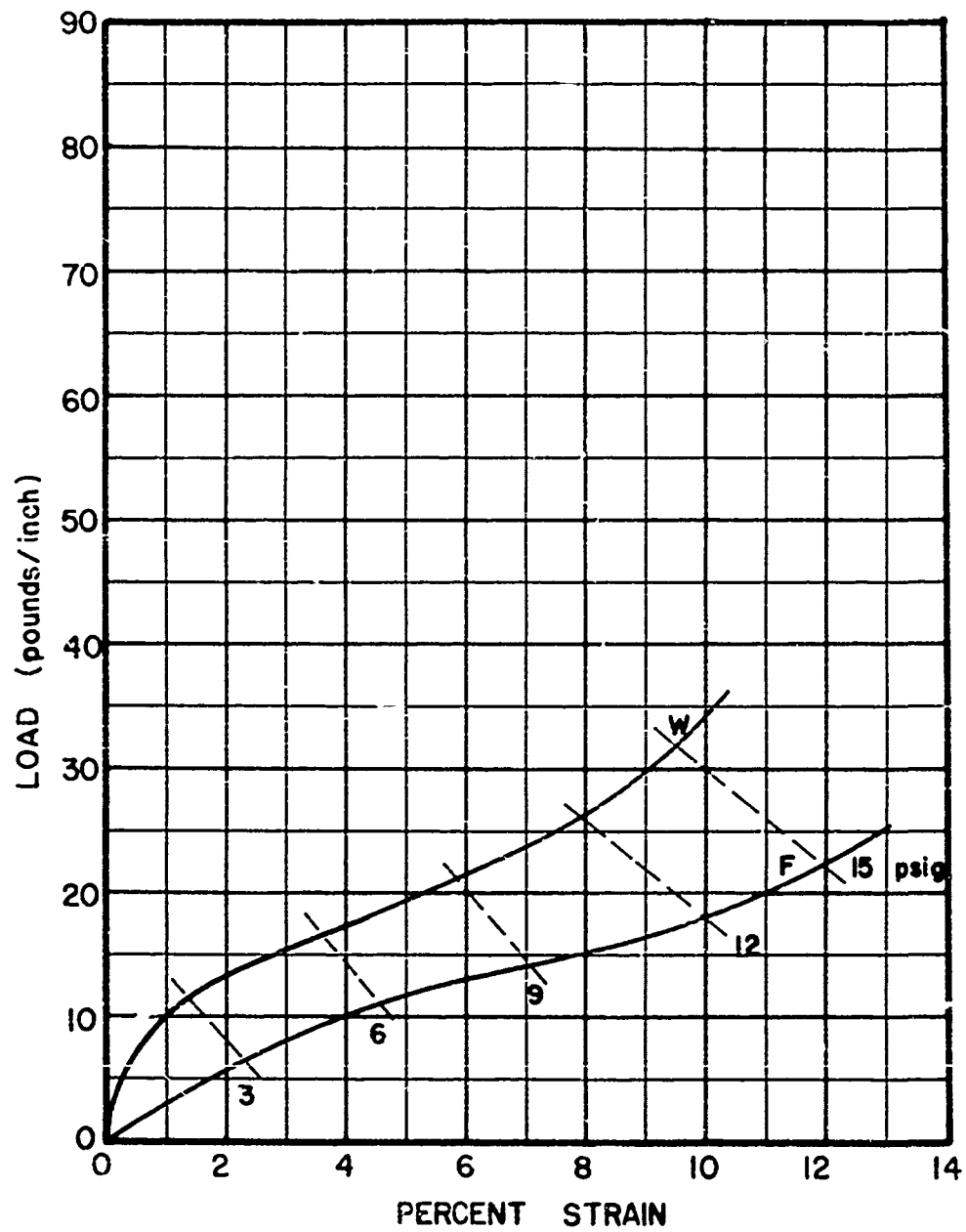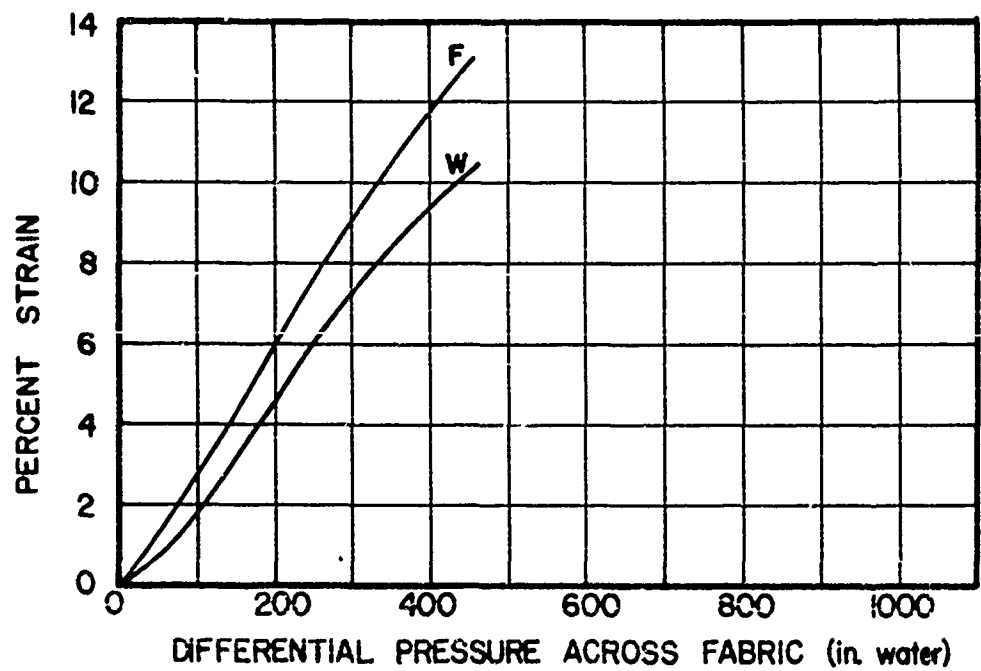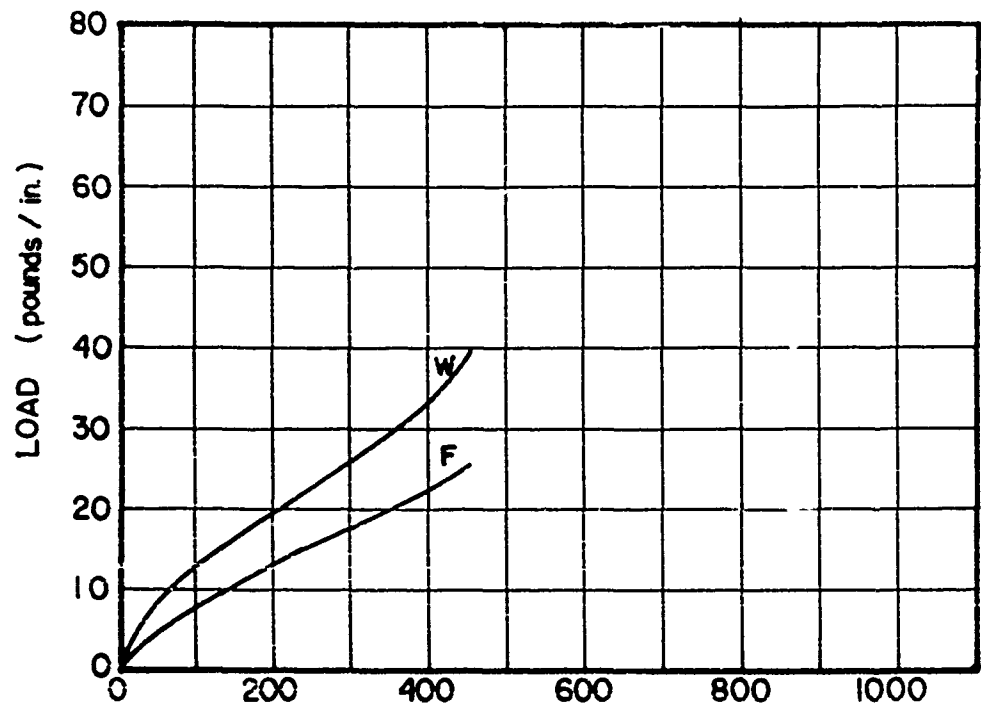Figure 45. Load and Strain vs. Pressure. S-8

WADC TR 59-374

Figure 46.   Load vs Strain. S-8

Figure 47. Load and Strain vs. Pressure. S-80AI
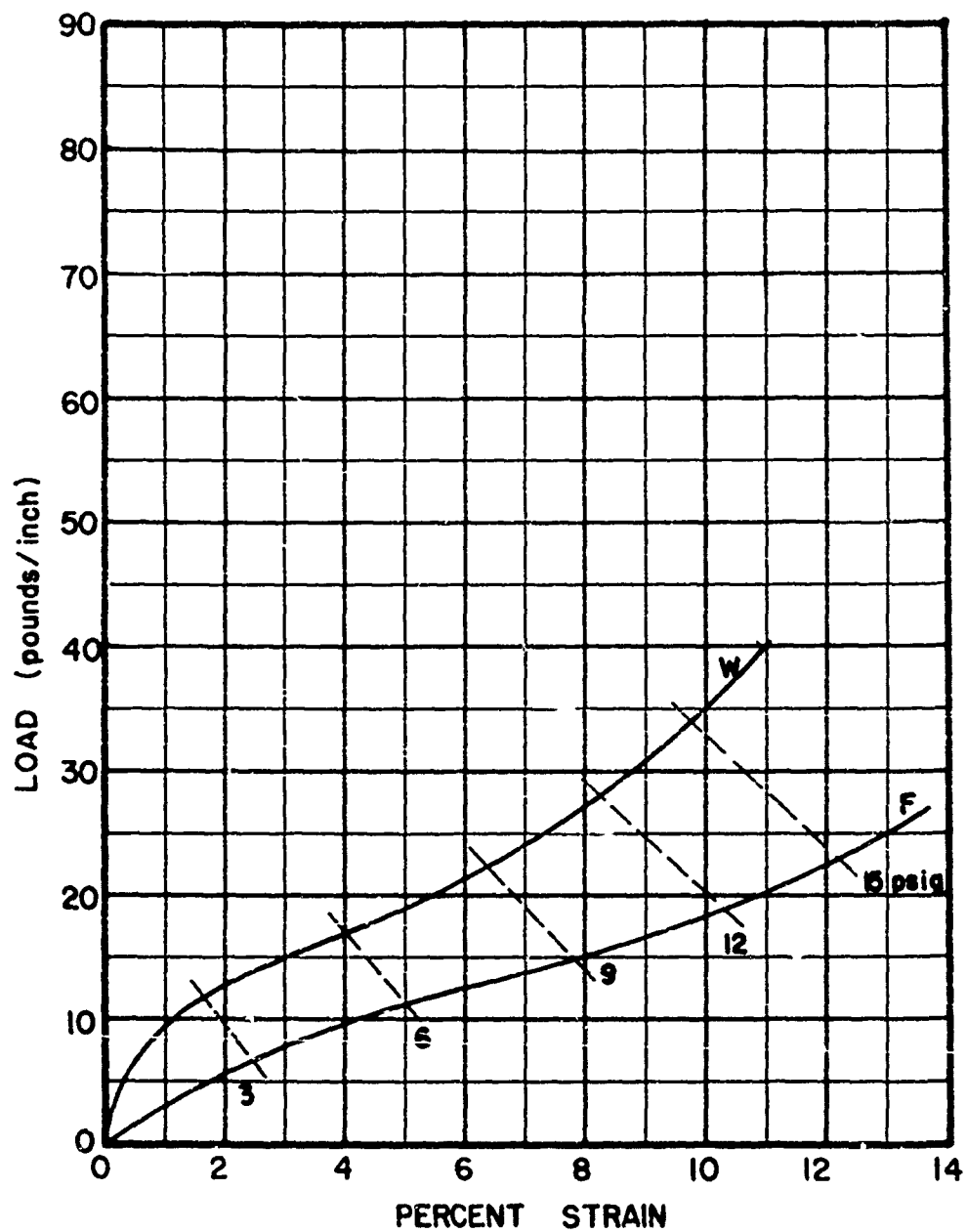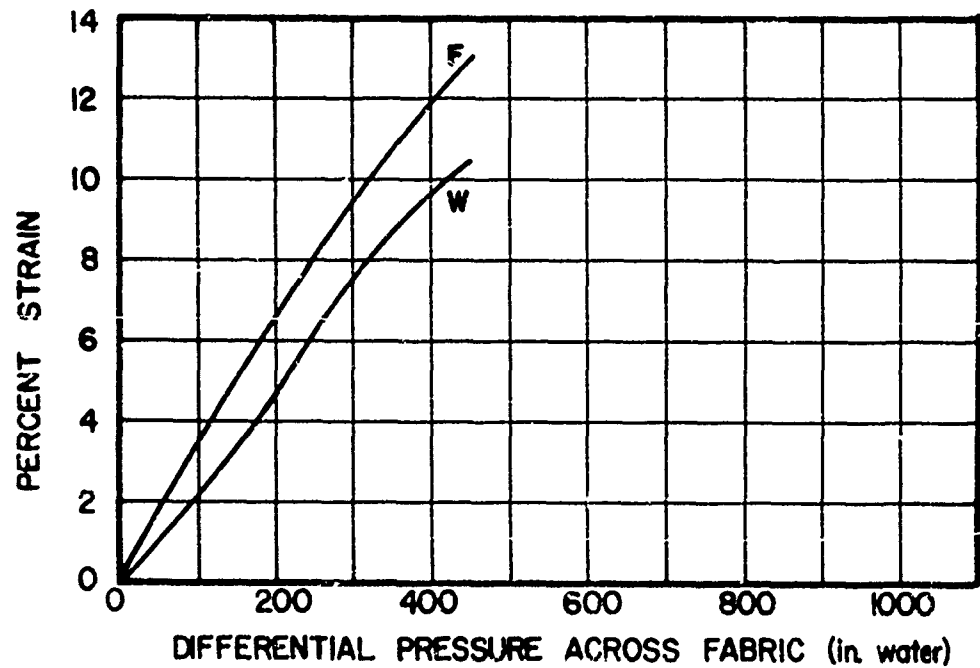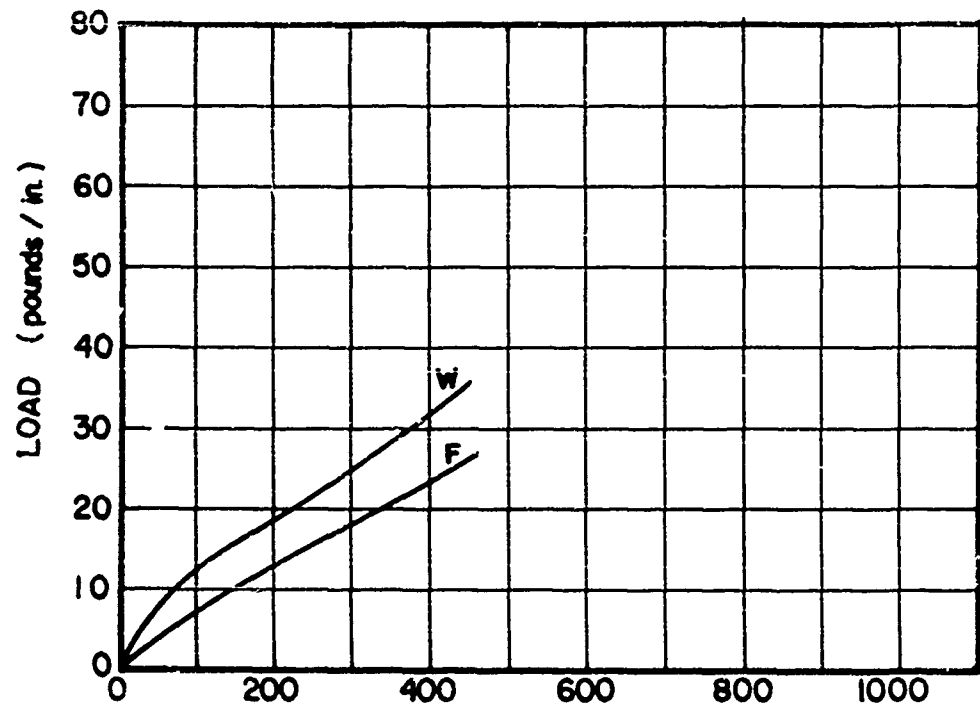
Figure 48.   Load vs. Strain.   S-8 OAI

SAMPLE S-80A2

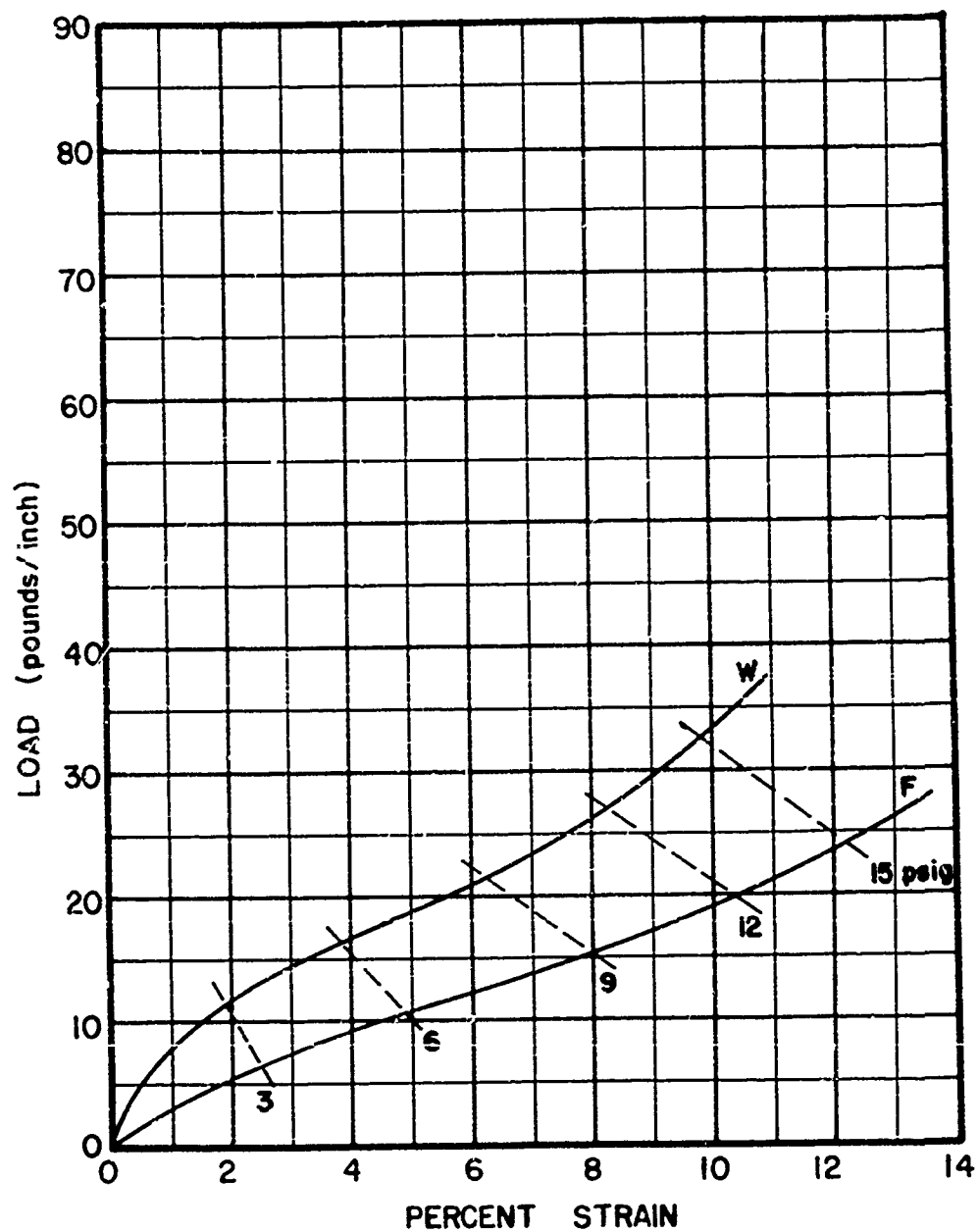Figure 49. Load and Strain vs. Pressure S-80A2

Figure 50.   Load vs. Strain.   S-8 OA2

Biaxial Stressing and Embedding Under Stress

To stress cloth samples biaxially the standard tensile tester INSTRON (Instron Engineering Corporation, Quincy, Mass.) Model TTB and a biaxial stress attachment (developed at M.I.T.) were used. The biaxial attachment (as shown in Figs. 51 and 52) consists of four vertical lead screws supporting a horizontal frame. The horizontal frame has two cross pieces to which an ordinary jaw and a swivel mounted jaw with a load cell can be attached. These two cross pieces can be moved in horizontal but opposite directions by means of a hand wheel attachment in the front. Each of the four lead screws has a sprocket at its top which can be connected by means of a chain to two sprockets on the Instron lead screws. This arrangement makes the horizontal frame move along with the lower jaw of the Instron at half its speed.

Another attachment used along with the biaxial attachment is a square clamp jaw, designed to clamp the stressed sample until it is embedded in the resin. The stress applied by the Instron is recorded by the Instron recorder. The stress applied in the horizontal direction is recorded by the Sanborn recorder (Sanborn Company, Cambridge, Mass.) which is connected to the load cell with swivel jaw on the horizontal frame. An electric saw is used to cut the cloth samples once embedded. A rough abrador and a polishing wheel are used to flatten and polish the two surfaces of the resin blocks containing the samples. A travelling stage microscope and a Leica (35 mm) camera specially adapted for micro-photography are used in sample measurements. Standard dark room equipment is used for processing and enlarging of the photographs from which the subsequent measurements were made. Camera lucida equipment is also used for direct drawing of the sections observed in the microscope.

The sample is cut in a cross pattern with tail strip width 2" and tail lengths 11". Marks at a distance of 3.5" from the center are made on each of the tails. These marks correspond with jaw position providing a gage length of 7" in warp and filling. Then a cardboard box 3" x 3" x 1½" (with its top open) is taken and slits of about 2½" length are cut on each of its sides, at the same level. The sample is threaded through the box slits in such a way that the 2" x 2" square central portion of the cross stays in the box and the four tails stick out. The warp and fill directions, the sample number and the stress level to be reached are marked on the side of the box for subsequent identification.

The biaxial attachment is mounted on the Instron in such a way that the gage length between the Instron jaws is 7" and the horizontal jaws are exactly in their middle. The Instron load cell is calibrated on the Instron recorder and the load cell for the horizontal jaws on the Sanborn recorder.
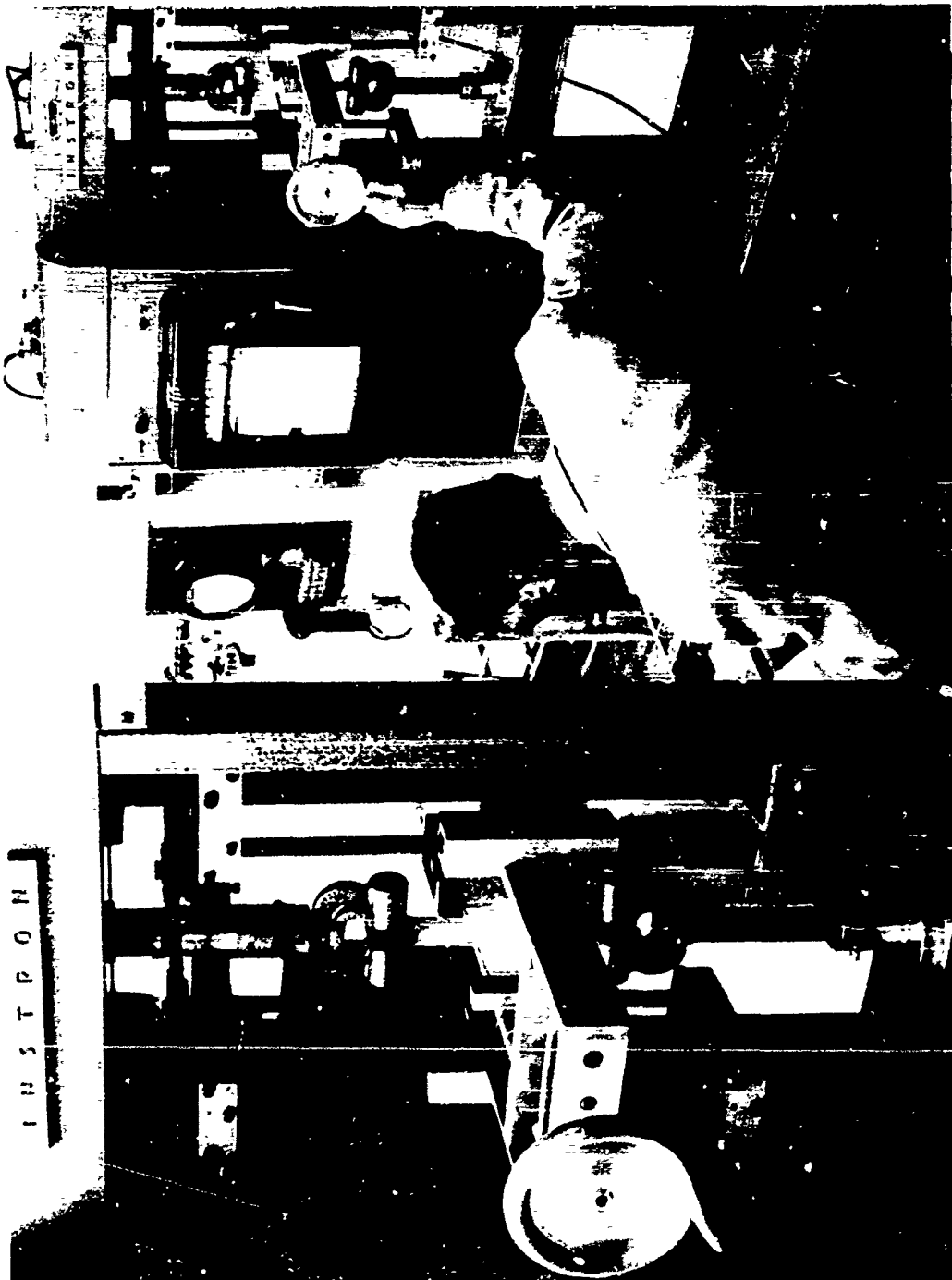
FIGURE 51. VIEW OF BIAXIAL STRESS DEVICE
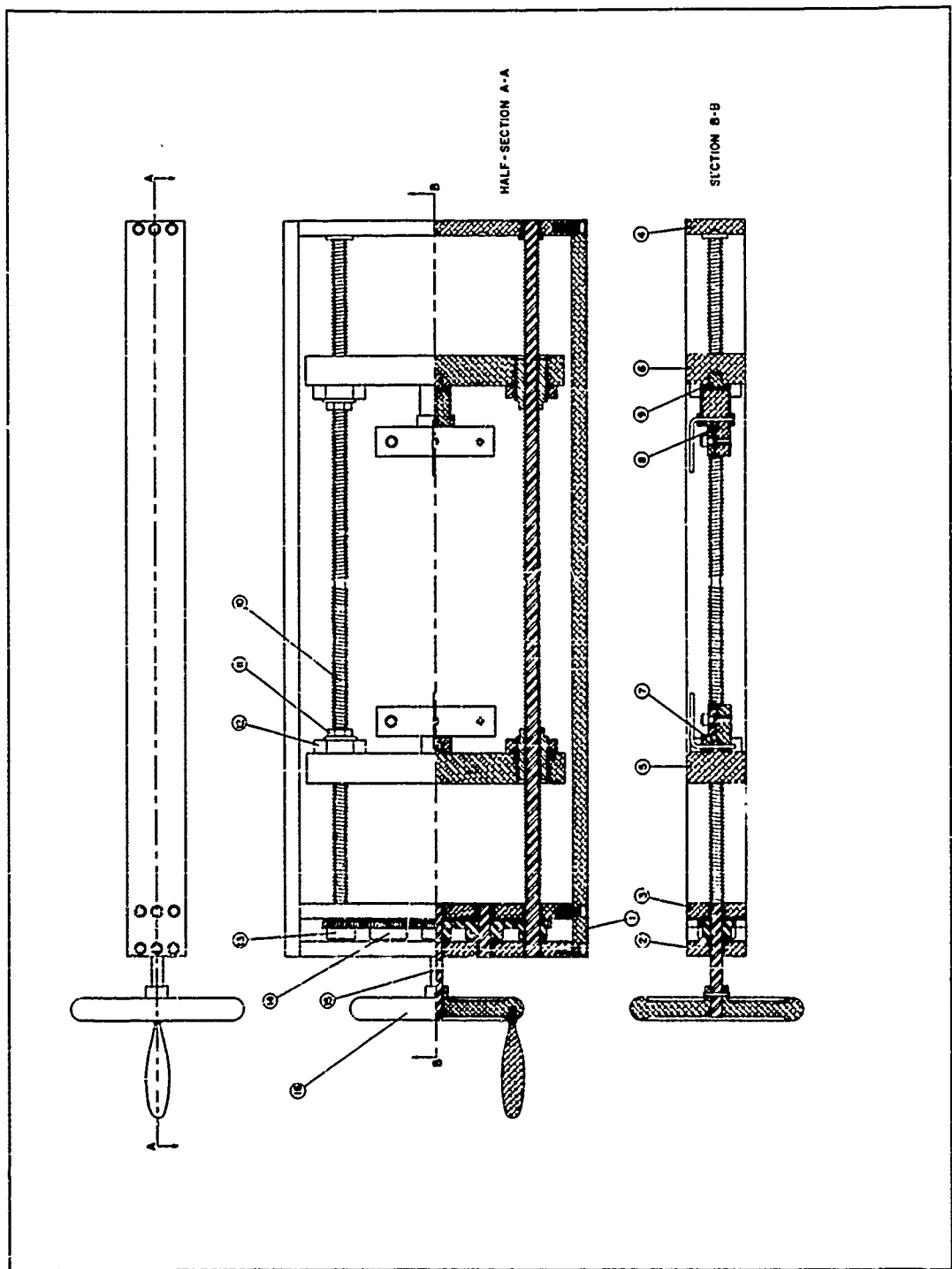
WADC TR 59-374

FIGURE 52. ESSENTIAL PLAIN VIEW BIAXIAL STRESS DEVICE

WADC TR 59-374

101

The load cell jaw assembly is then mounted on the biaxial attachment and the load cell is connected to the Sanborn recorder. The sample is then mounted in the two pairs of jaws such that the gage length is 7" in both directions. A suitable scale is selected on both the recorders according to the loads required. The Instron jaw speed is adjusted to 0.1'/min. The two recording charts are started and the "down" button on the Instron panel is activated. The loading in the horizontal direction is induced by rotating the hand wheel. Care is taken that the ratio between the two rates of loading is maintained equal to the ratio of the desired ultimate loads. Loading is stopped a few pounds beyond the required load and the sample is then allowed to relax at the fixed strain. After half an hour the loads are raised again to the desired level and once more allowed to relax. The cycle is continued until steady loads at the desired level are obtained. The slits are then sealed off from outside the box by means of a suitable cement. The sample is then clamped in a four clamp square jaw and taken out of the Instron with the stress maintained in the newly applied square jaw.

The top of the slits are then sealed off from inside the box with cement. Laminac* (99% vol.) is mixed with Lupersol** DPM (1% vol) in a 6 oz. paper cup. The mixture is thoroughly stirred and allowed to stay until the air bubbles escape. It is then poured into the box containing the sample. Care is taken that the mixture is not poured on the fabric but in a corner of the box and allowed to wet the fabric from below, forcing out practically all the air below the fabric. The box is then filled with the monomer mixture to a reasonable level.

The square jaw with the box containing the sample of the monomer then is kept in the oven at 80°C for 15 minutes to initiate polymerization. Care is taken that it does not remain in the oven longer than 10-15 minutes, otherwise the polymer cracks in the process of polymerization. The sample is taken out of the oven and allowed to sit at room temperature for 2 hours to complete the polymerization. The sample is then ready for cutting, polishing and photographing.

After the resin has polymerized, the cardboard box is taken out of the clamps and the cloth tails are cut. The box is then saw cut twice, in the middle of the two adjacent sides, taking out a rectangular corner piece from the whole sample. The corner which comes from the center of the sample is marked clearly, also, warp and fillingdirection, the sample number and the stress levels are

---

*Laminac is a polyester monomer made by American Cyanimde Co.
**Lupersol DPM is a catalyst made by Wallace and Tieraan Corp. Buffalo.

WADC TR 59-374

102

scratched on the top surface for easy identification. The two
adjacent sides of the marked corner are then polished for warp
and filling x-section on an abrader and a polishing wheel until
the desired sections are obtained. Fig. 55 shows the various
geometrical parameters measured. These are also listed below:

P_w spacing between two adjacent warp ends.

P_f spacing between two adjacent filling picks

L_w length of warp between two adjacent filling picks.

L_f length of fill between two adjacent warp ends.

θ_w angle of inclination between the warp yarn and the
horizontal plane of the fabric.

θ_f angle of inclination between the filling yarns and
horizontal plane of the fabric.

H   thickness of the fabric.

$C_{w,f}$ crimp of the yarns defined as $c_w = \dfrac{l_w - P_f}{P_f}$

$d_{w,f}$ yarn diameters in warp and filling

The biaxial stress conditions imposed on the fabrics were
initially selected at uniform intervals over a range proportional
to the tensile strength of each parachute cloth. Later in the
program measurements of the biaxial stresses developed in each
fabric on the hydrostatic test unit (at 3, 6, 9 and 12 p.s.i. res-
pectively) were used to set the stress levels of the Instron biaxial
stress device. In this way direct geometric studies could be under-
taken on the fabric under the specific conditions of the air flow
tests in the "prestress" series. The "successive slice" technique
which was so time consuming was restricted to fabric E9 (Figures
53 to 54.3, inclusive). The E9 stress levels in the successive
slice pore studies were 0/0 and 100/100 lbs/in., warp and filling.

The sections of E9 taken at other stress levels were limited
to the yarn centers, or unit cell boundaries. These latter sections
are shown in Figures 61.1 to 614 inclusive. Similar center yarn
sections taken of Fabric E10 are shown in Figures 62.1 to 62.7 in-
clusive. Fabric S3 sections are presented in Figures 63.1 and 63.2
while Fabric S6 sections appear in Figures 64.1 to 64.3 inclusive.

The weave structures and local yarn distortions of the various
parachute cloths are pictured in Figures 57 to 60 inclusive. The
original data of the various measurements made of the above listed
parameters are not included in this report. Suffice it to say that
the primary geometric information needed is contained in the cross
sectional representations. The measurements of spacings in the
distorted sections were used to check the strain readings made

directly on the hydrostatically stressed specimens (Figures 39-50 inclusive). The measurements of the horizontal diameter changes in warp and filling, are presented graphically in Figures 65 to 68 inclusive. These graphs also show the changes effected in crimp (length minus spacing divided by spacing, or the 'degree' of waviness). Change in angle of inclination is likewise shown.

A practical difficulty in using geometric measurements of fabric cross sections to check direct strain readings involves the matter of sampling. One is forced in a detailed section to deal with single or even a few unit cells. The direct strain reading on the other hand is based on 50, 100 or 150 unit cells, with no extra effort. It was therefore not unexpected to find wide discrepancies in local strains based on unit cell readings in one case and multiple cell readings in the other case. That the difficulty of attaching absolute quantities to the data based on the fabric sections is principally statistical is proved by a separate series of tests on fabric cross sections. In these tests a filar micrometer was used to traverse a variable number of unit cells to measure effective strain. As the number of unit cells traversed was increased, the agreement between 'sectional' strain readings and 'planar' strain readings (See Figure 38) improved to an acceptable level.

The wide variation between individual weave cell dimensions pointed up in the strain study throws some doubt on the absolute value of the detailed geometric representations recorded in the figures which follow this page. But it must be recalled that the strain reading taken at successive stress levels automatically includes a few pore readings in the unstrained condition as its basis of comparison. Thus a high variation for that pore grouping and the expected error in judging the boundaries of its unit cells, can combine to affect significantly all subsequent strain readings for the given fabric based on small sections of an embedded cross section.

Other geometric readings of pore and unit cell geometry do not depend on comparisons with the unstressed state. These include crimp, c, inclination angle θ and horizontal diameter, d. Their values based on single or a few pore readings will vary considerably. But in plotting the changes in these parameters with stress (Figures 65-68 inclusive and Table 9) an averaging process from stress level to stress level smooths the data and provides a consistent picture of the relative behavior of the different woven structures during airflow tests.

Fabrics S3, S6, E9 and E10 were studied in cross-sectional detail. Fabrics E9 and E10 are both basket weaves (2 x 2) as seen in Figure 69. Fabric S-3 provides a plain weaving end on either side of a block of two pick floats. It is the plain weave end of S-3 that is pictured in Figure 63.1 and 63.2. Likewise the plain weave end of Fabric S6
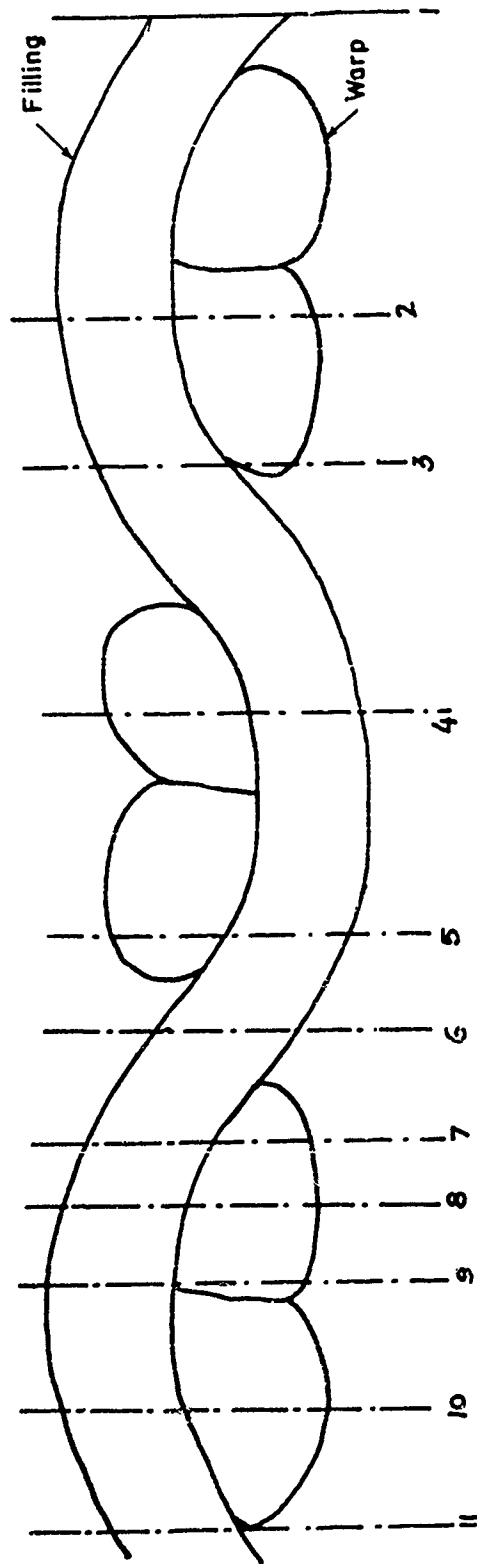
Filling

Warp

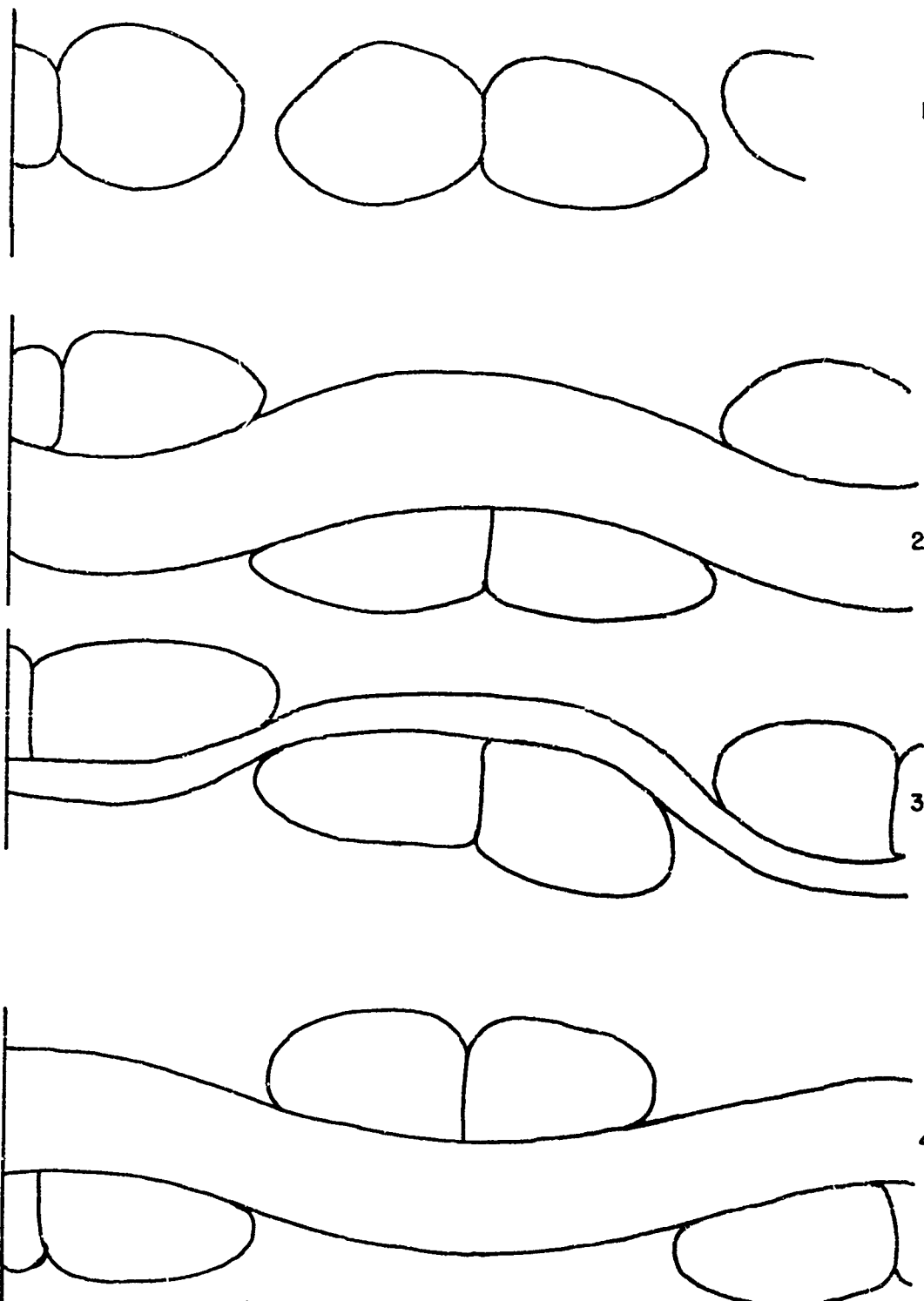Figure 53.   Successive Cross Sections of Fabric E-9.   Unstressed.
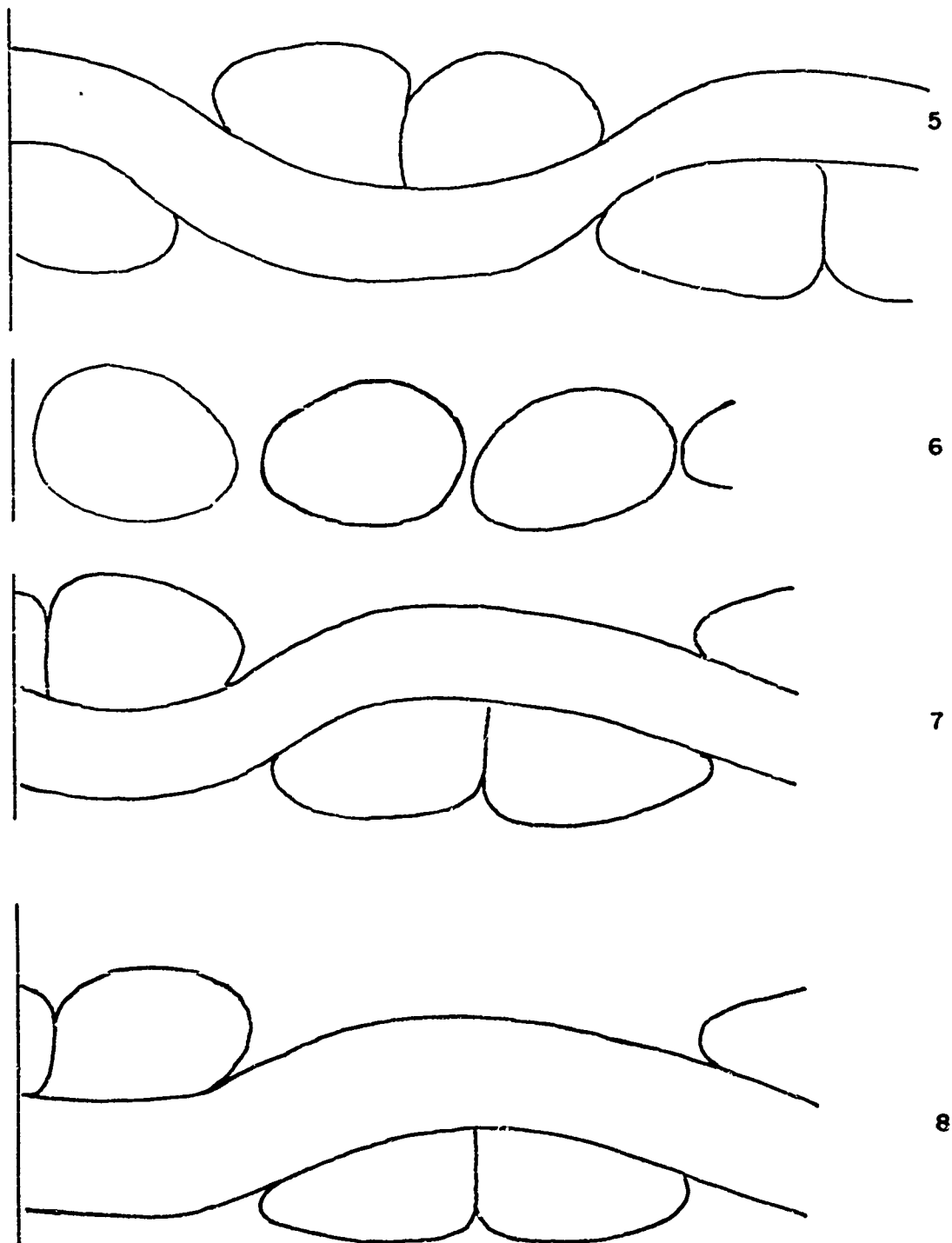
Figure 53.1 Filling Section of Fabric E-9. Unstressed.

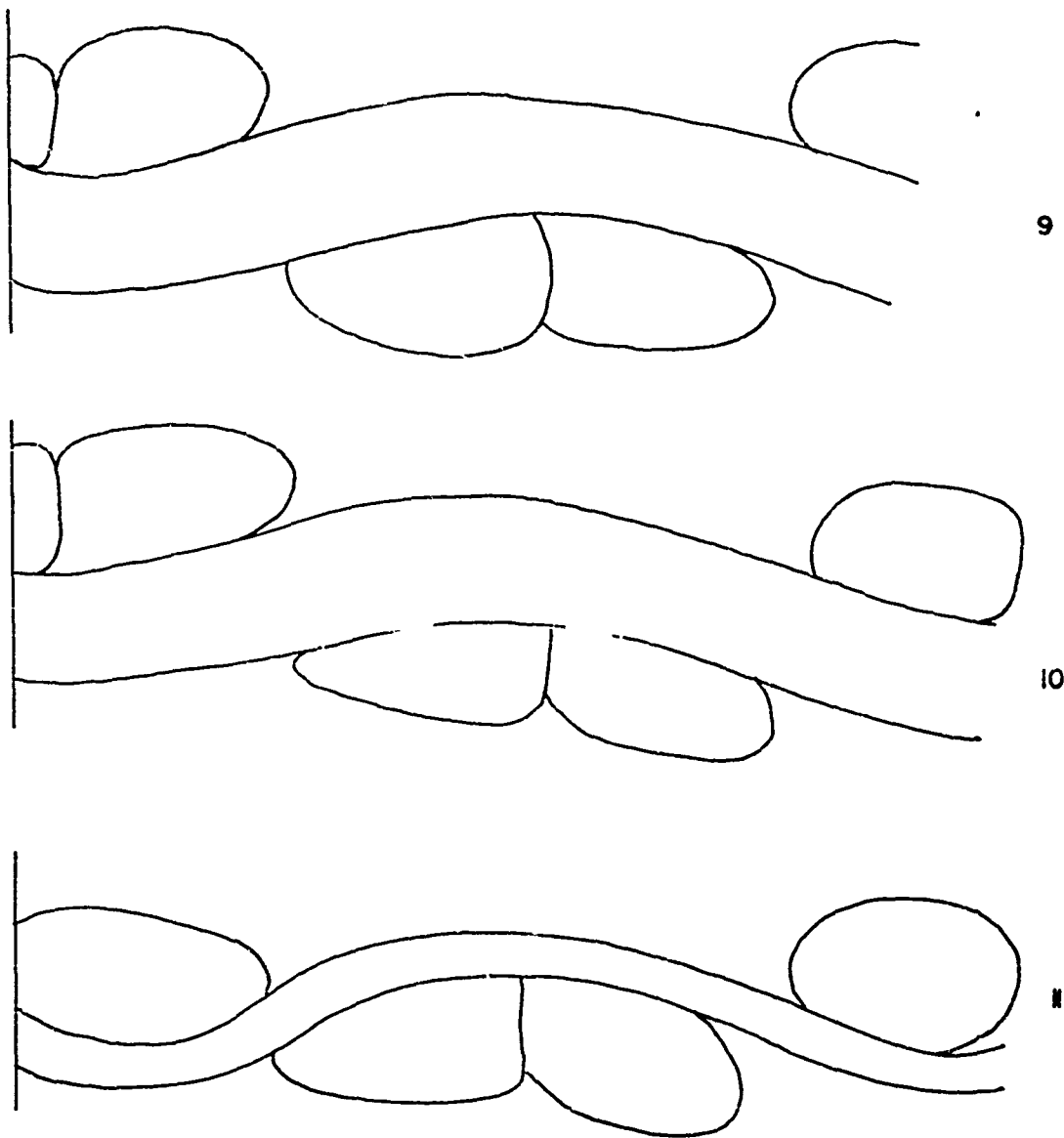Figure 53.2   Filling Sections of Fabric E-9.   Unstressed.

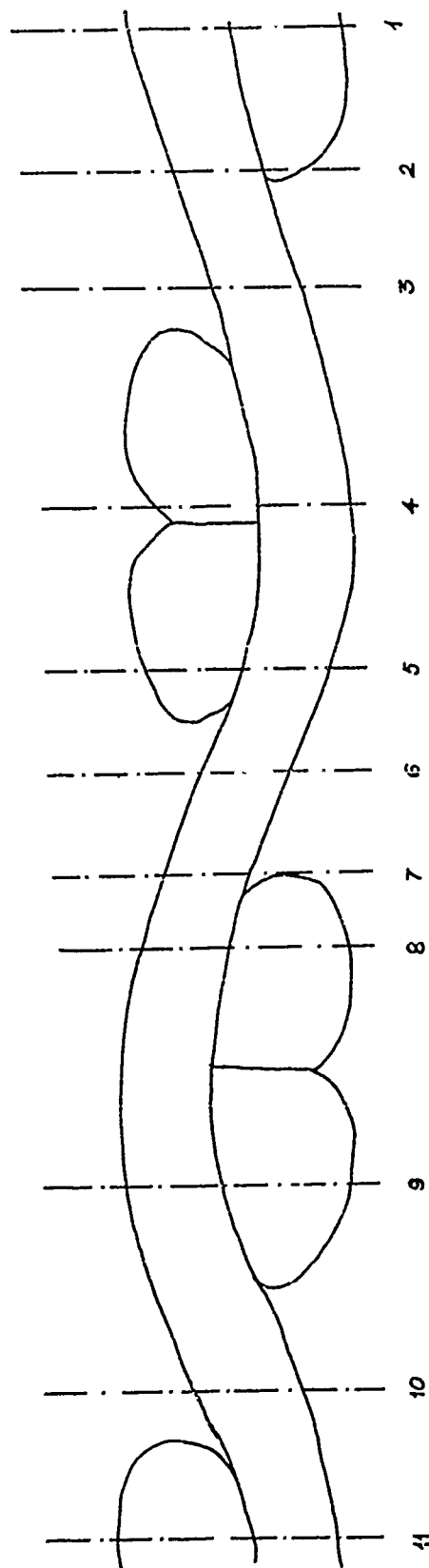Figure 53.3. Filling Sections of Fabric E-9. Unstressed.

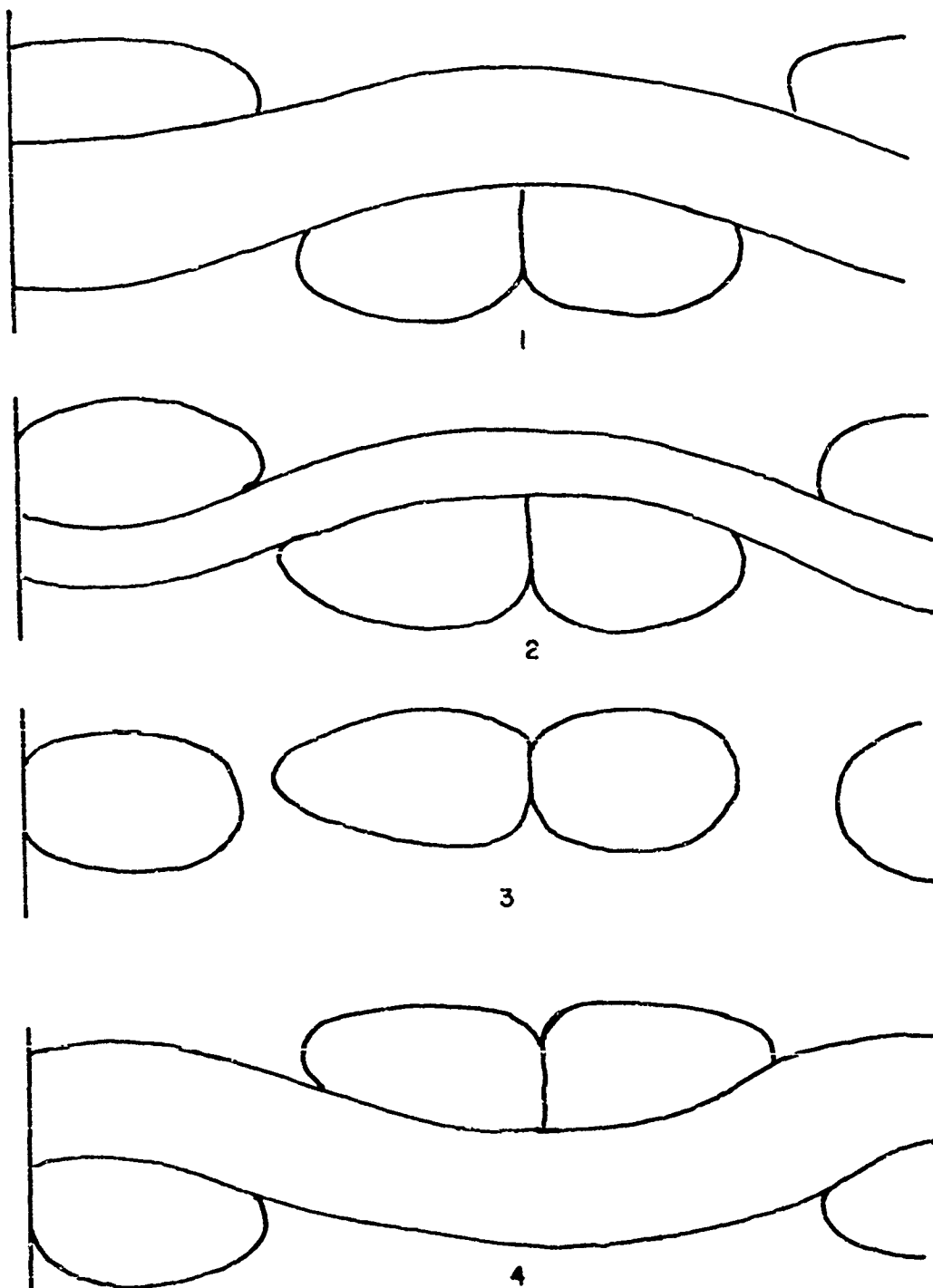Figure 54. Successive Cross Section of Fabric E-9. Stressed 100 x 100 lbs/inch
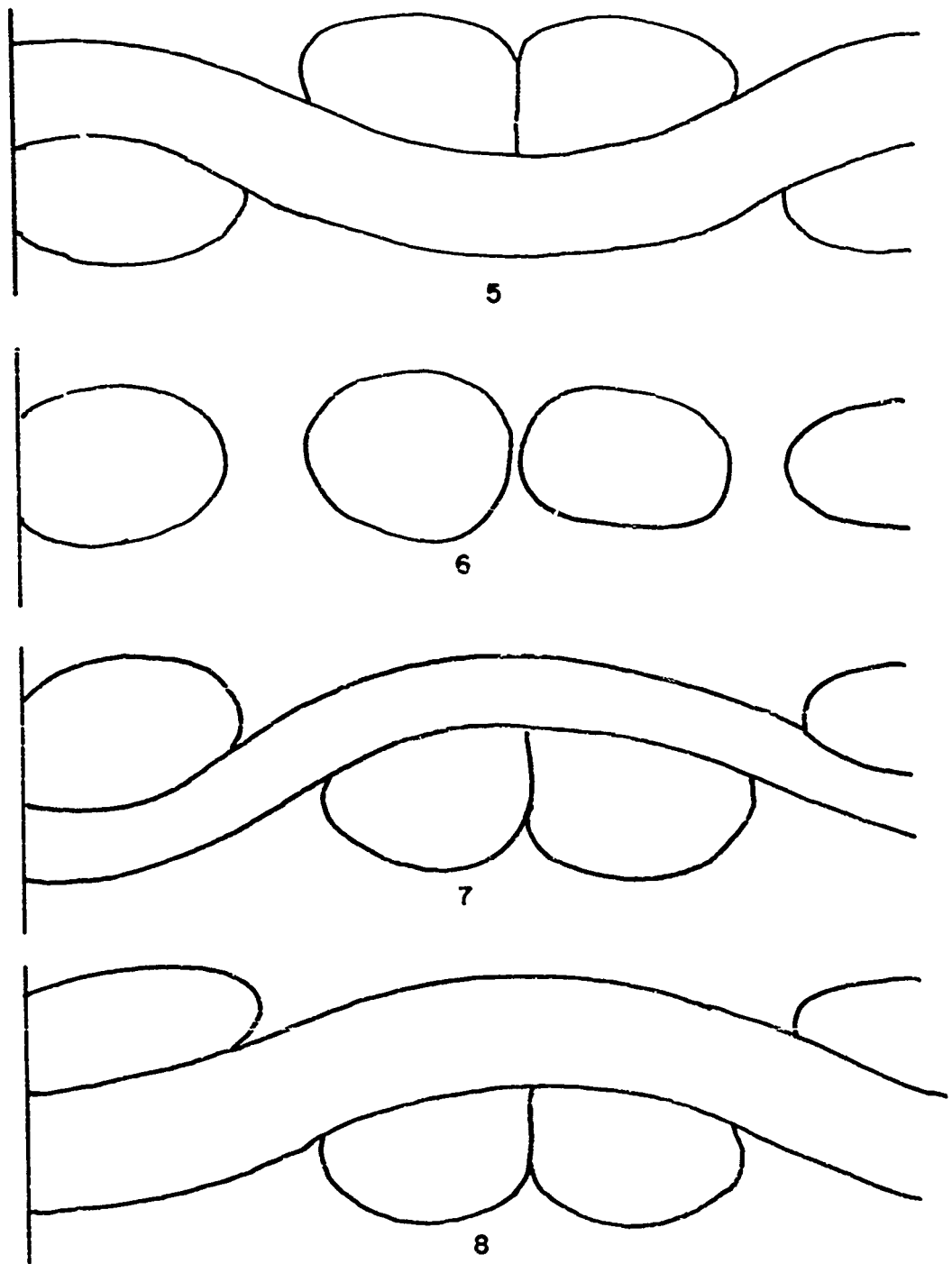
FIG·54.1   Filling Section of Fabric E- 9 Stressed
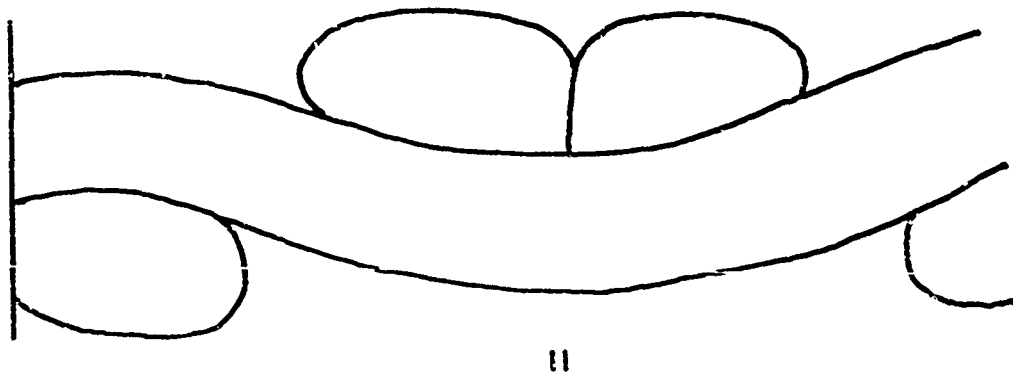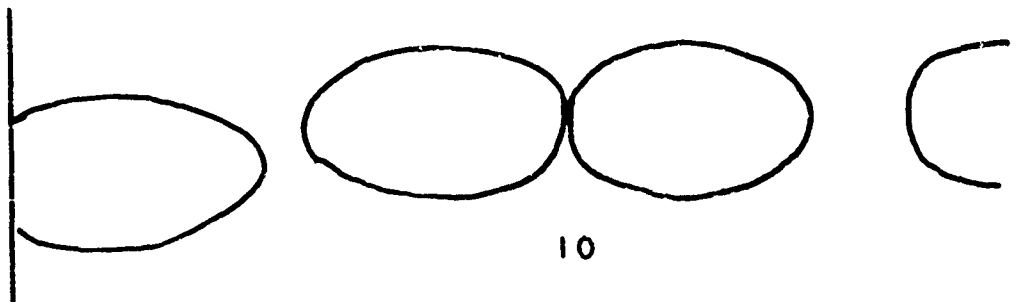
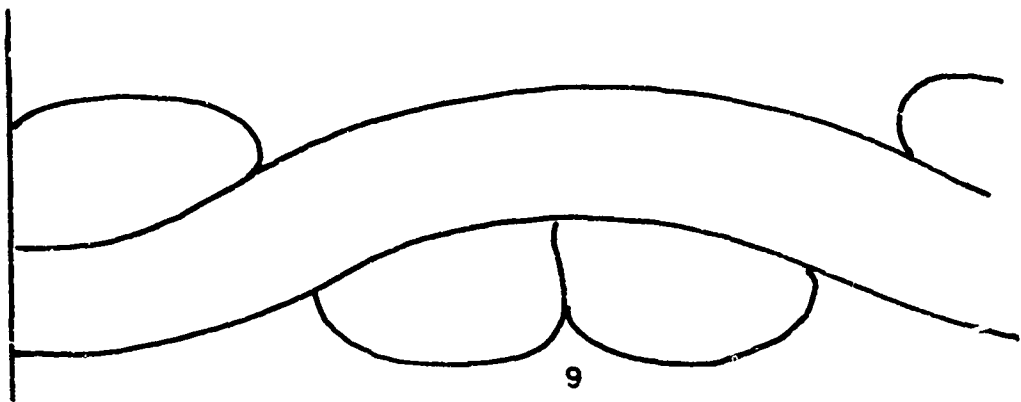FIG·54.2　Filling　Section　of　Fabric E- 9　Stressed

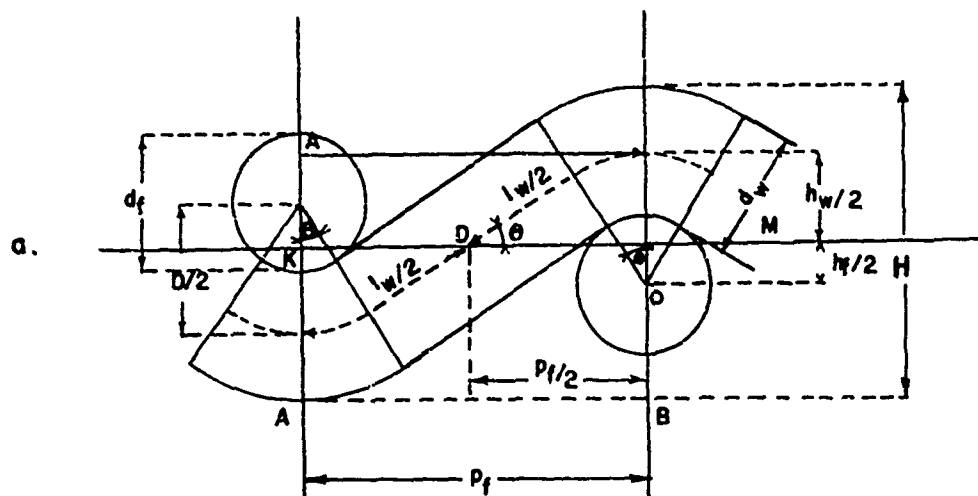FIG· 54·3 Filling Section of E- 9 Stressed
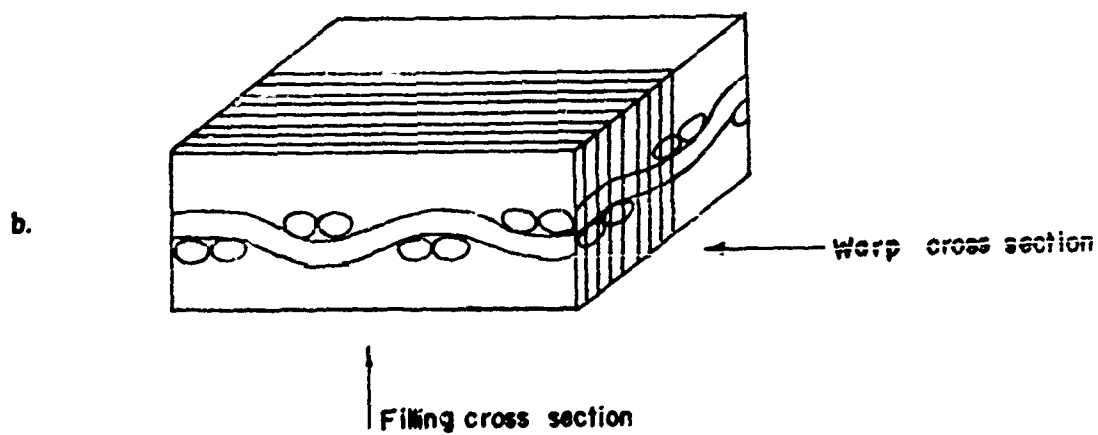
Figure 55   Geometry of Cloth Structure

Figure 56. Corner of Embedded Fabric Showing Successive Slices

FIGURE 57.   FABRIC S6   20X

WADC TR 59-374

114

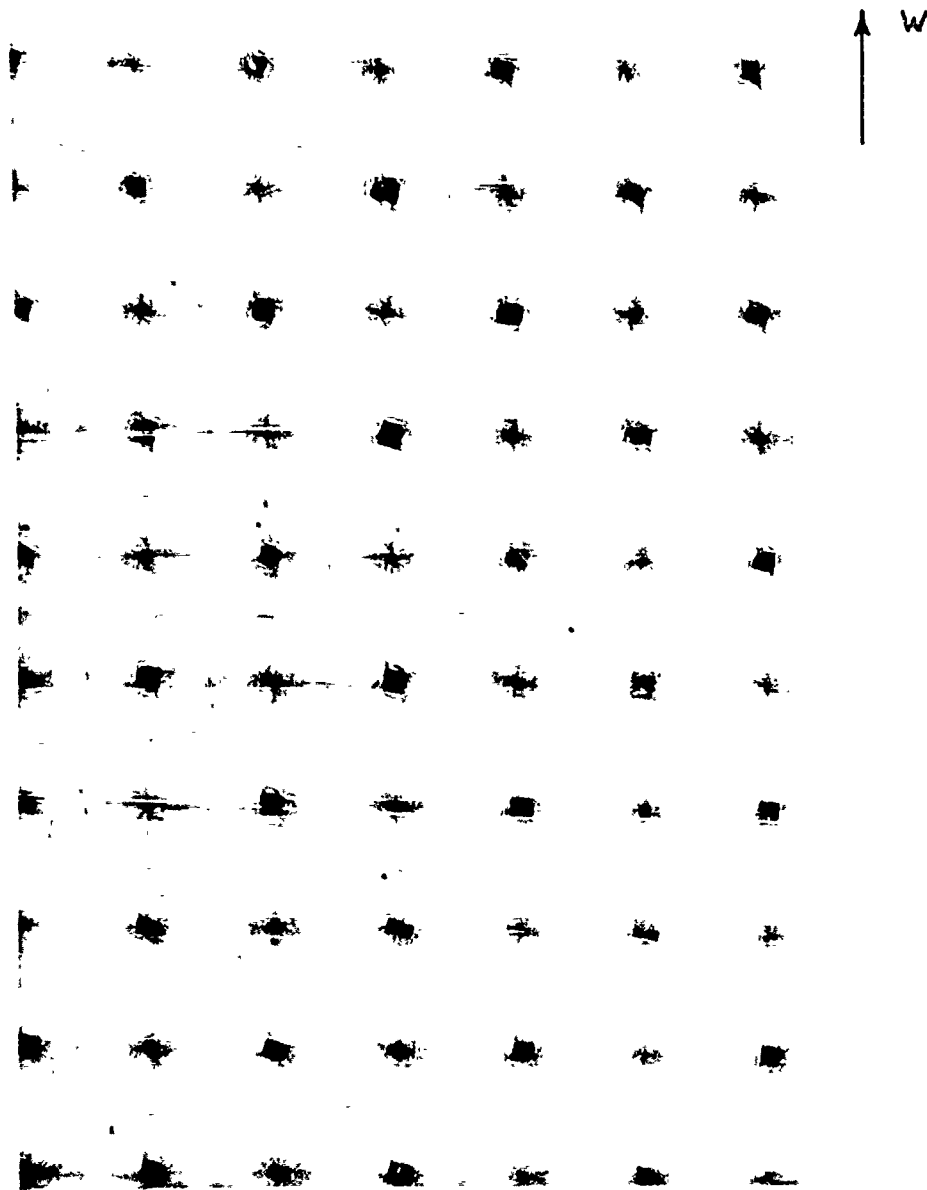FIGURE 58.   FABRIC E10   20X
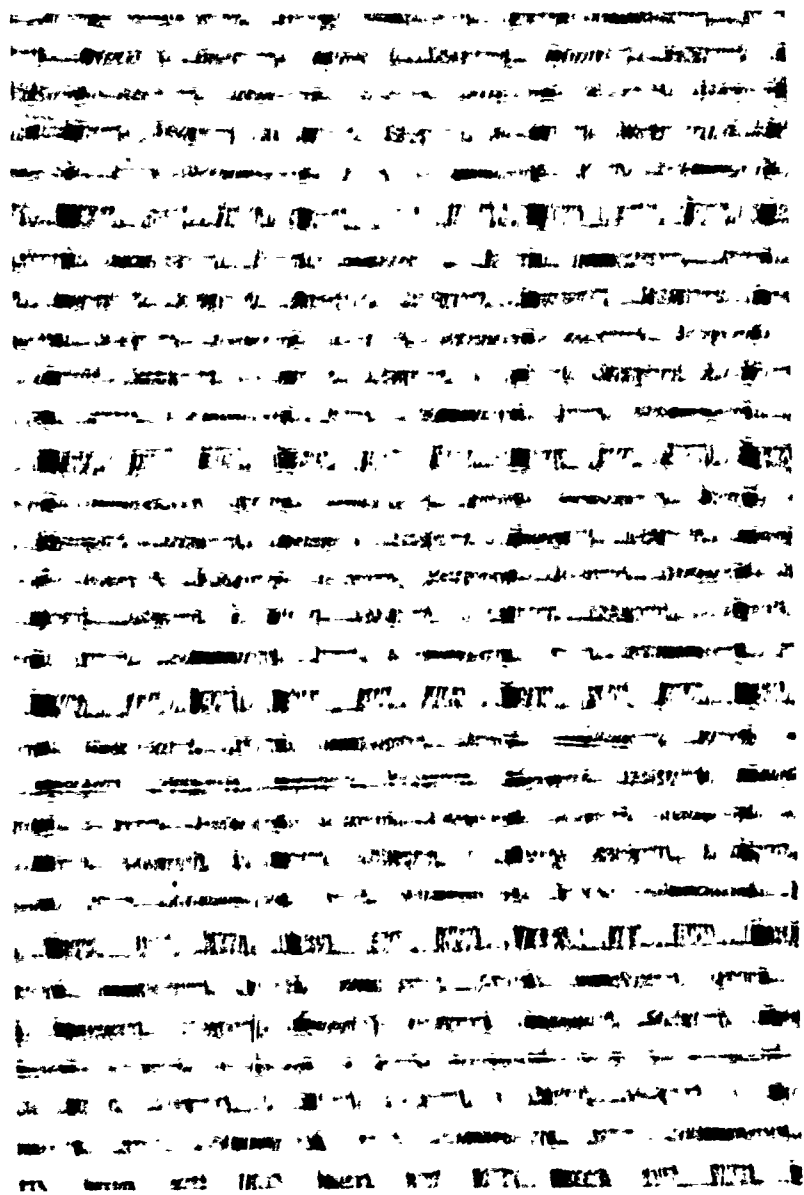
FIGURE 59.   FABRIC S3   20X
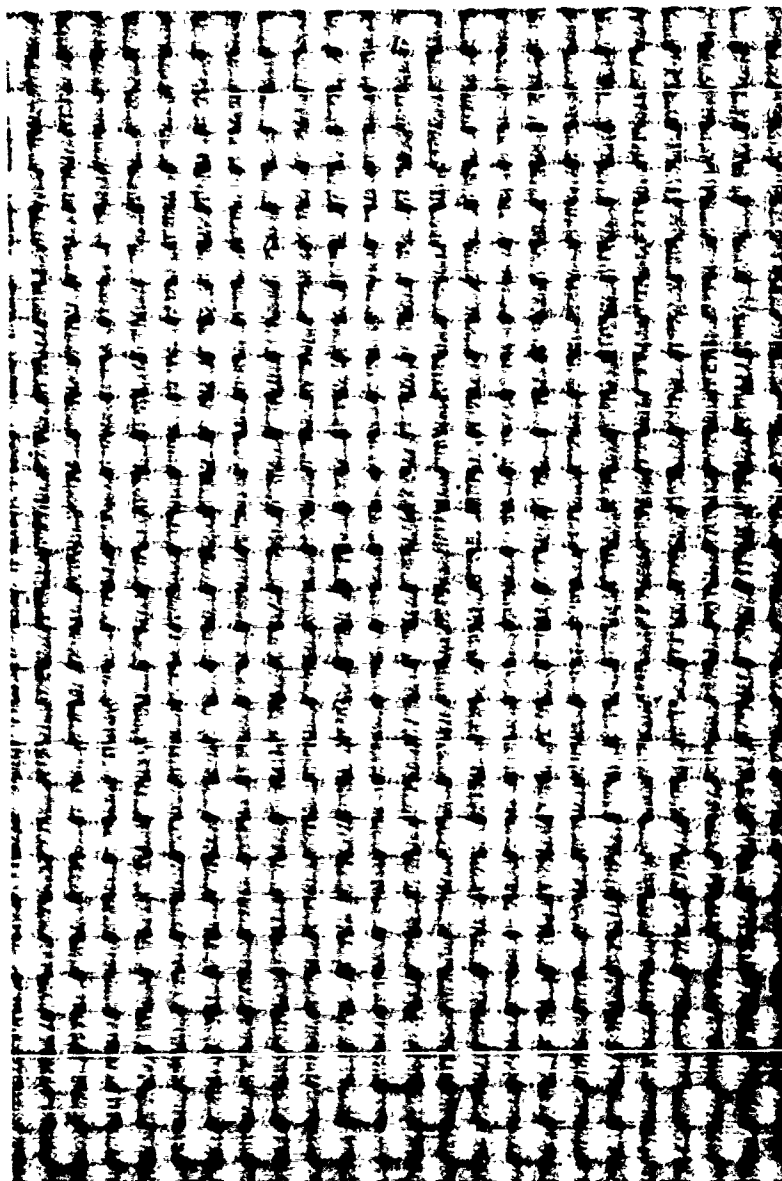
FIGURE 60. FABRIC S8 20X

E-9

0/0 W

0/0 F

25/25 W
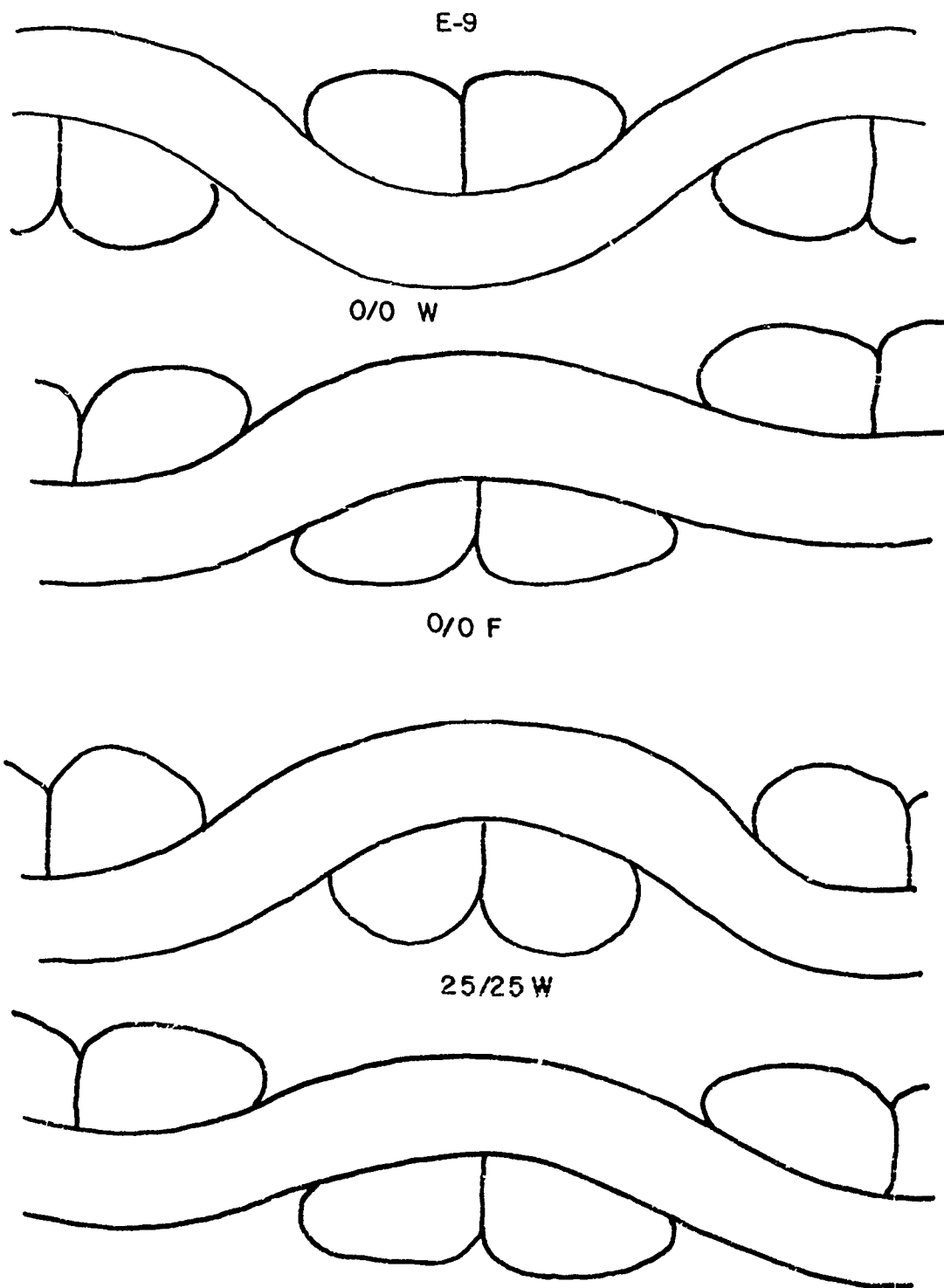
Figure 61.1. Section of Fabric E-9. 25/25F

E -9
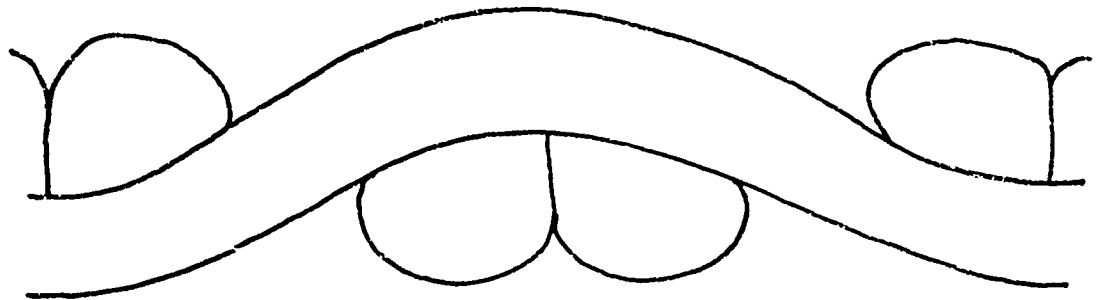
37·5/37·5 W
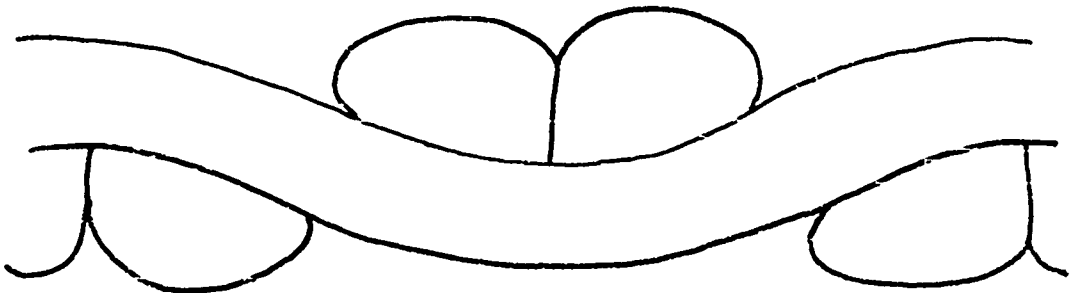
37·5/37·5 F
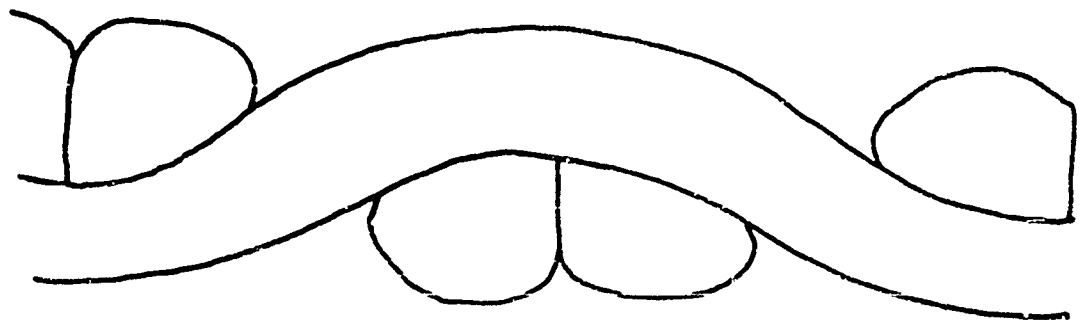
50/ 50 W
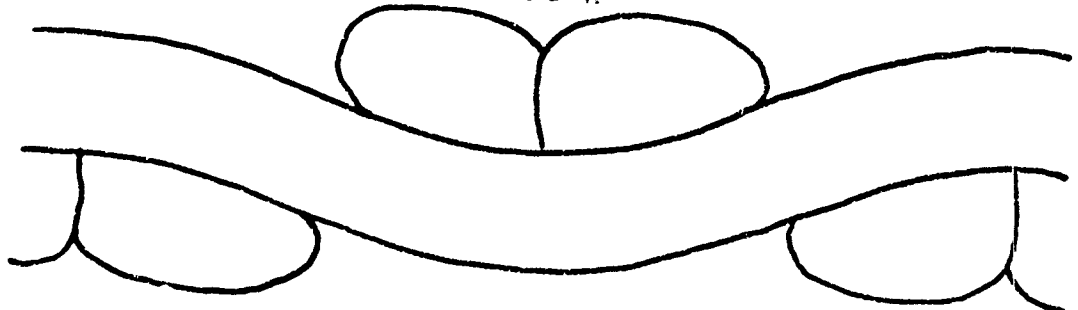
50/5 0F

Figure 61.2. Section of Fabric E-9.

E-9

75/75 W

75/7 5 F
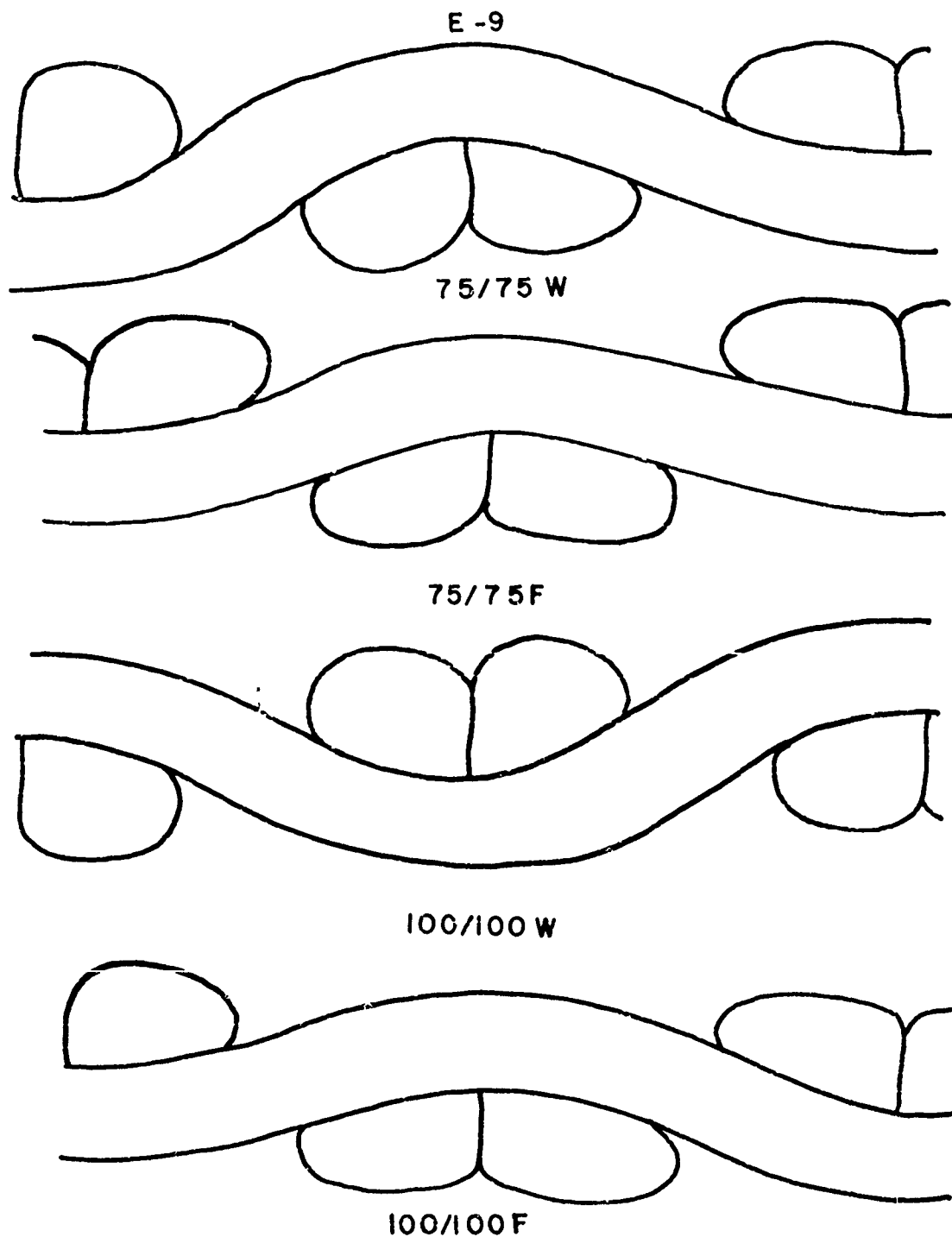
100/100 W

100/100 F

Figure 61.3. Section of Fabric. E-9.
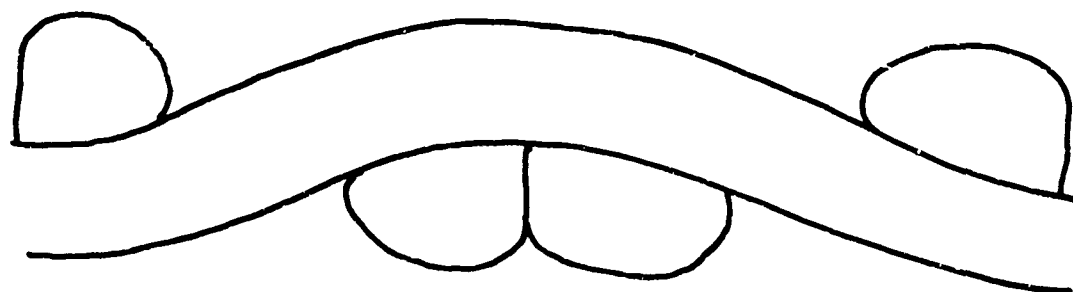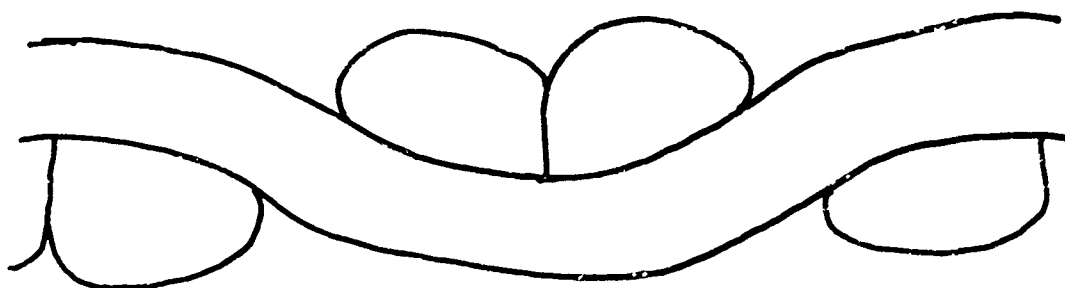
150/150 W

150/150 F

Figure 61.4. Section of Fabric E-9

E-10

O/O W

O/ O F

25/25 F W

25/25 F
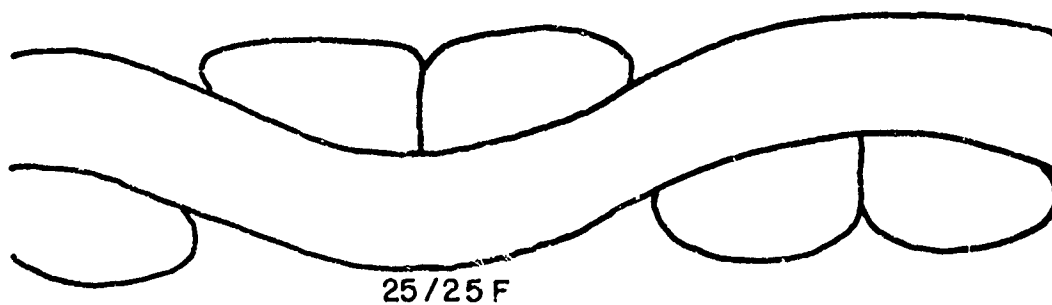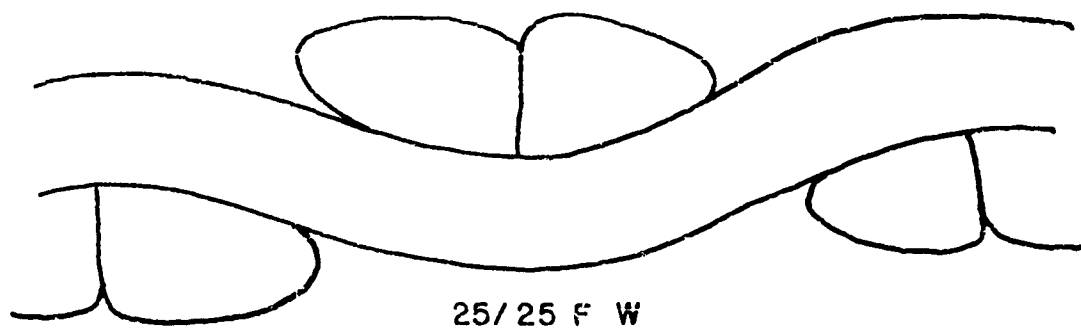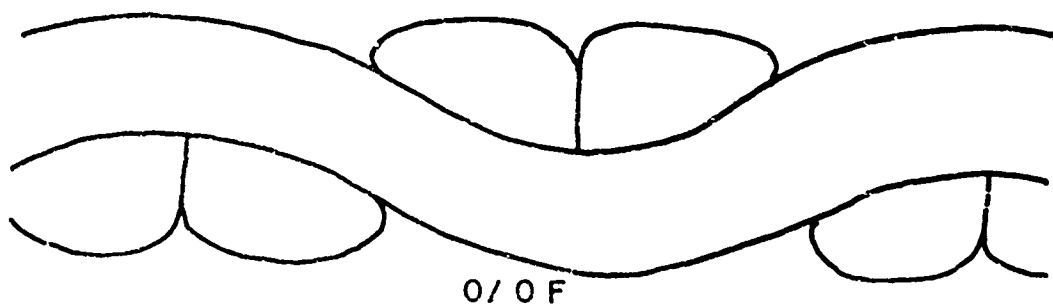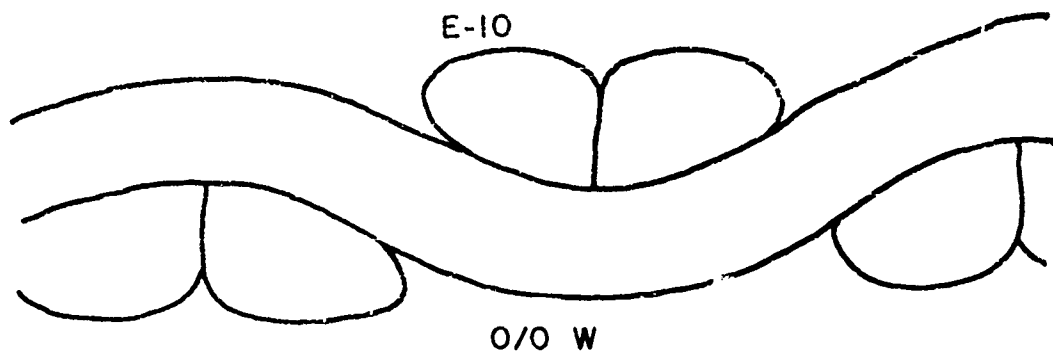
Figure 62.1, Section of Fabric E-10

E-10

75/75 W

75/75 F

125/125 W

125/125 F
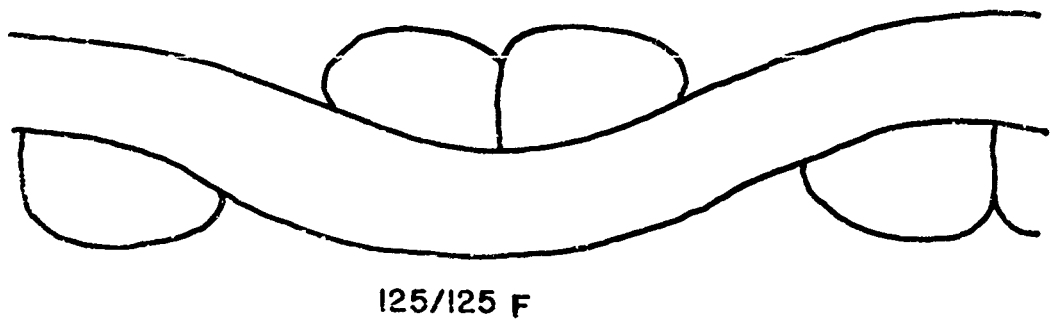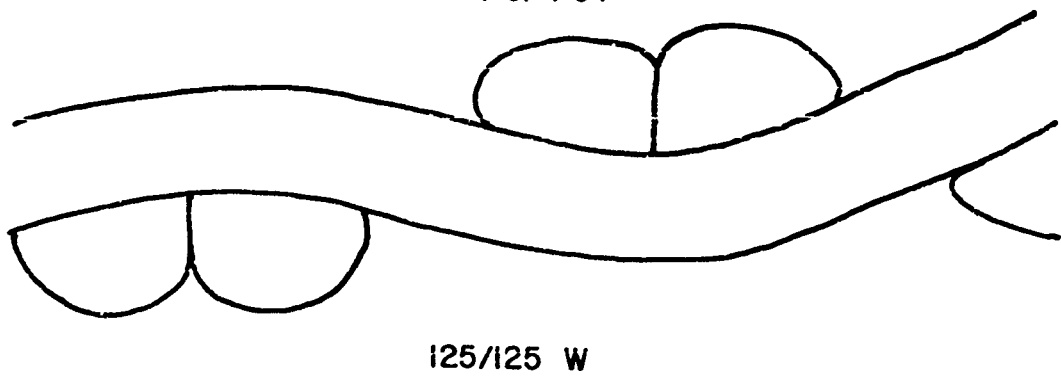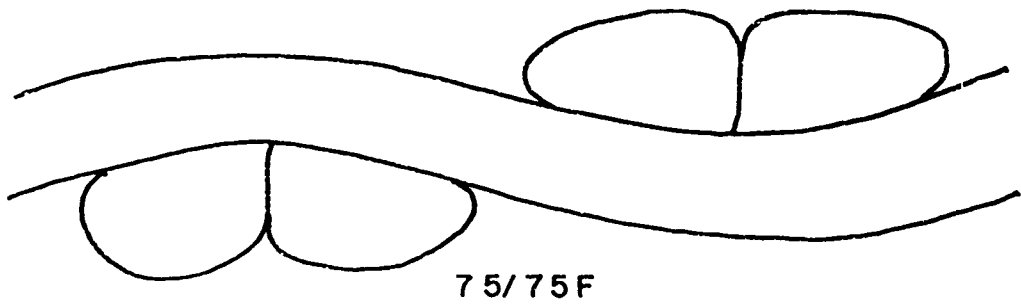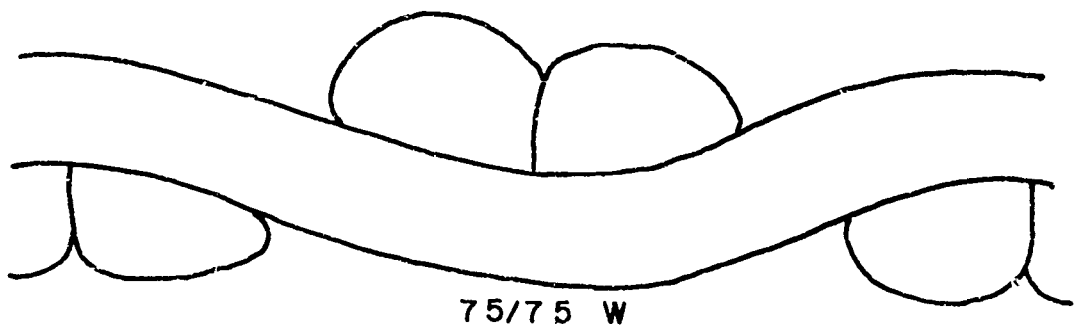
Figure 622. Section of Fabric E-10.

E-10
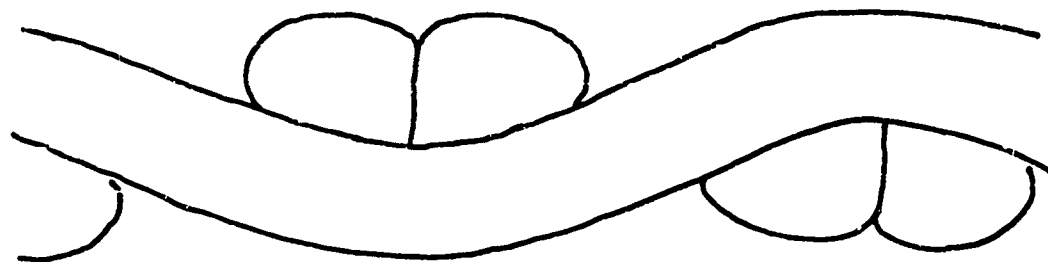
50/50 W
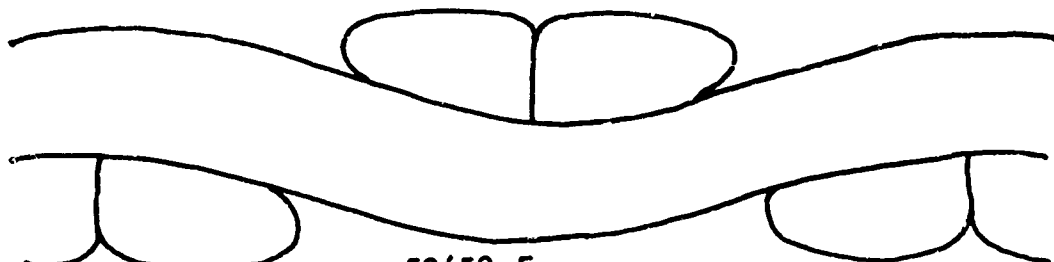
50/50 F

100/100 W
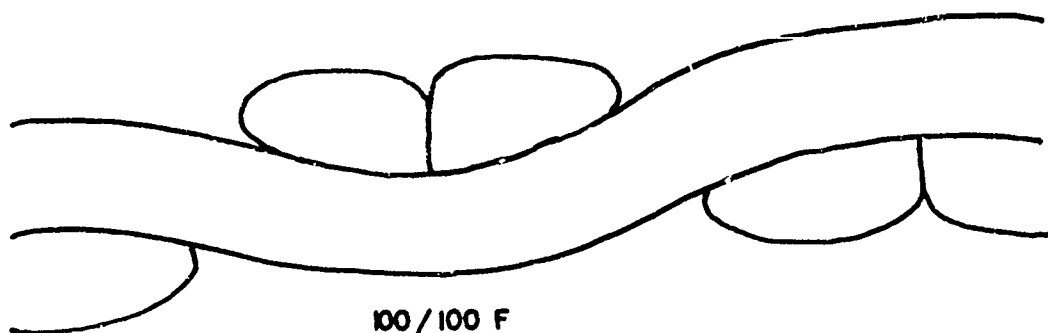
100/100 F

Figure 62.3. Section of Fabric. E-10.

E-10

150/150 W

150/150 F
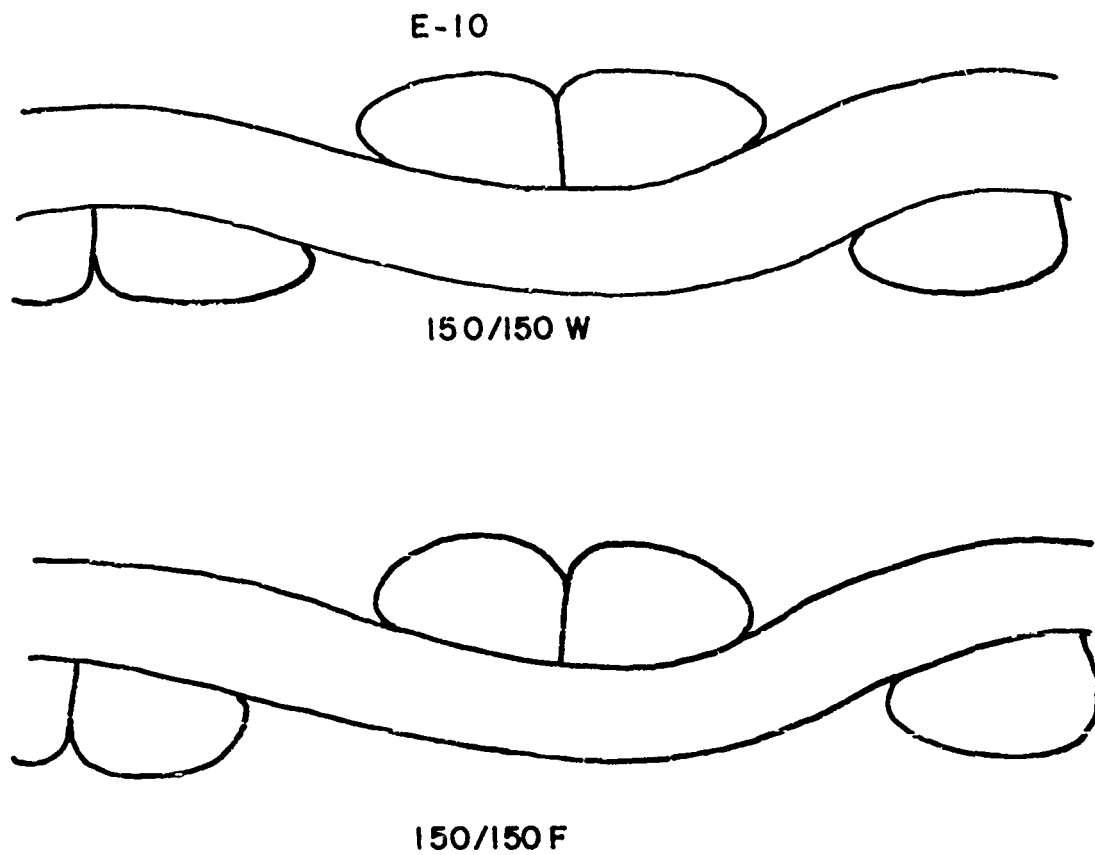
Figure 62.4. Sections of fabric E-10.

E-10

15·3/12 W

15·3/12 F

23/20 W

23/20 F
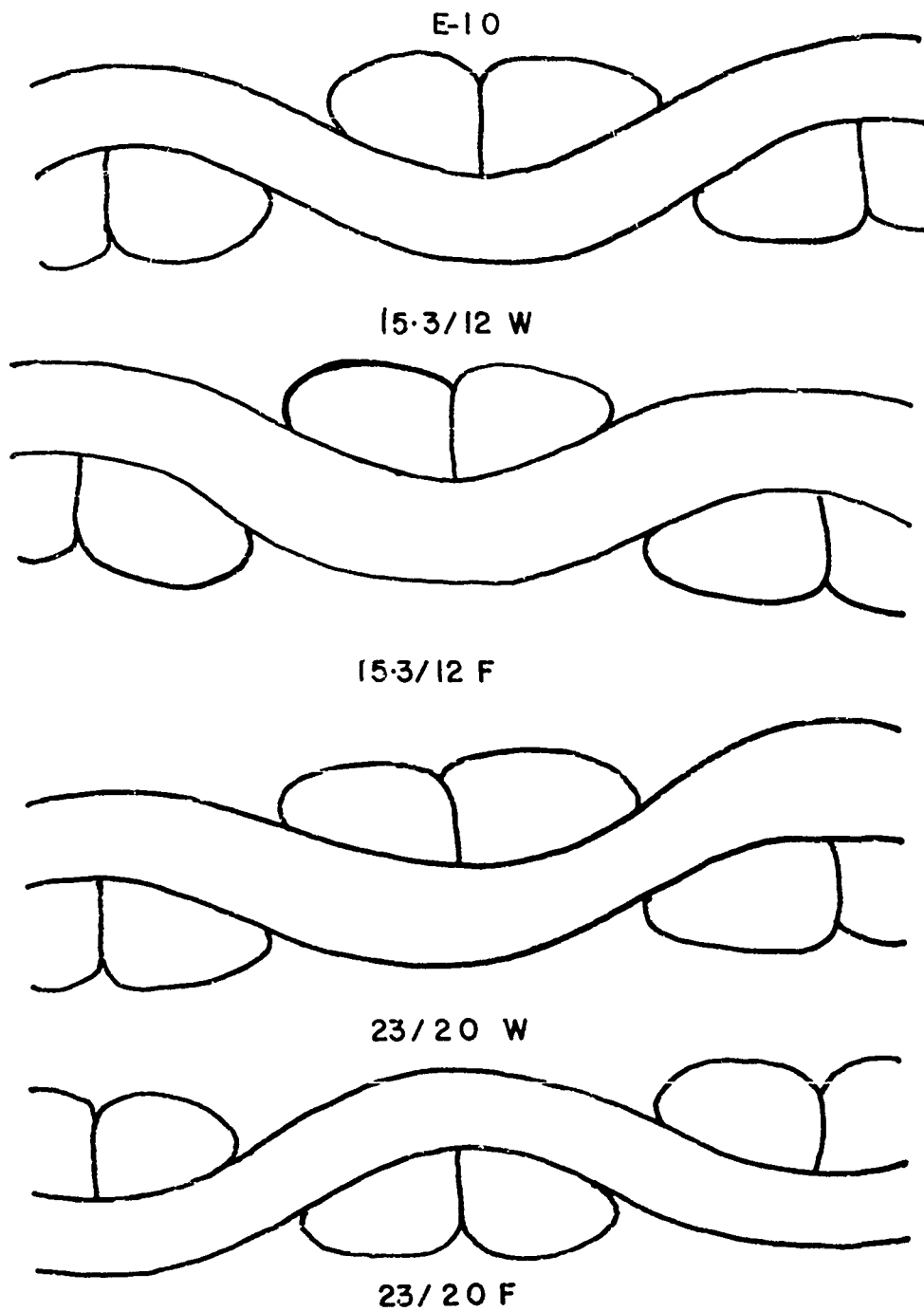
Figure 62.5.   Sections of Fabric E-10.

E-10
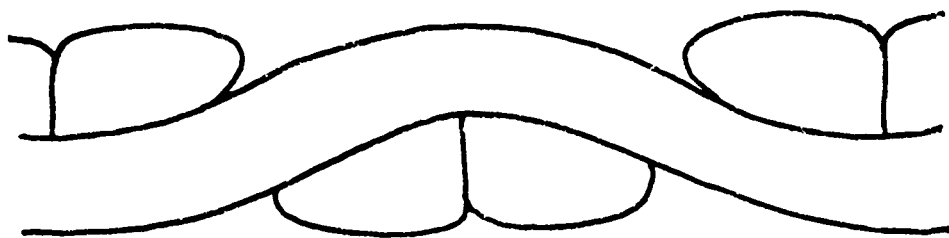
39/31.5 W
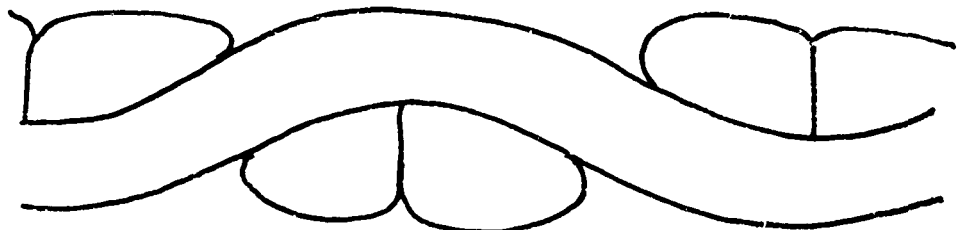
39/31.5 F
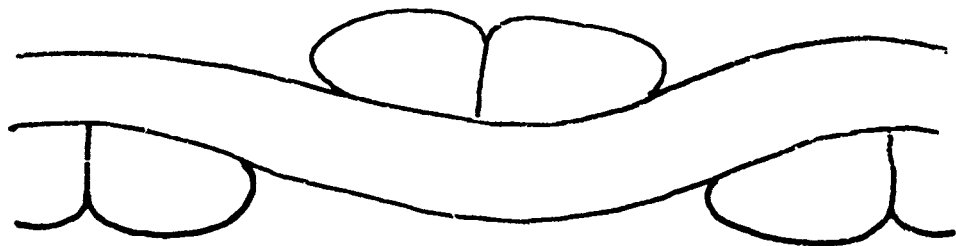
56/45 W
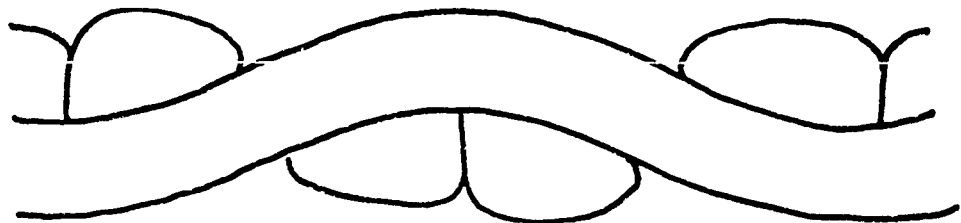
56/45 F

Figure 62.6. Section of Fabric E-10.

E- 10
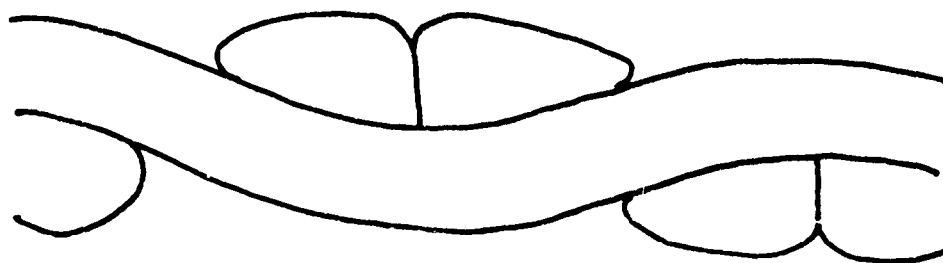
80/66 W
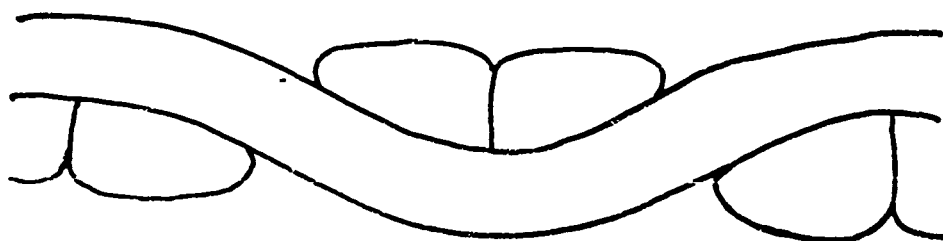
80/6 6 F

Figure 62.7. Sections of Fabric E-10.

S-3

0/0 W

0/0 F

14 / 10 W

14 / 10 F

16/12 W

16/12 F

Figure 63.1   Section of Fabric S-3.
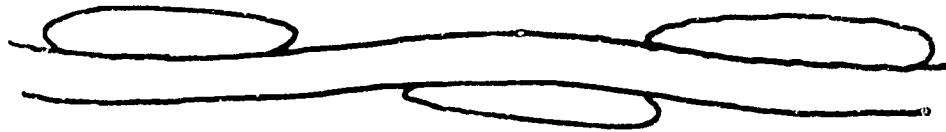
23/17 W
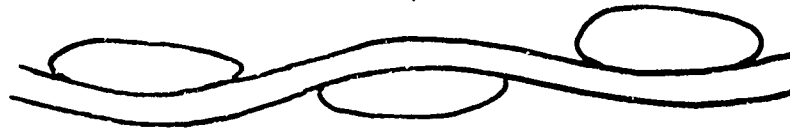
23/17 F

30/23.5 W
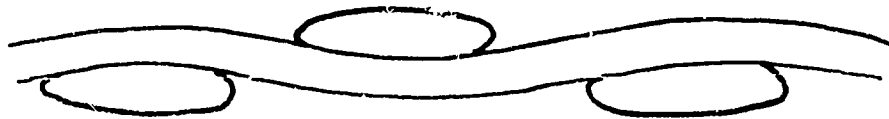
30/23.5 F

46/35 W

46/35 F

Figure 63.2 Section of Fabric S-3.

S - 6

0/0 W

0/0 F

10/10 W

10/10 F

17/17 W

17/17 F

Figure 64.1. Section of Fabric S-6.

S - 6

35/ 35 W

35/ 35 F

50/50 W

50/50 F

75/75 W

75/75 F
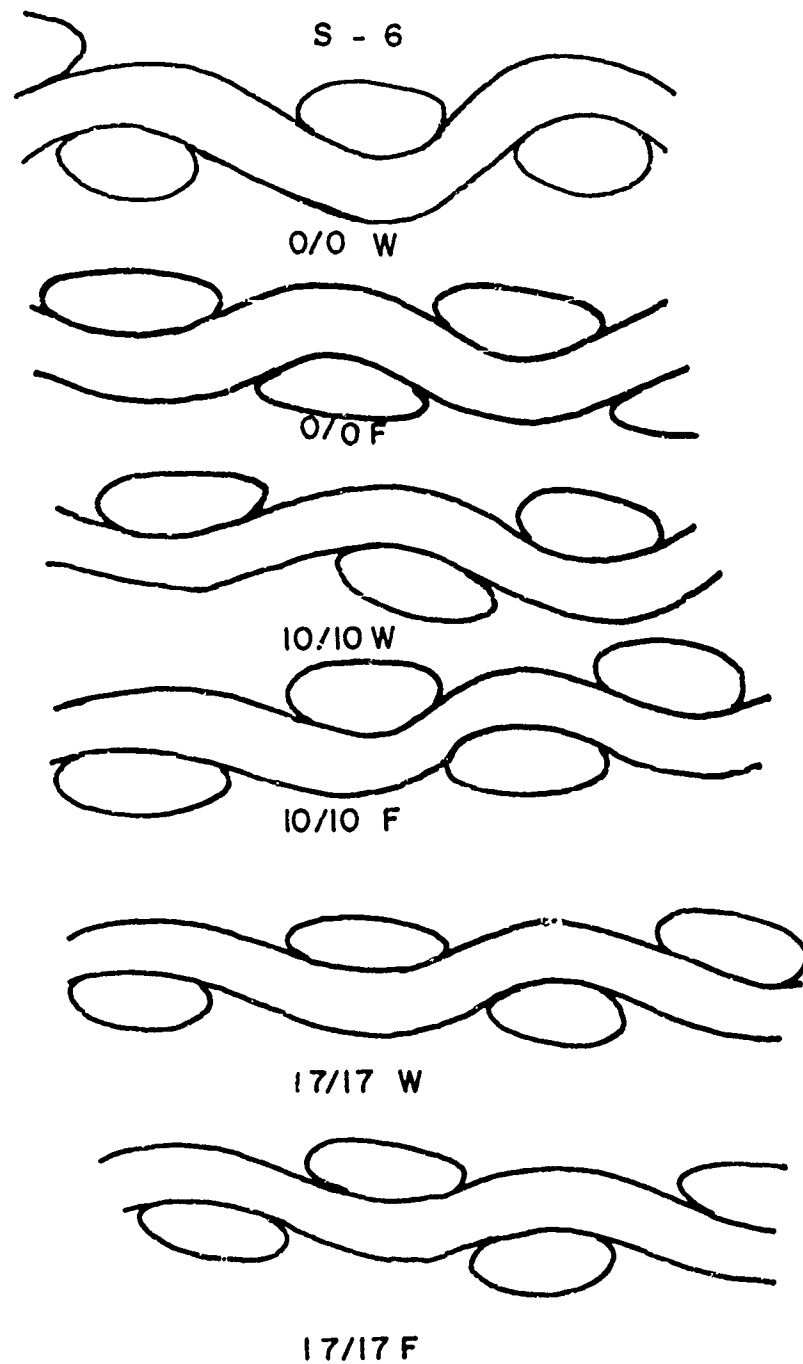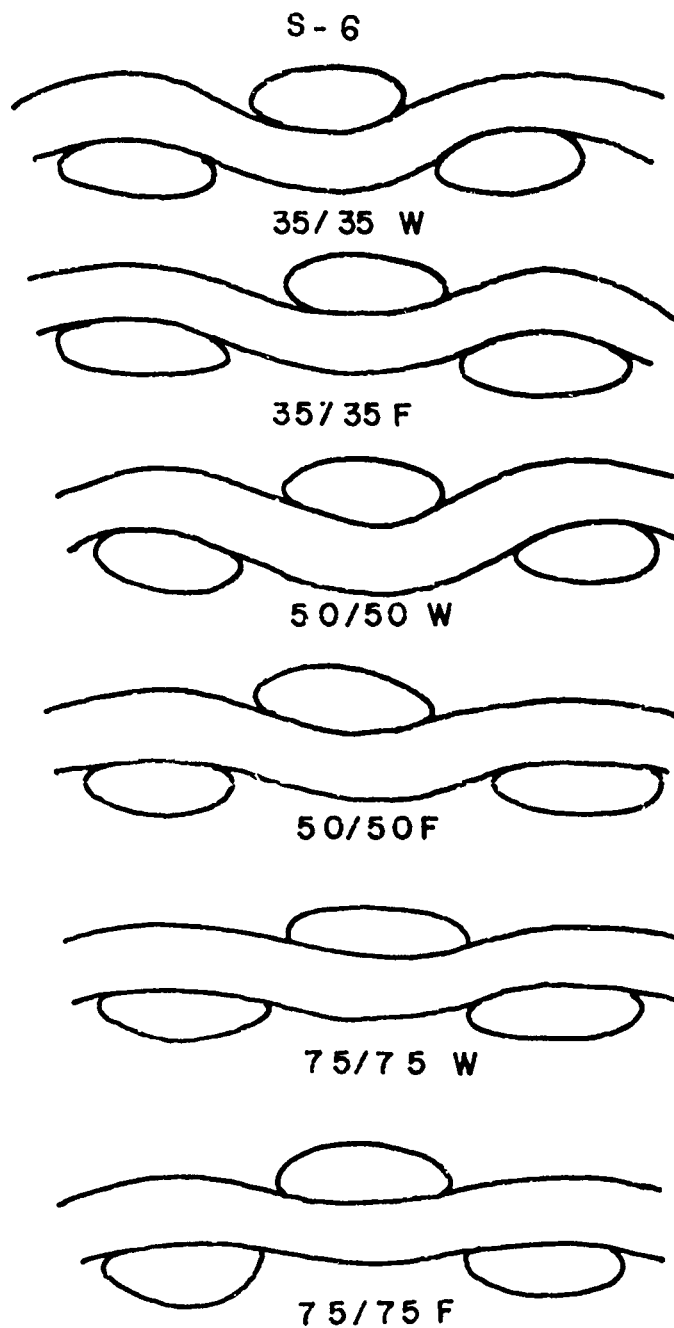
Figure 64.2. Section of Fabric. S-6.

S-6
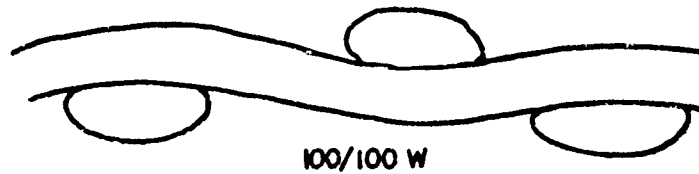
100/100 W

100/100 F

Figure 64.3. Sections of Fabric S-6.
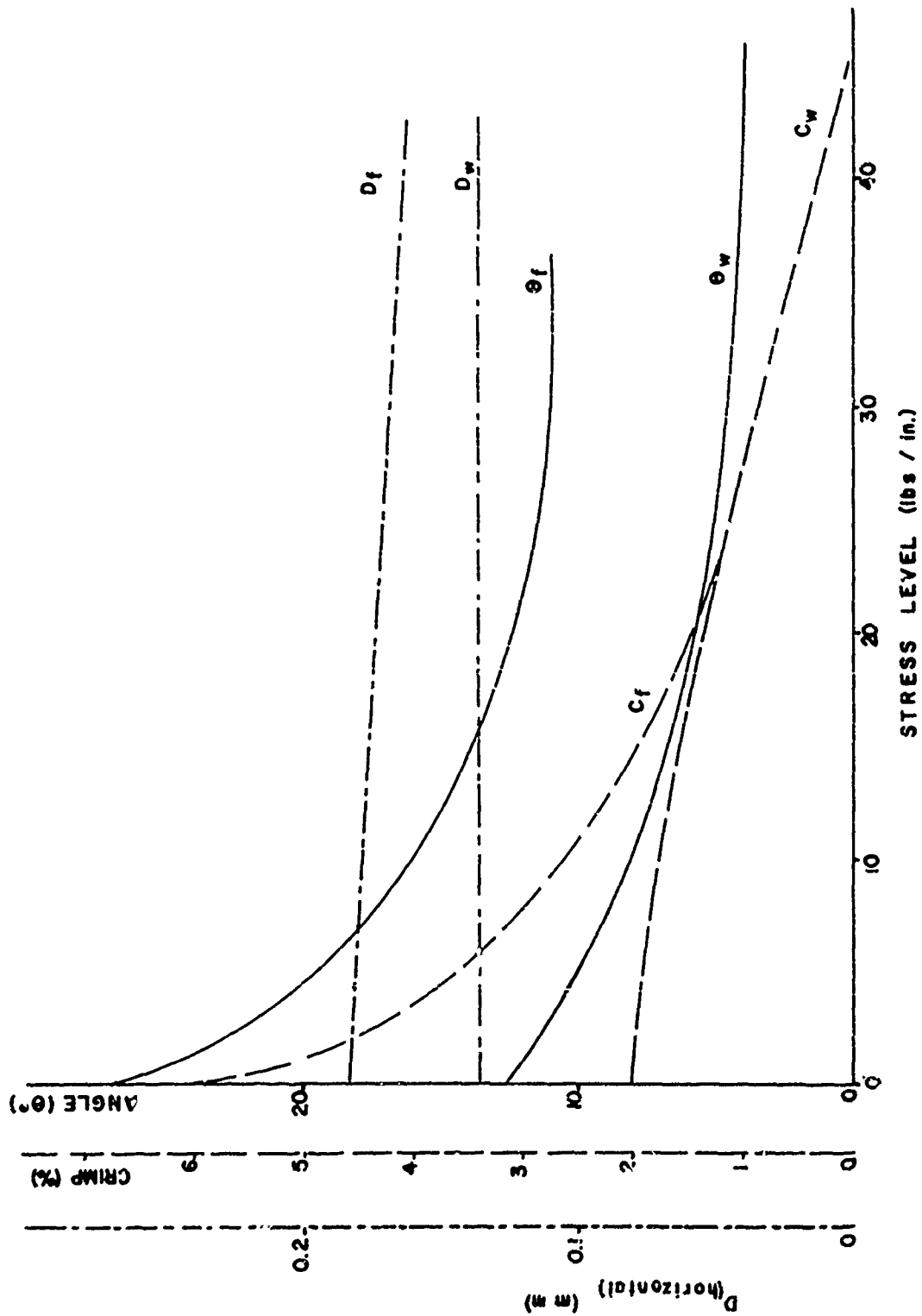
Figure 65. Changes in Fabric Geometry Induced by Stress in S-3
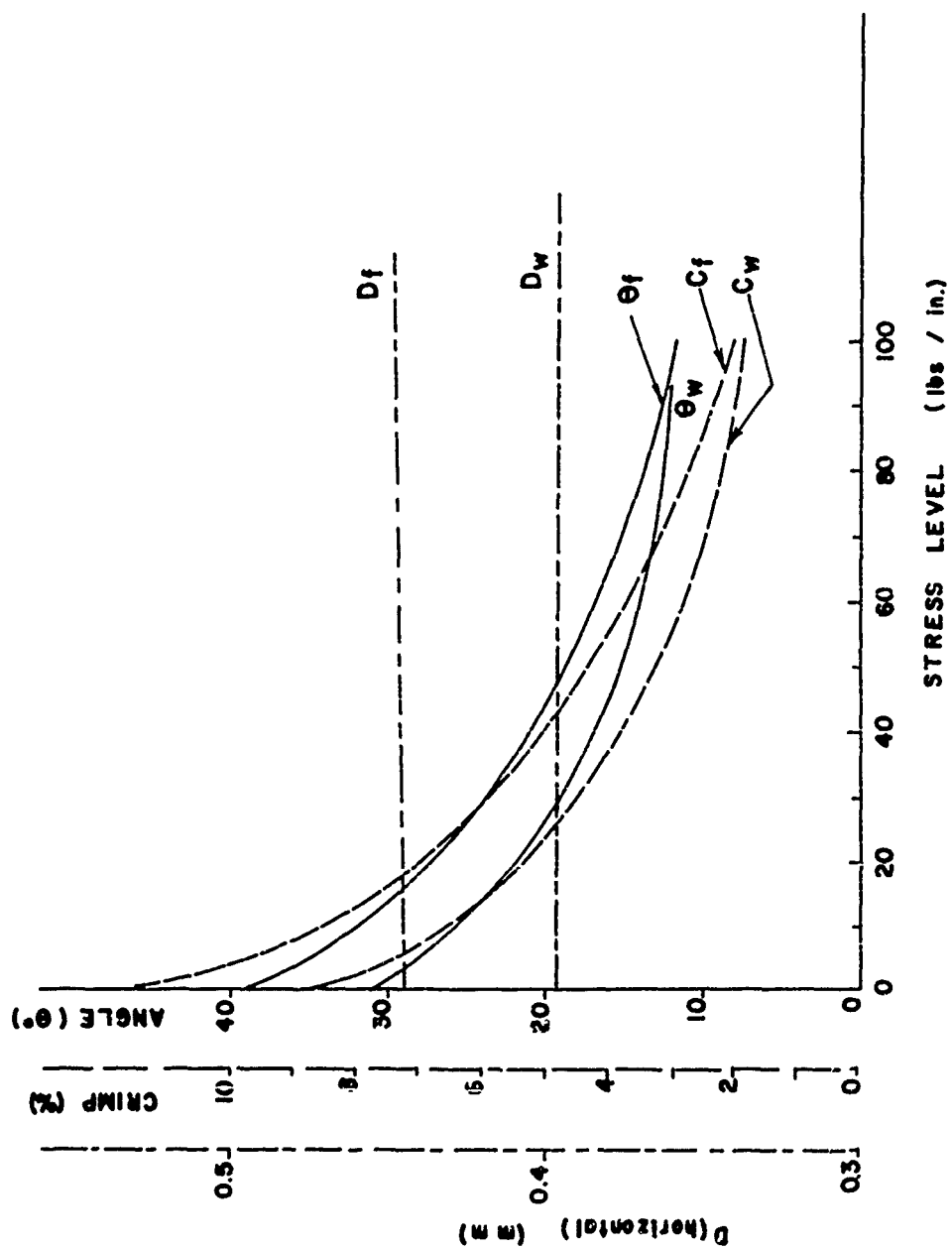
Figure 66. Changes in Fabric Geometry induced by Stress in S-6
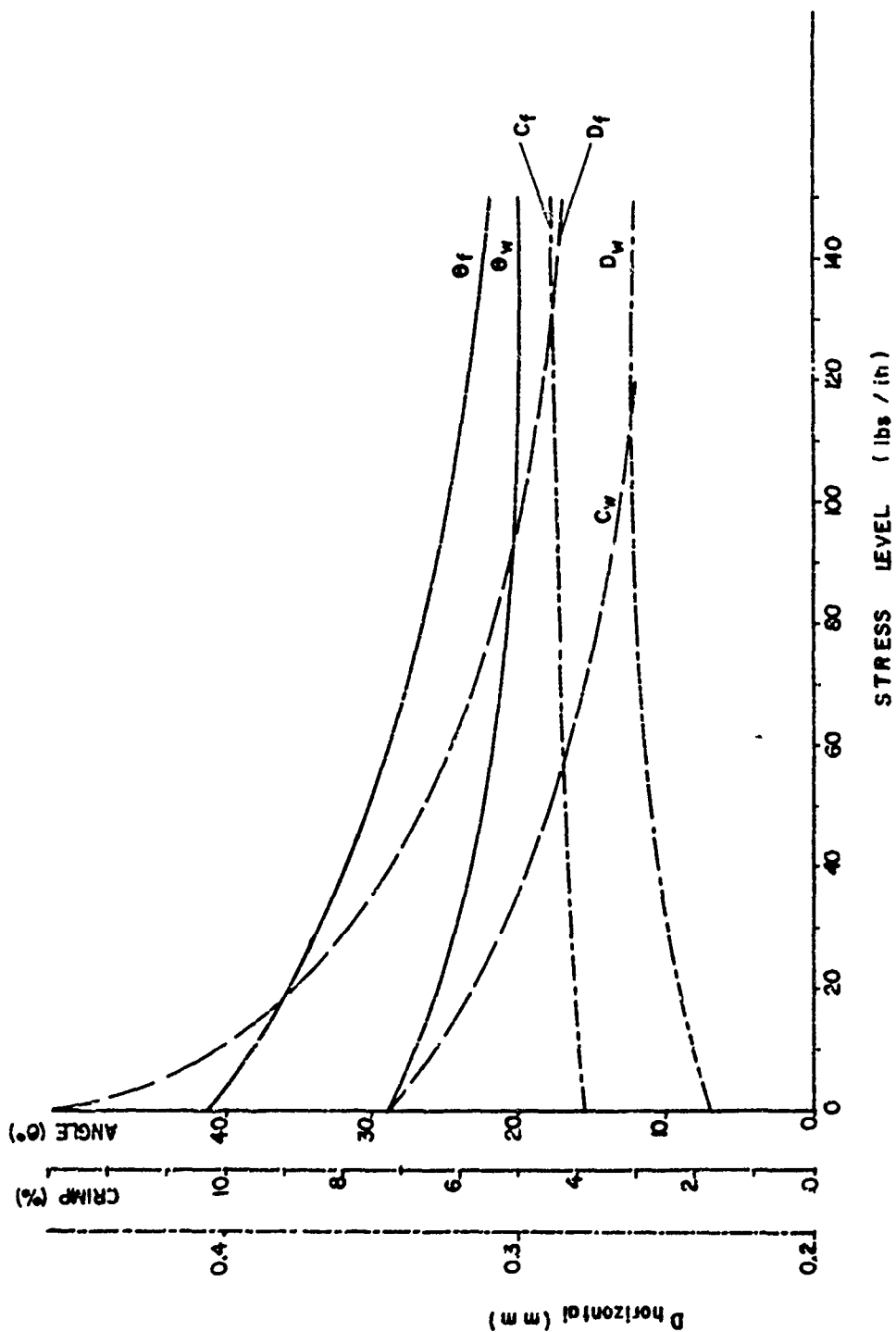
Figure 67. Changes in Fabric Geometry Induced by Stress in E-9
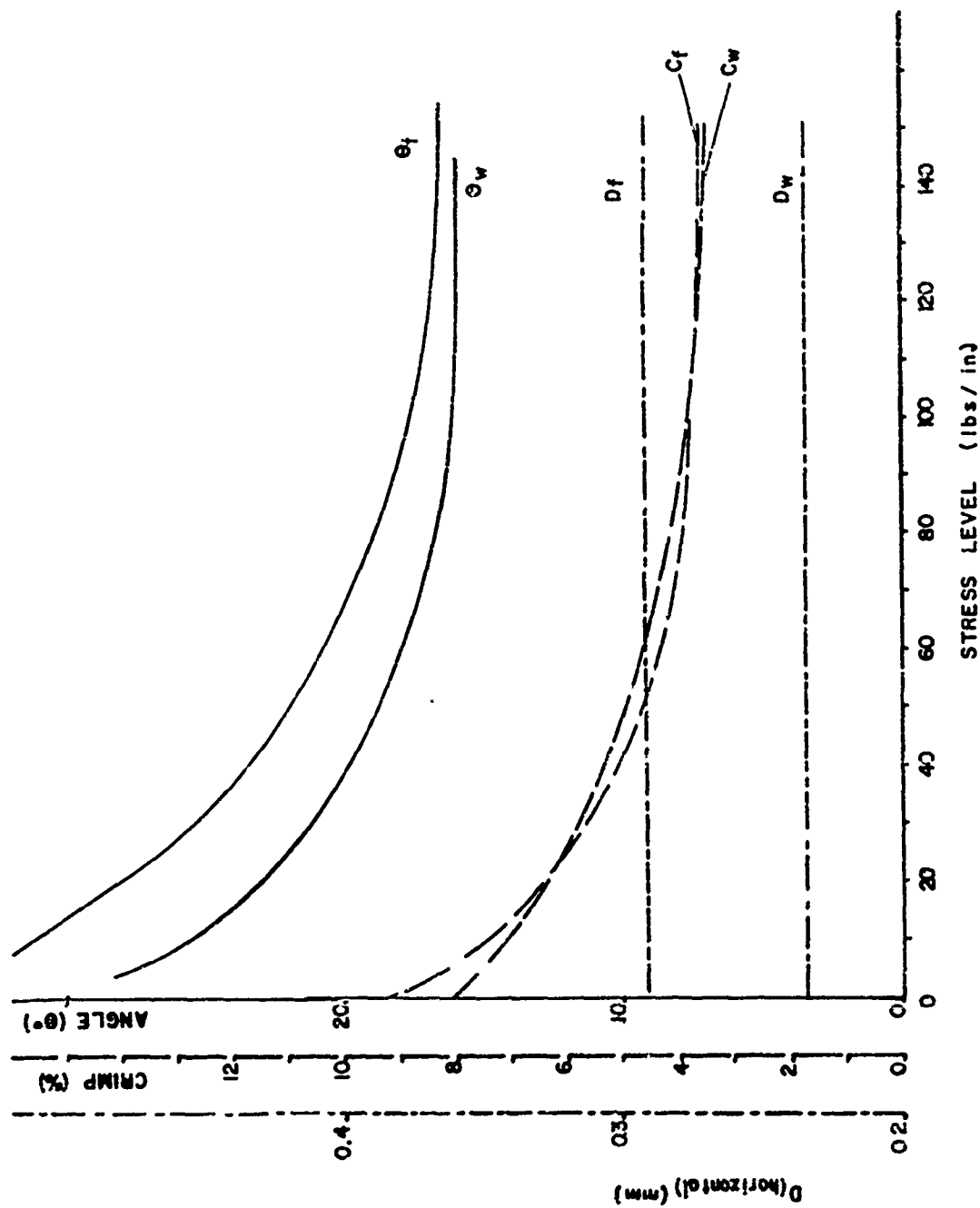
Figure 68. Changes in Fabric Geometry Induced by Stress in E-IO.

TABLE 9

Biaxial Stress Tests on Parachute Cloth

Specimen   Stress   Conditions   (lbs/in)   warp/filling

Specimen								
E9	0/0		25/25	37½/37½	50/50	75/75	100/100	150/150
E10	0/0	25/25	50/50	75/75	100/100	125/125	150/150	15.3/12
		23/20	39/31.5	56/45	80/66			
S3	0/0	14/10	16/12	23/17	30/23.5	46/35		
S6	0/0	25/25	50/50	75/75	100/100	10/10	17/17	35/35

is represented in Figures 64.1 - 64.3 as it flanks a three pick float (Figures 57 and 69.) Fabric S6 proved particularly difficult to section along the plain weaving yarn because of the extensive lateral yarn distortion which takes place in the plane of the cloth. This is characteristic of the 'pinching' tendency of the three pick float. Similar lateral distortion is observed for Fabric S3, and even in the 2x2 basket weaves of E9 and E10 a marked in-cloth-plane distortion is present. These distortions do affect the pore dimensions and shapes in a way which is discussed in the next section of this report.

Geometry Stress and Airflow

It remains to discuss the results obtained in the prestress airflow experiments, the hydrostatic pressure tests and the biaxial stress embedding process. For all three phases were conducted with a view to understanding the distortion of parachute cloth during an airflow test and the way this distortion influences the flow. In addition it was expected that the biaxial stress embedding studies could throw some light on the "air stream deflection" tendencies of certain of the fabrics tested during the program. Consider the "deflection tendency" first.

It has been reported that the thin fabrics S3, S6 and S8 do not deflect the airstream passing through them to a significant degree. These fabrics are constructed of 115x115, 470x565, and 115x125 denier yarns respectively - decidedly on the thin side. Fabrics E6 and E9 show strong deflection tendencies, depending on the conditions of test, and have 903x917 and 1250x1290 denier yarns respectively. The relative thickness and channelling of S3, S6 and S8 versus E6 and E9 can be easily realized by comparisons of the sections of E9 and E10 (940x980 denier yarns) in Figures 61 and 62 with those of S3 and S6 in Figures 63 and 64 respectively.

In addition to the thickness of their yarns, Fabrics E6 and E9 which show maximum deflection tendencies, share another constructional feature. They are both basket weaves (2x2), as is Fabric E10. But the basket weave appears to be completely symmetrical at first glance. Why then should an air stream entering its pores be deflected in a preferred direction. The answer appears in our consideration of the complex interaction between yarn and cloth structure. Two factors tend to disturb the ortho-symmetry of the fabrics at hand: the planar non-symmetry of the weaving operation and the inclination of the fibers to the yarn axes--that is the direction of yarn twist.

One can readily observe the presence of small pores and large pores across the surface of the basket weave. This difference in pore sizes is systematic and follows directly from the buckling

WADC TR 59-374

139

tendency of the crimped twisted yarns. One observes it easily in Fig. 58, the surface photograph of fabric E10 and in the sectional tracings of Figures 53 and 54 (in particular at sections 3 and 6 and 3, 6 and 10 respectively. The instability of crimped and twisted yarns is well known in the field of textile technology. It is responsible for such effects as local buckling, shrinkage, creping and twill dominance. Where the asymmetry of the weave assists the natural buckling tendency of the yarn the yarn twist will be relieved locally when the yarn axis forms a helix of the same direction). The weave asymmetry may, on the other hand, prevent the yarn from buckling (as occurs when twill and twist directioı ᴉ are crossed).

In an ortho-symmetric weave like a 2x2 basket, the weave neither assists nor prevents buckling and it proceeds to a level which depends on the relative tightness of the supporting weave structure and the twist unbalance in the yarns. In open weaves, such as in certain industrial filters, the buckling tendency is pronounced and it imparts an added extensibility to the cloth structure. In the case at hand, the degree of buckling is moderate, but it is still sufficient to rotate the basket weave float clockwise into a Z helix (corresponding to the Z twist direction). This rotation serves to reduce the size of the fabric pore at the upper right hand corner of the float, and at its lower left hand corner. The pores at the lower right and upper left hand corners are correspondingly enlarged. Rotation of the floats takes place on the front and back of the fabric in warp and in filling, all rotation serving to reinforce the enlargement of pores along alternate diagonals.

This selective enlargement of fabric pores may account for directional deflection effects in air flow tests if it can be shown that air streams through the large pores deflect in one direction while those through the smaller pores deflect in the other direction. One can then credit the larger pores with dominance over the scene. But a closer view of the enlarged pore, as say in the successive sections of Figures 53 and 54 does not provide overwhelming evidence of a directional tendency in air flow through the pore. One pertinent feature noticeable is the asymmetry of the float in its vertical plane. In the weaving process the loom shedding motion is asymmetric, as is the beat up motion. As a result the floats of the warp yarns are not perfectly symmetric relative to the center plane of the fabric. Nore are they symmetric fore and aft, that is forward and backward along their length (about the center point). This 'longitudinal asymmetry' can be observed in these basket weaves by moving the cross section along under the microscope from warp float to warp float, but it is not practical to reproduce here the numerous cross sections necessary to illustrate the point. Suffice it to say that the longitudinal asymmetry of floats in the weaving of wire cloth has so reduced the uniformity of float abrasion that the wire cloth weavers have designed a special tensioning device to level out the float surface.

The asymmetric behavior of the warp float serves to explain the deflection tendency of the large pores in the basket weaves, Fabrics E6, E9 and E10 Looking at a contiguous pair of warp floats in E9 under a stereoscopic microscope, one can observe evidence of different warp bending curvatures at the top and bottom of the warp floats. Thus, the warp entering a given large pore at the top of its float has a different curvature than one entering the same pore (from the other side) at the bottom of its float. As a result, the warp yarns which bound the pore are not symmetric about the center plane of the cloth. The yarn cylinder which is further downstream along the line of air flow in the pore will bend the stream away from it, thus contributing to the overall stream deflection. This influence of the yarn downstream in a pore model has been shown experimentally by Penner et al. (15).

One would expect that if the warp yarn behavior controls the stream deflection that the deflection angle β would far exceed angle α (Fig. 25.2). This is seen to be the case in Tables 6,7 and 8 for Fabrics E6 and E9. Further one would expect a reversal of the fabric to alter the sign of angle β and leave angle α relatively untouched. This happens in Fabric E9 as expected, but in E6 the results do not show a significant trend.

One would also expect that the asymmetry of the warp float will be reduced if the fabric is subjected to high tension in both warp and filling, or in warp alone. Thus, at high biaxial stress levels the fabric should flatten and the floats become more symmetric. Both of these conditions should reduce the amount of deflection of air flow through the pores. The uniaxial warp tension should have the greatest effect in reducing deflection. The data of Table 6 shows a reduction in airstream deflection for Fabric E6 with increased pressure drop. In Table 8 Fabric E9 exposed over the full air flow channel shows a marked reduction in overall deflection angle ϕ as higher pressure differentials, hence higher biaxial stresses, are put across the fabric. But the reduction with stress application of angle β is accompanied by a similar reduction in α. Thus, it appears that while the asymmetry of the warp is a principal cause of the airstream deflection, it develops a corresponding asymmetry in the filling yarn with which it interlaces to form the boundaries of a fabric pore. Specimens $E9_1$, $E9_2$ and $E9_3$ were exposed to airflow only at the center square inch of uniformly, biaxially stressed cloth. At this central point the stress level appears to have much less effect on the deflection angles than for the case of E9 exposed over the entire specimen.

We now consider the influence of stress on the airflow characteristics of the test fabrics. The summary of prestress test data can

WADC TR 59-374

141

be found in Figs. 32 to 35 inclusive. These data are to be compared with the hydrostatic test data plotted in Figs. 39 to 50 inclusive and with the stress-embedding studies of Figs. 61 to 68 inclusive.

Fabric S3 is the lightest material of the group and it is expected that prestressing will have the greatest influence on the permeability of this material. The relatively thin construction of S3 is seen in Fig. 63. Its relative softness to stress application is seen in Fig. 44, with the warp acting significantly stiffer than the filling at all levels of hydrostatic pressure. Thus one expects considerably more reduction in filling crimp and inclination angles, a feature observed in Fig. 65. And for such high extensibilities of about eight (8) per cent at 20 lbs/in biaxial load (corresponding to the 0 psig prestress pressure), one expects that the 'prestress' permeabilities will range far above the zero prestress tests. In fact, at low Δp's across the fabric, prestress permeabilities are from 50 to 100% higher than the zero prestress values.

Fig. 46 shows Fabric S8 to be initially stiffer than Fabric S3, but unbalanced in similar fashion warp vs. filling. While increased fabric stiffness should decrease the effect of prestressing on permeability it must be remembered that the prestress in the experiments reported here is provided by a hydrostatic pressure. Thus, for the same 3 psig, Fabric S8 encounters 12 x 7 lbs/in tension in warp and filling, while fabric S3 encounters only 8 x 6 lbs/in. At 5 psig Fabric S8 encounters 17 x 11 lbs/in and Fabric S3 17 x 12 lbs/in. It is expected then, that Fabric S8 at the lower pressure differentials and lower prestress values is in fact being subjected to a harsher test condition. Despite this, the prestress permeability of Fabric S8 up to 40 inches of water, is about 25% greater than the unprestressed permeability.

Sample S6 data are reported in Fig. 40. Here we observe a balanced performance for warp and filling. This is reflected to some extent in the parallel behavior of crimp and inclination angles in Fig. 66. The average extension of S6 at the low prestress levels is of the same order as that of S8 (averaged for warp and filling) and the prestress permeabilities are about equally higher than the zero prestress values for both S8 and S6. But at the higher hydrostatic prestress levels S6 is much stiffer than S8 and the prestress extensions are significantly lower (despite the higher biaxial stress levels). As a result the prestress permeability increases (at this higher prestress level) are less for S6 than for S8. Thus, the full stress-strain behavior of the fabric under biaxial stress conditions is seen to influence the relative permeabilities to a significant degree.

Fabric E10 data are plotted in Figs. 35, 42 and 68. In Fig. 68 we observe a marked change in crimp levels at low stress levels, in warp and filling. This accounts for the lower fabric modulus at low stresses shown in Fig. 42, followed by the higher modulus at higher stresses. The permeability increase due to prestress extensions for E10 are of the same order of magnitude as for S6 at low pressure drops. At higher pressure drops across the fabric the higher prestress permeability data are also grouped together as in S6 reflecting high sample stiffness, while in the softer fabric S3 the prestress permeability data are markedly separate. Again the stress-strain behavior of the cloth is seen to have a dominant effect on its relative permeability under the prestress test conditions.

CONCLUSIONS

Based on the results of the high altitude flow studies the following conclusions were reached.

1. Good experimental data were obtained for Fabrics S3, S, and E10 over a range of altitudes from 50,000 to 150,000 feet and for pressure differences up to 1000 inches water. The values of the flow rates at these altitudes are the correct order of magnitude based on a simple nozzle flow analogy. The observed variation of flow rate with altitude, for a given Δp, did not always follow the expected trend that lower flow rates should occur at higher altitudes. However, this discrepancy may be due to the variability of the geometric porosity of fabric samples.

2. The variation of flow rate, at a given Δp, with altitude is very difficult to measure even with an accurate flow measurement system since the geometric porosity of fabric samples is liable to vary considerably even for samples taken from the same fabric lot. The accurate measurement of this variation becomes progressively more difficult as the altitude is increased, especially beyond altitudes of 50,000 feet.

3. The calculated values of effective porosity and geometric porosity for Fabrics S3, S6 and E10 are in good agreement with values from the literature.

4. A method of predicting flow rate data for fabrics used under high altitude conditions from the corresponding data under sea-level conditions has been developed and verified. The agreement between the measured and predicted flow rates for Fabrics S3 and S is excellent. The discrepancy between measured and predicted flow rates for Fabric E10 is not yet clearly understood but may be due to difficulties in obtaining reproducible data for this fabric. Additional experimental work should be done on Fabric E10. This method has been verified for values of Δp greater than 100 inches water, but further careful experimental studies should be done for values of Δp less than 100 inches water.

5. Since the method of predicting flow rate data for fabrics under high altitude conditions has proven so successful, it would seem that further experimental programs to obtain flow rate data for fabrics at altitudes beyond 150,000 feet are unnecessary unless the area of interest is restricted to rather low values of Δp, i.e. 100 inches of water or less. As new fabrics are produced, flow rate data can be obtained under sea-level conditions using standard permeometers and then the high altitude data can be predicted. Additional tests should be made on fabrics in order to determine any limitations on the method of predicting high altitude data.

Based on the results of the prestress, hydrostatic, stream deflection, and geometric studies the following conclusions were reached:

1. Deflection of an airstream as it passes through a woven parachute fabric is dependent on the initial geometry of the fabric pores and on the state of stress to which the fabric is subjected during the test. The effect is not observed in thin cloths. In thick cloth the deflection can be traced to the influence of pore asymmetry arising from twist-weave interactions and from the basic asymmetry about the cloth-center-plane introduced by the weaving operation. The deflection angle for a given cloth is dependent on airflow test conditions on fabric stress, and pressure differentials. It is therefore unlikely that the deflection phenomenon can be used effectively as a practical design parameter in construction of parachutes. Its existence and order of magnitude, however, should be kept in mind in any critical study of the influence of permeability on parachute performance.

2. In tests on Fabric S8 taken from six jump and thirteen jump canopies respectively, no significant change from the original permeability or stress-strain behavior was observed. The aging effect of thirteen jumps can be termed negligible in this case.

3. Air flow tests on woven cloths based on fixed specimen dimensions can give misleading results if no account is taken of fabric stress buildup during the air flow measurements. The cloths tested in this program extend significantly at low biaxial tensions. Airflow differences at low pressure differentials which result from these extensions range from 25 to 100% of the measurements taken in the conventional manner. This early extension is not the result of crimp interchange but rather the result of overall crimp reduction following from yarn flattening and yarn extension. These effects have been demonstrated in independent tests of prestress air flow behavior, in hydrostatic-biaxial stress tests, and in extensive geometric studies of stress-embedded samples.

RECOMMENDATIONS

As a result of the air flow studies which have been done during this research program, the following recommendations are made:

1.   A critical study should be made of methods for using flow rate data taken under sea-level conditions to predict flow rate data under high altitude conditions. Special attention should be given to the range of pressure differences across the fabric extending from 0 to 100 inches water, since in this range the nozzle flow analogy described in this report may not be valid due to Reynolds number effects. The methods developed should be tested using available data taken under sea-level and high altitude conditions. The development of such methods would obviously eliminate a large amount of testing of fabrics under high altitude conditions, since only sea-level data would have to be taken.

2.   An experimental program should be started to measure air flow characteristics of fabrics under a range of altitude conditions extending from sea-level to about 150,000 feet and a range of pressure differences extending from 0 to 100 inches water. Such data would be useful in themselves and for purposes of studying the methods described above. This program could also include tests on some metal screens where the geometric porosity could be controlled and measured.

3.   An experimental program should be started to measure air-flow characteristics of textile and metallic fabrics over a temperature range extending up to about $1000^{\circ}F$. The altitude and pressure difference conditions should be as broad as possible but concentrated in these regions of present practical interest.

4.   A critical study should be undertaken to extract from current parachute research all evidence of canopy stress buildup during deployment and steady state descent. Time and temperature factors pertinent to parachute usage and stress application should be observed. An experimental program should be undertaken so as to provide information on the air flow characteristics of canopy cloths and the specific restricted range of temperature, stress-level, and rate of stress application which they meet in critical uses.

BIBLIOGRAPHY

1. Johns, T. F. and Anterson, E. I., R&M No. 2335 (British Ministry of Supply, Aeronautical Research Council)

2. Hoerner, S. F., Aerodynamic Properties of Screens and Fabrics. Textile Research Journal, 22, 275, (1952)

3. Krizik, J. G., Victory, E., Cheatham, J., and Backer, S., Design Data on Biaxial Forces Developed in Parachute Fabrics. WADC Technical Report TR 57-443, December 1957

4. Standard Atmosphere - Tables and Data for Altitudes to 65,800 Feet NACA Report 1235, 1955

5. Warfield, Calvin N., Tentative Tables for the Properties of the Upper Atmosphere, NACA TN 1200, January, 1947.

6. Shapiro, A.H., The Dynamics and Thermodynamics of Compressible Fluid Flow, Volume I, Ronald Press New York (1953)

7. Lavier, H.W.S., and Boteler, W.C., WADC Technical Report 52-283 Part V

8. Lavier, H.W.S., Air Permeability of Parachute Cloths, WADC Technical Report TR 52-283 Part 3.

9. Chu, C. C., Lermond, C. A., and Platt, M. M., Study of the Effect of Twist in Yarns on Parachute Fabrics, WADC Technical Report TR 55-104 February 1956

10. Klein, W. G., Lermond, C. A., and Platt, M. M., Development of Design Data on the Mechanics of Air Flow Through Parachute Fabrics WADC Technical Report 56-576, September 1957

11. Klein, W. G., Lermond, C. A., and Platt, M. M., Research Program for the development of a Design Procedure to Engineer Parachute Fabrics, WADC Technical Report TR 58-65, May 1958

12. Heinrich, Helmut G., Parachute Engineering and Retardation, Chapter V. The Variation of the Air Resistance of a Low Porosity Screen with Reynolds Number, University of Minnesota, Center for Continuation Study, July 14-25, 1958.

13. Peirce, F. T., Geometrical Principles Applicable to the Design of Functional Fabrics, Textile Research Journal 17, 123 (1947)

14. Backer, S., The Relationship Between the Structural Geometry of a Textile Fabric and Its Physical Properties, Part IV Interstice Geometry and Air Permeability, Textile Research Journal XXI, 703 (1951)

15. Penner, S. E., and Robertson A. F., Flow Through Fabric Like Structures, Textile Research Journal, XXI, 775, (1951)

16. Keenan, J. H. and Kaye, J. 'Gas Tables,'' John Wiley & Sons Inc., New York, 1950

APPENDIX I
CONSTRUCTION OF TEST FABRIC

TABLE 10

	Fabric E9		Fabric E10		Fabric S3 MIL-C-7350B-TI		Fabric S6 MIL-C-8021A-TII		Fabric S7 MIL-C-25174T-1		Fabric S8 MIL-C-25174-TII	
	Spec.	Actual	Spec.	Actual	Spec.	Actual	Spec.	Actual	Spec.	Actual	Spec.	Actual
1. Yns'in warp	-	42	-	48	70	71	53	53	-	63	80	84
Fill.	-	43	-	46	70	71	48	48	-	65	80	76
2. Weight oz/yd²(max)	-	15.22	-	11.59	2.25	2.10	7.00	6.46	-	-	7.90	2.69
3. Breaking strength (lb/in) warp	-	627	-	563	90	90	300	350	-	-	100	118
Fill.	-	630	-	560	90	90	300	313	-	-	100	105
4. Air Permeability (ft³/min/ft²) min.	-	-	-	-	100	-	50	-	-	-	100	-
max.	-	-	-	-	150	-	90	-	-	-	160	-
5. Thickness (mils)	-	25	-	24	6	6	24	22	-	7.5	6.5	6.5
6. Yarn Denier warp	-	1250	-	940	-	115	-	470	-	185	-	115
Fill.	-	1290	-	980	-	115	-	565	-	195	-	125

```
X O X O X O          O X O X O X
O X O O X X          X X X O X O
X O O X O O    S-3   O X O X O X    S-6
O O X O O X          X O X O X O
X X O O X O          O X O X X X
O X O X O X          X O X O X O


X O X O X O          O X O X O X
O X O X O X          X O X O X O
X O X O X O    S-7   O X O X O X    S-8
O X O X O X          X O X O X O
X O X O X O          O X O X O X
O X O X O X          X O X O X O


X X O O X X O O      X X O O X X O O
X X O O X X O O      X X O O X X O O
O O X X O O X X      O O X X O O X X
O O X X O O X X E-9  O O X X O O X X E-10
X X O O X X O O      X X O O X X O O
X X O O X X O O      X X O O X X O O
O J X X O O X X      O O X X O O X X
O O X X O O X X      O O X X O O X X
```

Figure 69.   Weave   Patterns   of   Test   Fabrics

APPENDIX II

DETAILS OF AIR COMPRESSOR AND AIR EJECTOR SYSTEMS

Air Compressor

The air supply for the permeometer was a two-stage, motor driven, reciprocating air compressor manufactured by the Joy Manufacturing Company of Michigan City, Indiana. The low pressure stage has a 10 inch diameter bore and a 7 inch stroke, while the high pressure stage has a 5 inch diameter bore and a 7 inch stroke. This compressor is a Class WN-112, Size 10-5x7, Model K Joy Compressor. The compressor has an intercooler and an aftercooler. The air from the compressor enters a receiver tank and then flows to the permeometer. A by-pass control system has been installed on the line from the receiver tank which permits extremely accurate control of the air pressure at the permeometer. At a discharge pressure of 150 psia, the compressor has a volumetric efficiency of 80.4%, a volume flow rate of 293 SCFM, and a mass rate of flow of 22.2 lbm air/min.

Air Ejector

The low pressure source for the downstream side of the fabric was a three stage, steam driven, air ejector. Manufactured by the Elliott Company, Inc., of Jeannette, Pa. The official Elliott designation was 8 N 8 B32 three stage ejector.

The ejector is supplied with steam at 185 psia and 380 F. Normally, air enters the suction of the first stage and is mixed with about 250 lbm steam/hr. This mixture then flows to the suction of the second stage where another 1000 lbm steam/hr are added. The air and 1250 lbm steam/hr then enter a barometric intercondenser where about 160 gpm of cooling water are used to condense the steam. Instead of using a barometric leg on the intercondenser of 34 feet of water, a centrifugal pump is used to remove the condensate and cooling water from the intercondenser. The cooling water is supplied to the intercondenser by means of a vacuum lift. The air and a small amount of steam leave the inter-condenser and enter the suction of the third stage where another 1100 lbm steam/hr are added. The air and this final steam flow leave the third stage and pass to an aftercondenser where most of the steam is condensed. The aftercondenser is a four-pass, shell and tube heat exchanger. The air is then discharged from the after-condenser to the laboratory. When all three stages are used, the

WADC TR 59-374

pressure at the suction of the first stage will vary between 1 and 35 mm Hg. abs. depending on the air flow rate. The first stage has a discharge pressure of about 1.25 inch Hg. abs. while the second stage discharges to the intercondenser at a pressure of about 5.5 inch Hg. abs. The third stage discharge pressure is about 31.5 inch Hg. abs.

The air ejector was designed to maintain a pressure of 4 mm Hg. abs. at the suction of the first stage while handling 120 lbm air/hr. At "dead-end" conditions, the pressure was to be less than 1 mm Hg. abs. The ejector was also designed to operate in a stable manner for flow rates up to 370 lbm air/hr at a pressure 35 mm Hg. abs.

For tests at the lower altitudes only the third stage ejector was used.

APPENDIX III

FLOW MEASURING SYSTEM

The air flow rate through the fabric was measured using a calibrated Fischer and Porter Company rotameter. The rotameter employed a Number 10-1735, Size 8 glass tube. The Number BSx267 float was used for mass flow rates from 2 to 23 lbm air/hr. when the rotameter was supplied with air at 2 psia and 70F. For higher flor rates, a Number B-NSVT 84 float was used. This latter float covered mass flow rates from 50 to 510 lbm air/hr when the rotameter was supplied with air at 36 psia and 70F. The method of calculating the mass flow rate through the rotameter when the inlet conditions are different than those mentioned above has been discussed in the main body of this report.

In order to obtain the greatest possible accuracy from the rotameter it was calibrated against the gasometer in the Mechanical Engineering Laboratory at M.I.T. For rotameter inlet pressures greater than atmospheric pressure, air was supplied to the rotameter by the Joy air compressor. After steady state flow conditions had been established, the air flow from the rotameter was switched to the gasometer for a mass flow rate measurement. For rotameter inlet pressures less than atmospheric pressure, air was drawn through the rotameter using the air ejector. After steady state flow conditions had been established, the air flow to the rotameter was supplied from the gasometer for a mass flow rate measurement. The entire piping system was carefully tested for leaks.

The calibration data for the Number B-NSVT 84 float were taken at an inlet pressure of 36 psia and were within less than $\pm 1\%$ of the calibration curve supplied by the Fischer and Porter Company over the entire mass flow rate range. In order to check the use of Equation (1) to predict mass flow rates at inlet pressures other than 36 psia, data were taken at inlet pressures between 16 psia and 22 psia. When these flow rates were referred back to an inlet pressure of 36 psia by Equation (1), these values were also within less than $\pm 1\%$ of the Fischer and Porter calibration curve.

At a mass flow rate of about 24 lbm air/hr, the average calibration curve for float Number BSx867 indicated a mass flow rate which was about 5% higher than that indicated by the Fischer and Porter calibration curve. However, all the calibration data taken at an inlet pressure of 2 psia were within less than $\pm 1\%$ of their own mean curve.

MASSACHUSETTS INSTITUTE OF TECHNOLOGY,
TEXTILE DIVISION, MECH. ENG. DEPT.,
Cambridge, Mass. AIR FLOW CHARACTERISTICS
OF PARACHUTE FABRICS AT SIMULATED HIGH
ALTITUDES, by C. V. Seshadri, G. A. Brown,
S. Backer, J. G. Krizik and D. H. Mellen.
August 1959. 153p. incl. illus. tables.
(Proj. 7320; Task 73201)(WADC TR 59-374)
(Contract AF 33(616)-5864)
          Unclassified report

The air flow characteristics of parachute
canopy cloth have been measured over an
unusually wide range of test conditions.
High altitude simulated tests (up to 150,
000 feet) have shown the cloth to have
markedly low flow rates, as may be predict-
ed from a nozzle flow analogy. A method

(over)

of prediction high altitude behavior has
been proposed. Permeabilities of four
cloths have been shown to be significantly
dependent on their state of stress at the
time of air flow measurement.

MASSACHUSETTS INSTITUTE OF TECHNOLOGY,
TEXTILE DIVISION, MECH. ENG. DEPT.,
Cambridge, Mass. AIR FLOW CHARACTERISTICS
OF PARACHUTE FABRICS AT SIMULATED HIGH
ALTITUDES, by C. V. Seshadri, G. A. Brown,
S. Backer, J. G. Krizik and D. H. Mellen.
August 1959. 153p. incl. illus. tables.
(Proj. 7320; Task 73201)(WADC TR 59-374)
(Contract AF 33(616)-5864)
          Unclassified report

The air flow characteristics of parachute
canopy cloth have been measured over an
unusually wide range of test conditions.
High altitude simulated tests (up to 150,
000 feet) have shown the cloth to have
markedly low flow rates, as may be predict-
ed from a nozzle flow analogy. A method

(over)

of prediction high altitude behavior has
been proposed. Permeabilities of four
cloths have been shown to be significantly
dependent on their state of stress at the
time of air flow measurement.

MASSACHUSETTS INSTITUTE OF TECHNOLOGY,
TEXTILE DIVISION, MECH. ENG. DEPT.,
Cambridge, Mass. AIR FLOW CHARACTERISTICS
OF PARACHUTE FABRICS AT SIMULATED HIGH
ALTITUDES, by C. V. Seshadri, G. A. Brown,
S. Backer, J. G. Krizik and D. M. Mellen.
August 1959. 153p. incl. illus. tables.
(Proj. 7320; Task 73201)(WADC TR 59-374)
(Contract AF 33(616)-5864)
                    Unclassified report

The air flow characteristics of parachute
canopy cloth have been measured over an
unusually wide range of test conditions.
High altitude simulated tests (up to 150,
000 feet) have shown the cloth to have
markedly low flow rates, as may be predict-
ed from a nozzle flow analogy. A method

(over)

of predicting high altitude behavior has
been proposed. Permeabilities of four
cloths have been shown to be significantly
dependent on their state of stress at the
time of air flow measurement.

MASSACHUSETTS INSTITUTE OF TECHNOLOGY,
TEXTILE DIVISION, MECH. ENG. DEPT.,
Cambridge, Mass. AIR FLOW CHARACTERISTICS
OF PARACHUTE FABRICS AT SIMULATED HIGH
ALTITUDES, by C. V. Seshadri, G. A. Brown,
S. Backer, J. G. Krizik and D. M. Mellen.
August 1959. 153p. incl. illus. tables.
(Proj. 7320; Task 73201)(WADC TR 59-374)
(Contract AF 33(616)-5864)
                    Unclassified report

The air flow characteristics of parachute
canopy cloth have been measured over an
unusually wide range of test conditions.
High altitude simulated tests (up to 150,
000 feet) have shown the cloth to have
markedly low flow rates, as may be predict-
ed from a nozzle flow analogy. A method

(over)

of predicting high altitude behavior has
been proposed. Permeabilities of four
cloths have been shown to be significantly
dependent on their state of stress at the
time of air flow measurement.